

UNIVERSITY OF STRATHCLYDE
DEPARTMENT OF DESIGN MANUFACTURING & ENGINEERING
MANAGEMENT

WEAR ASSESSMENT OF SUPERPLASTIC
FORMING CERAMIC DIES:
A STUDY ON PROTECTIVE COATING
PERFORMANCE

ANDREA STAIANO

A thesis presented in fulfilment of the requirements for the degree of
Doctorate of Engineering

2019

Declaration of Authenticity and Author's Rights

This thesis is the result of the author's original research. It has been composed by the author and has not been previously submitted for examination which has led to the award of a degree.

The copyright of this thesis belongs to the author under the terms of the United Kingdom Copyright Acts as qualified by University of Strathclyde Regulation 3.50. Due acknowledgement must always be made of the use of any material contained in, or derived from, this thesis.

Date:

Signed:

Publications

Staiano A., Ion W., O'Hare L. *Thermal sprayed protective coatings for superplastic forming ceramic dies: a monitoring system of die condition*, Proceedings of the International Thermal Spray Conference (May 21-23, 2014, Barcelona, Spain). Dusseldorf: DVS Media, p. 301-305, 2014

Staiano A., Ion W., O'Hare L. *Monitoring of ceramic die condition under hot forming processes*, The 23rd International CAPE Conference (Nov 5, 2015, Edinburgh, UK)

Staiano A., Ion W., O'Hare L., Zuelli N. *Protective coatings for superplastic forming ceramic dies: An initial study on protective coatings performance*, Proceeding of the European Superplastic Forming Conference (Sep 7-9, 2016, Toulouse, France)

Staiano A., Ion W., O'Hare L., Zuelli N. *Protective coatings for ceramic superplastic forming dies*, Materialwissenschaft und Werkstofftechnik, Vol. 48, Issue 10, p.1009, 2017

Gomex Gallegos A.A., Staiano A., Farrell M., Zuelli N. *A comparative study assessing the wear behaviour of different ceramic die materials during superplastic forming*, Materialwissenschaft und Werkstofftechnik, Vol. 48, Issue 10, p.983, 2017

Abstract

Superplastic forming (SPF) is an advanced manufacturing process, typically restricted to low volume and high value products, where metallic sheets are heated at the superplastic temperature and blow formed into a metallic die. Refractory ceramics are a low cost option to substitute the high temperature resistant steels and other alloys conventionally used in SPF dies, but their brittle nature is a limiting factor for most SPF applications. Suitable surface coatings have shown a significant effect on wear resistance in different applications and can be employed to improve the SPF ceramic performance in terms of tool life.

This thesis addresses the lack of testing methods available to assess wear of dies under SPF conditions. A die-part interface (DPI) test method has been developed to assess wear of ceramic dies for sheet metal forming applications. In addition, the thesis discusses the employment of the DPI test to take strategic decisions in different material selection studies. A study is conducted on the comparison of two uncoated ceramic materials, Ceradyne ThermoSil[®] 220 (ceramic CT) and Horizon Chrome infiltrated (ceramic HC), where DPI test results show that Ceradyne ceramic material has overall better performance under SPF conditions, thus its outcomes from the DPI test are considered the baseline to be compared with in further studies.

Two deposition procedures of the same coating material, petalite, have been developed resulting in coating PET-A and PET-B. The resulting coatings are compared through DPI test, resulting in a better performance of the coating fired at higher temperature (PET-B).

Three coating materials are assessed with the DPI test, which shows that two coatings soften under SPF conditions (F-50 and JK-N8), while another coating shows poor adhesion to the substrate (F-40).

The thesis concludes presenting a DPI test protocol that proposes guidelines for die surface wear assessment under SPF conditions.

Acknowledgements

This work has been supported by the department of Design, Manufacture and Engineering Management (DMEM) of the University of Strathclyde, the Advanced Forming Research Centre (AFRC) and the Engineering and Physical Sciences Research Council (EPSRC).

I am grateful to my parents, Maria and Pantaleone, who have always believed in my skills and supported my ideas. I am also grateful to my siblings, Vincenzo and Riccardo, who are growing up.

I would like to acknowledge Prof. Ion and Dr. O'Hare for their great support during the whole four years and especially when I was struggling with motivational issues. In addition, I would like to acknowledge Mr. Zuelli and all the forming team who supported me during the experimental work.

I am grateful with the AFRC people, who made the AFRC a great place where to work and they are always making the effort to improve and to grow.

A special mention goes to Dr. Daniel Sanders from Boeing, who helped me along the doctorate with his deep insight and technical recommendations.

I am also grateful to Prof. Luca Lusvarghi and his research team who were really supportive in the last stage of my doctorate.

A very special gratitude goes to Dorothy and the EngD students, Marine, Bilal, Moe, Subha, Mike, Muftooh, James, Colin, Nicola, Nicolas; to my flatmates, Samir, Daniele, Gurkan, Joel and Jareth; to my friends, Meryem, Riccardo, Pier, Ben and Ergun; to my travel friends, Roberto, Michele, Valery, Mirco and Ivan; to my terrons friends, Chiara, Gianni, Mario and Vittorio

And finally, I am grateful to my *piccole donne*, Brunella, Alessia, Gea and Giulia, who have supported me along the way of this doctorate.

Thanks for all your encouragement!

C'amm fat!

Contents

Abstract	iii
Abbreviations	xii
1 Introduction	1
1.1 Background and significance of the project	1
1.2 Aim and objectives	2
1.3 Structure of the thesis	3
2 Literature review	5
2.1 Superplastic forming	5
2.1.1 Requirements for superplasticity	5
2.1.2 Characteristics of superplastic metals	6
2.1.3 Superplastic alloys	7
2.1.4 Superplastic forming processes	8
2.1.5 Superplastic forming equipment and tools	10
2.2 Surface wear of ceramic	12
2.2.1 Sliding and adhesive wear	13
2.2.2 Surface damage	15
2.2.3 Friction and wear of ceramics	17
2.3 Wear assessment	19
2.3.1 Laboratory testing	19
2.3.2 Laboratory characterisation techniques	25
2.4 Coating materials and release agents for SPF ceramic dies	33
2.4.1 Cordierite	33
2.4.2 Release agents	34
2.5 Conclusion	34
2.6 Summary	36
3 Research methodology	37
3.1 Motivation of the research	37
3.2 Research question	38
3.3 Research strategy	39

4	Equipment and materials	42
4.1	The wear assessment method	42
4.1.1	The test selection	42
4.1.2	The test rig	44
4.1.3	Tool design	44
4.1.4	Correlation between strain rate and rotation	47
4.2	Characterisation methods	50
4.2.1	Die resistance and surface degradation	50
4.2.2	Titanium part scale accumulation	51
4.2.3	Chemical interaction	52
4.2.4	Coefficient of friction	53
4.3	Limitations of the test	53
4.4	Substrate, coating and metal sheet materials	55
4.5	Summary	56
5	Comparison of different ceramic die materials and validation of the DPI test	58
5.1	Comparison of different ceramic die materials	58
5.1.1	Materials	58
5.1.2	Design of experiment	59
5.1.3	Results	62
5.2	Experimental validation	71
5.2.1	Ceramic die design	72
5.2.2	Superplastic forming trials	73
5.2.3	Results	74
5.3	Conclusion	78
5.4	Summary	79
6	Coating deposition optimisation	81
6.1	Introduction	81
6.2	Coating deposition procedure	82
6.3	Experimental conditions	85
6.4	Results	86
6.4.1	Coating hot cracking and surface degradation	86
6.4.2	Titanium part surface degradation	88
6.4.3	Chemical interactions	90
6.5	Conclusion	91
6.6	Summary	94
7	Performance evaluation of protective coating solutions	96
7.1	Introduction	96
7.2	Experimental conditions	97
7.3	Results	98
7.3.1	Coating hot cracking and surface degradation	98
7.3.2	Titanium part surface degradation	103

7.3.3	Chemical interactions	106
7.3.4	Friction	110
7.4	Conclusion	111
7.5	Summary	112
8	Discussion of collated results	114
8.1	Introduction	114
8.2	Die hot cracking and surface degradation	114
8.3	Wear mechanisms	118
8.4	Chemical interaction	122
8.5	Friction	125
8.6	The die-part interface test protocol	127
8.7	Summary	127
9	Conclusion	129
9.1	Recommendations for future work	130
	Appendices	132
A	Coating materials	133
A.1	Coating materials for ceramic dies employed in similar applications	133
A.1.1	Rare earth alumino-silicates glasses	134
A.2	Coatings and materials that fulfil thermal expansion requirements	134
A.2.1	Adjustable thermal expansion materials	134
A.2.2	Low thermal expansion ceramic-glasses	135
A.3	Anti-oxidation barrier coatings	137
A.4	Summary	137
B	Surface roughness data acquisition and processing	139
B.1	Data acquisition	139
B.2	Data processing	139
B.2.1	Selection of the coordinate system	139
B.2.2	Form removal	140
B.2.3	Roughness filter	140
B.2.4	Roughness parameters extrapolation	140
C	Ferro coatings: technical information	141
D	James Kent coating N8-JK: technical information	142
E	Coating deposition procedures	143
E.1	Deposition procedure of coating PET-A	143
E.2	Deposition procedure of coating PET-B	144
E.3	Deposition procedure of coating F-50	144
E.4	Deposition procedure of coating JK-N8	144
E.5	Deposition procedure of coating F-40	145

List of Figures

2.1	Typical structures made with the SPF process.	6
2.2	Schematic representation of single sheet forming process.	9
2.3	Schematic representation of multi-sheet SPF.	10
2.4	Schematic of two sliding solid surfaces.	14
2.5	Classification of surface damage.	16
2.6	Ceramic die-titanium part interactions.	20
2.7	Laboratory test techniques.	21
2.8	Surface roughness parameters.	27
2.9	Abbott-Firestone curve.	27
2.10	Confocal microscopy.	30
2.11	Electron-sample interaction.	31
3.1	Technology readiness levels.	40
3.2	Research strategy diagram.	40
4.1	Test methods limitations.	43
4.2	The DPI test rig.	44
4.3	Design of the end tools for the DPI experiment.	45
4.4	End tools for the DPI experiment.	48
4.5	Correlation between strain rate and rotation.	49
4.6	Coefficient of friction calculation.	54
5.1	Schematic of the static mode DPI test.	60
5.2	Schematic of the dynamic mode DPI test.	62
5.3	Hot cracking of uncoated ceramics.	63
5.4	Thermal images of ceramic CT surface	65
5.5	Ceramic CT surface before and after dynamic DPI test	66
5.6	Ceramic HC surface before and after dynamic DPI test	67
5.7	Normalised titanium sample roughness versus sample sequence	68
5.8	Normalised titanium sample volume parameters versus sample sequence	69
5.9	Coefficient of friction comparison	72
5.10	Ceramic die design for validation test.	73
5.11	Ceramic die after SPF trials.	74
5.12	SEM images of uncoated ceramic CT tested under low pressure static mode DPI test.	76

5.13 SEM images of uncoated ceramic CT tested under high pressure static mode DPI test.	77
5.14 SEM images of ceramic die surface after SPF trials.	78
6.1 Coating deposition flow chart	82
6.2 Particle size distribution of the powder raw material	83
6.3 Firing cycle	85
6.4 XrD pattern of petalite coating	86
6.5 Coating deposition flow chart	87
6.6 Coating PET-A conditions before and after DPI test	87
6.7 Coating PET-B conditions before and after DPI test	88
6.8 Normalised titanium sample roughness versus sample sequence	89
6.9 Normalised titanium sample volume parameters versus sample sequence	90
6.10 SEM images of coating PET-A	92
6.11 SEM images of coating PET-B	93
7.1 Static mode DPI test outcomes of Coating F-50	98
7.2 Static mode DPI test outcomes of Coating JK-N8	99
7.3 Static mode DPI test outcomes of Coating F-40	100
7.4 Dynamic mode DPI test outcomes of all the coatings	102
7.5 Normalised titanium sample roughness versus sample sequence for coatings F-50, JK-N8 and F-40	103
7.6 Normalised titanium sample volume parameters versus sample sequence for coatings F-50, JK-N8 and F-40	105
7.7 SEM images of Coating F-50	107
7.8 SEM images of Coating JK-N8	108
7.9 SEM images of Coating F-40	109
7.10 Coefficient of friction comparison for coatings F-50, JK-N8 and F-40	111
8.1 Materials response to static mode DPI test	115
8.2 Control charts of surface roughness	117
8.3 Materials response to dynamic mode DPI test	118
8.4 Normalised titanium sample volume parameters versus sample sequence for coating F-50 without considering cracked area	121
8.5 COF from dynamic mode DPI test for all the tested materials	125
8.6 DPI test protocol	126

List of Tables

2.1	Superplastic properties of several titanium alloys	8
2.2	Summary of test methods.	23
2.3	Summary of pros and cons of each laboratory test.	24
2.4	Roughness amplitude parameters.	26
2.5	Roughness parameters.	28
4.1	Test rig tools design.	46
4.2	Key metrics evaluated.	50
4.3	SEM sample preparation procedure.	52
5.1	Test parameters of static mode DPI test.	60
5.2	Test parameters of dynamic mode DPI test.	62
5.3	Ceramic die roughness parameters.	74
7.1	Coatings technical properties.	97
8.1	Summary of wear mechanisms	120
8.2	Observations from SEM analysis.	123
A.1	CTE of zirconia, titania and Titanium alloy (Ti-6Al-4V)	135

Abbreviations

AFRC	Advanced forming research centre
ANOVA	Analysis of variance
COF	Coefficient of friction
CTE	Coefficient of thermal expansion
DPI	Die-part interface
EDX	Energy dispersive X-ray (spectroscopy)
FEA	Finite element analysis
FRRC	Fibre reinforced refractory castable
HP	High pressure
LAS	Ternary system lithia-alumina-silica
LP	Low pressure
MAS	Ternary system magnesia-alumina-silica
NASA	National aeronautics and space administration
NZP	Ceramic material $NaZr_2P_3O_{12}$
SEM	Scanning electron microscopy
SPF	Superplastic forming
TRL	Technology readiness level
WDS	Wavelength dispersion spectroscopy
XRD	X-Ray diffractometry or X-Ray diffractometer

Chemical formulas nomenclature

Al_2O_3	Aluminium oxide, alumina
BN	Boron nitride
B_2O_3	Boron oxide, boria
CeO_2	Cerium oxide, ceria
Li_2O	Lithium oxide, lithia
MgO	Magnesium oxide, magnesia
SiO_2	Silicon oxide, silica
SiC	Silicon carbide
TiO_2	Titanium oxide, titania
ZrO_2	Zirconium oxide, zirconia
Y_2O_3	Yttrium oxide, yttria

Chapter 1

Introduction

The research in this thesis concerns the development of a laboratory test that is able to study the interaction at the die-part interface during high-temperature forming processes. The following chapter introduces the technological background and the research project significance. In addition, the reader will find the aim and objectives of this work. The last part of the chapter presents the structure of the thesis.

1.1 Background and significance of the project

Superplasticity is a deformation mode associated with exceptional ductility that certain materials exhibit when deformed under specific strain rate and temperature. This phenomenon is widely employed in manufacturing processes such as superplastic forming (SPF), where a metal sheet is formed into a die at high temperature. Titanium alloys are commonly used in SPF for a wide number of applications for aerospace, chemical, automotive, biomedical and marine [1, 2]. SPF is an attractive manufacturing process due to the complexity of shapes that can be formed and low residual stresses induced in SPF formed parts [3].

SPF dies are commonly made of heat resistant nickel-chromium cast steels, but such materials are expensive and have very long manufacturing lead-time. The total time to design, cast, machine and polish a metal die is typically three to eight months [1, 4], which is a critical limiting factor for the improvement of the SPF process in mass production. Lutjering et al. [5] evaluated the cost of the SPF manufacturing process and identified the principal cost elements as the titanium sheet and the tool materials, which must withstand prolonged time at elevated temperatures.

Recently, high temperature steels are being challenged by emerging materials such as ceramic refractories, which present a lower production cost and exhibit shorter lead-time [6, 7]. Low-cost ceramic materials are being used by a number of companies in high-value aerospace tooling applications. These materials have the potential to revolutionise the

process economics of hot forming by reducing capital investment in existing processes and shortening lead times for new product/process development. Ceramic materials are brittle, but, as ceramic dies become more widely used, their design has been focused on enhancing the overall ductility and increasing their lifespan employing reinforced structures (particles, fibres or rods) [8, 7]. Consequently, brittle fracture is becoming a secondary issue to the failure mode of ceramic tooling; instead, die surface wear and spalling are still a major issue that reduces both die life and part quality, increasing process costs [9].

Ceramic wear mechanisms have been studied for several manufacturing processes conditions [10, 11, 12, 13], but limited work has been done to assess wear of ceramic dies under SPF conditions. This work addresses the lack of knowledge on wear mechanisms that take place on the ceramic die working surface during the SPF process, through the development of a laboratory test that simulates SPF conditions at the die working surface. The outcomes of this research work deliver scientific knowledge of the ceramic die wear mechanisms involved during the SPF process that are useful to prevent or retard brittle fracture of ceramic dies. In addition, the laboratory test methodology proposed in this thesis enables further research work on systematic testing of die materials and coatings combinations in order to generate a database of materials wear behaviour under SPF condition. Die design engineers can benefit from such outcomes during the material selection process, by determining the appropriate die material and coating for a sustainable wear ceramic die that can replace expensive metallic dies in the SPF process.

1.2 Aim and objectives

The SPF process, due to its features, is restricted to low volume and high cost products. This is a limitation for the development of new tool materials and tool improvements. Nevertheless, there is high interest from the manufacturers to decrease the cost of the overall process in order to extend it to further applications. The replacement of metallic with ceramic dies goes in that direction. In order to do so, it is crucial to know the wear mechanisms that occur on the ceramic surface during the SPF process. Thus, the aim of this work is to develop a laboratory test, which will assess the surface wear of ceramic materials under high temperature forming conditions. In addition, this test will be able to evaluate different protective coatings' performances.

The author, with this work, wants to fill the knowledge gap existing in surface wear testing of ceramic materials and coatings in order to get a better understanding of the interactions that take place during the SPF process at the die-part interface.

In order to achieve the project aim the author will:

Objective 1: Conduct a review of the testing methods available to characterise surface wear of ceramic materials;

Objective 2: Develop a laboratory test to assess coating performances and surface degradation and coatings performance under high temperature forming conditions;

Objective 3: Validate the developed laboratory test assessing different ceramic materials and protective coatings.

Further out-of-scope objectives have been identified, which are complementary to the objectives listed above:

1. Identify and down-select high-temperature resistant coatings for ceramic materials;
2. Demonstrate the efficacy of different protective coating materials with the developed test.

1.3 Structure of the thesis

This work is structured in nine chapters. **Chapter 2** gives an overview of the SPF process, materials and tools based on the literature. Furthermore, the chapter describes surface wear mechanisms of ceramic materials and experimental techniques for wear assessment.

Chapter 3 discusses the research methodology followed to achieve the aim and objectives. This chapter discusses the main research question regarding the laboratory test developed and the supplementary research questions regarding coating solutions.

Chapter 4 focuses on the developed laboratory wear assessment method. The chapter presents the materials and equipment employed to carry out the research work. Attention is paid on the test rig and its operating modes (static and dynamic).

At this point the work shows three studies where the developed test method is used to assess wear under SPF conditions. **Chapter 5** evaluates two different uncoated ceramic materials. The outcomes of the experiment are relevant for the selection of the ceramic material to employ for the protective coating studies. In addition, a comparative SPF trial have been conducted with a 200 ton SPF press.

From the literature review in chapter 2 an alumino-silicate coating material, made of petalite, has been selected to investigate its performance as protective coating for SPF ceramic dies. In **Chapter 6** the use of the developed test is employed to evaluate the optimal firing procedure of the petalite coating.

In addition, a market screening has been conducted to identify possible coating candidates that could be employed on ceramic SPF dies. Three coatings have been

selected, and in **Chapter 7** coating performance assessment is conducted under SPF conditions.

Chapter 8 gives a general discussion of all the results from chapters 5, 6 and 7. In addition, in this chapter the die-part interface protocol test is described: a guideline procedure developed from the experience on the conducted studies, which can be used to carry out future research on surface wear assessment of materials under SPF conditions.

The work ends with **Chapter 9**, where conclusions and suggestions for future work are made.

Chapter 2

Literature review

This chapter identifies the requirements for an SPF die wear assessment. The first section focuses on the superplastic forming process, its requirements and materials involved, paying more attention to titanium alloys as the metal forming parts and ceramic materials as dies. The chapter moves into the discussion of surface wear mechanisms of ceramic materials. The chapter then deals with the state-of-the-art test methods employed to assess wear of surfaces under high-temperature forming conditions, in order to identify a suitable laboratory method to assess wear on SPF ceramic surfaces. The last part of the chapter is dedicated to protective coatings and release agents available for SPF ceramic dies.

2.1 Superplastic forming

Superplasticity is a phenomenon observed in certain materials where they exhibit exceptional ductility when deformed under defined conditions. Superplasticity is commonly referred to as ductile tensile behaviour of the material; however, superplastic deformation is manifested also under compression deformation [14, 15]. Superplastic metals typically present tensile elongation from 200% to 1000% [16], and under certain conditions elongation can reach up to 5000% [17]. Elongations of this magnitude are more common with plastic materials rather than metals; while considering formability of metals, ductility is a limiting factor of sheet forming process capabilities, thus superplasticity is a significant advantage for metal forming processes. Figure 2.1 shows some typical structures made with the SPF process.

2.1.1 Requirements for superplasticity

In order to understand the SPF process, it is necessary to review the superplastic behaviour of materials. The material grain structure is determinant for the achievable

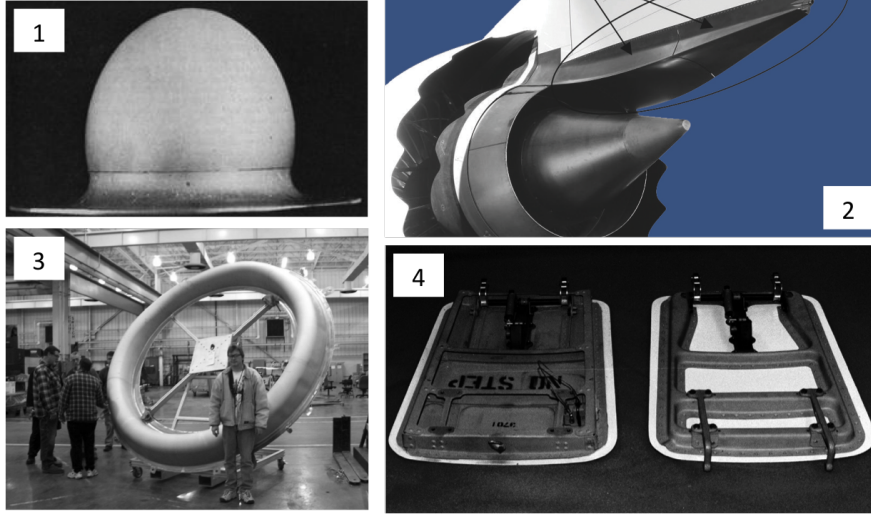


Figure (2.1) Typical structures made with the SPF process: the fist superplastically formed bubble in 1964 (1) from [18]; a heat shield assembly (2) from [19]; a nacelle inlet superplastically formed (3) from [20]; in (4) a traditional access door on the left and a simpler assembly made of superplastically formed 7475 aluminium [7].

tensile elongation and the superplasticity involved refers to the micrograin superplasticity [21, 22]. The basic requirements to observe micrograin superplasticity are:

- Ultrafine grain size material ($10 \mu\text{m}$ or finer),
- Relatively high temperature ($\geq 0.5 T_m$), and
- Controlled strain rate (10^{-5} to 10^{-3} s^{-1}).

Only a limited number of alloys available in the market exhibit superplasticity. However, research effort has been spent to develop new superplastic materials, and an increasing number of alloys have been grain-refined to induce the superplastic effect [23].

2.1.2 Characteristics of superplastic metals

The superplasticity of metals under tensile test can be observed above a temperature value, which depends on the material. The superplastic forming behaviour of materials can be described as a non-Newtonian viscous flow. Such materials' flow stress, σ , can be described with the constitutive equation [16, 24, 25]:

$$\sigma = K\epsilon^n\dot{\epsilon}^m, \quad (2.1)$$

where K is a constant, ϵ is the strain, $\dot{\epsilon}$ is the strain rate, n is the strain hardening

parameter and m is the strain rate sensitivity index, defined as:

$$m = \frac{\partial \ln(\sigma)}{\partial \ln(\dot{\epsilon})}. \quad (2.2)$$

Equation 2.1 is also known as the Norton-Hoff power law relationship between Cauchy stress, σ , strain ϵ and equivalent strain rate $\dot{\epsilon}$. The strain-rate sensitivity (m) of a material determines the forming capability in the SPF process, where the control of forming process parameters become significant for obtaining the full potential of this class of material, thus the process control behind SPF is more demanding than in conventional forming processes (process temperature and material strain rate sensitivity have a major impact on the achievable elongation). However, SPF's unique capability of fabricating complicated components in a single steps offers great advantages for several applications.

2.1.3 Superplastic alloys

The grain size requirement for a metal to be superplastic restricts the number of commercially available alloys that exhibit this characteristic. Several materials have been produced in laboratories, but very few of them are available in the market [22]. As SPF technology improves, the process has been employed not only for aerospace and architecture but as well in automotive. The most common materials are aluminium, titanium and magnesium alloys [20, 23]. This work is restricted to the application of the SPF process with titanium alloys. Future work might extends this investigation to other superplastic materials.

2.1.3.1 Ti-6Al-4V

Titanium alloy Ti-6Al-4V is extensively used in engineering and, according to Ghosh and Hamilton [26], it covers approximately 60% of total titanium production while unalloyed grades constitute approximately 20% of production and all other alloys constitute the remaining 20%. The selection of the alloy type and grade depends on desired mechanical properties, forming process employed, service requirements and cost. Table 2.1 summarises the most common commercially available superplastic titanium alloys.

Ti-6Al-4V is a unique alloy regarding oxygen and nitrogen solubility at the interstitial positions. This solubility makes possible a particular bonding technique, so called diffusion bonding. However, its solubility creates problems that are not of concern in most other metals when heated in air. The interstitial solubility of oxygen results not only in a common surface oxidation, but in solid solution hardening of the surface (alpha-phase), which reduces fatigue strength and ductility [16], therefore this layer has

Table (2.1) Superplastic properties of several titanium alloys [26].

Titanium alloy	Test temperature (°C)	Strain rate (s^{-1})	Strain-rate sensitivity	Elongation (%)
<i>α/β</i>				
Ti-6Al-4V	840 - 870	1.3×10^{-4} to 1.3×10^{-3}	0.75	750 - 1170
Ti-6Al-5V	850	8×10^{-4}	0.70	700 - 1100
Ti-6Al-2Sn-4Zr-2Mo	900	2×10^{-4}	0.67	538
Ti-4.5Al-5Mo-1.5Cr	871	2×10^{-4}	0.63 - 0.81	>510
Ti-6Al-4V-2Ni	815	2×10^{-4}	0.85	720
Ti-6Al-4V-2Co	815	2×10^{-4}	0.53	670
Ti-6Al-4V-2Fe	815	2×10^{-4}	0.54	650
Ti-5Al-2.5Sn	1000	2×10^{-4}	0.49	420
<i>β and near β</i>				
Ti-1.5V-3Cr-3Sn-3Al	815	2×10^{-4}	0.5	229
Ti-13Cr-11V-3Al	800	<150
Ti-8Mn	750	...	0.43	150
Ti-15Mo	800	...	0.60	100
<i>α</i>				
CP Ti	850	1.7×10^{-4}	...	115

to be removed before parts are put in service.

2.1.4 Superplastic forming processes

Superplastic alloys have been employed in several sheet metal forming processes, and the superplastic forming processes can be divided into two main families, which are:

- Single sheet forming, and
- Multi-sheet forming/diffusion bonding.

In the following sections these techniques will be discussed.

2.1.4.1 Single sheet forming

During single sheet forming a gas pressure is imposed on the metal sheet, causing the material to deform into a die configuration. The applied pressure is usually in the range of 0.7 to 3.4 MPa [27], and for some shapes the pressure can reach values up to 7.0 MPa [28]. The single sheet forming method is illustrated in Figure 2.2, which shows a cross section of the dies and forming sheet. Dies and sheet material are normally maintained at the forming temperature, and the gas pressure is imposed over the sheet, causing the sheet to form into the lower die; the gas within the lower die chamber is

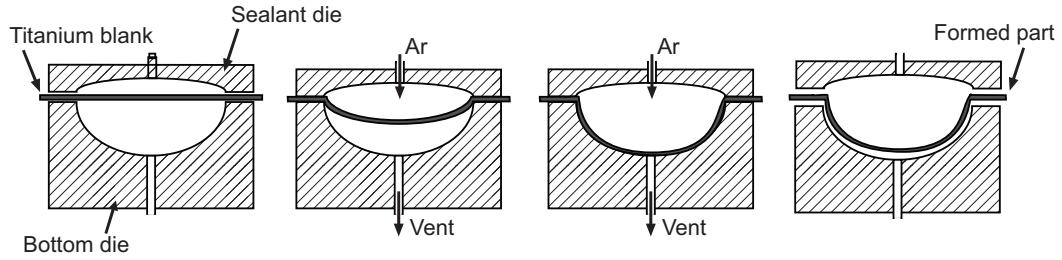


Figure (2.2) Schematic representation of single sheet forming process. The blank is loaded onto hot dies and clamped with a top die. The blank is then heated to the superplastic temperature (depending on the blank material). The inlet valve on the top die allows the introduction of an inert gas (such as argon). Controlling the gas pressure it is possible to regulate the blank superplastic deformation and strain rate [26].

simply vented to atmosphere. The lower die chamber can also be held under vacuum, or a back pressure can be imposed to suppress cavitation if necessary [16]. The gas flow is controlled such that the induced strain rate in the forming sheet is maintained in the superplastic range and the rate of pressurisation is nowadays determined by finite element simulations citeNazzal2004,Sorgente2010. This pressure is generally applied slowly, avoiding abrupt pressure changes, in order to prevent rapid strain rate that may damage the forming part. The periphery of the sheet is held in a fixed position and is dimensioned to be large enough to give space to a seal bead, which prevents the sheet from slippage and draw-in and to form a gas-tight seal in order to avoid leakage of the forming gas. Therefore, the sheet alloy stretches into the die cavity, and almost all the material is used to form the part. The finished part shows considerable gradients in thickness for complex and deep-drawn parts.

This process has been widely used to fabricate structural parts from titanium alloys, aluminium alloys and other metals. Large and complex parts can be readily formed, therefore, single-sheet superplastic forming is considered a near net-shape manufacturing process. Multiple parts can be formed in a single process cycle; it has no moving die components and it does not require mated dies.

2.1.4.2 Multi-sheet forming/diffusion bonding

Multi-sheet forming/diffusion bonding process, also known as SPF/DB, is a unique process that combines the characteristics of SPF process with the ability of some materials to bond through material diffusion at a certain temperature. The SPF/DB process evolved as natural combination of SPF and DB, as the process requirements (temperature and pressure) are similar [29]. The SPF/DB process can be done with two or more

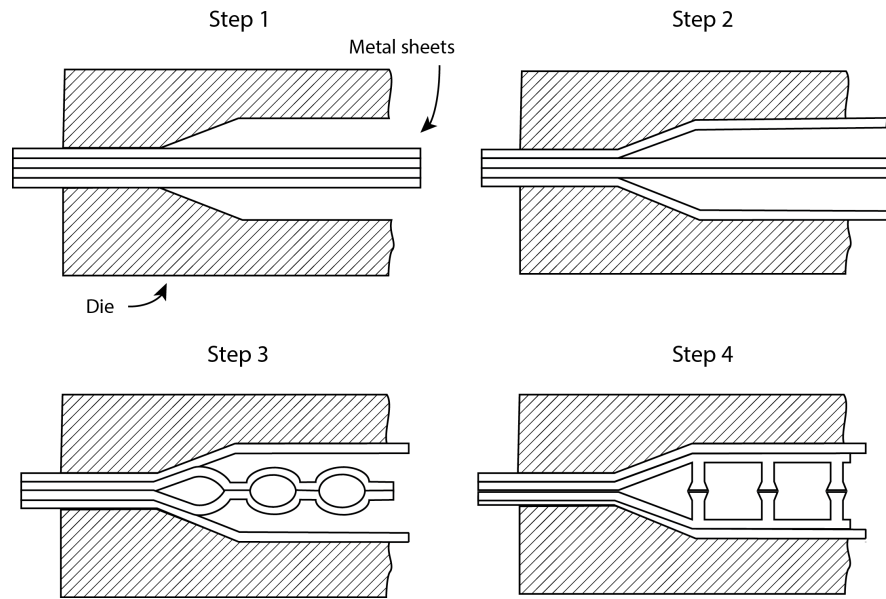


Figure (2.3) Schematic representation of multi-sheet forming/diffusion bonding process from [16].

metal sheets. A sandwich structure is formed with the SPF/DB process, as showed in figure 2.3, increasing the mechanical properties of the final part, reducing weight [26].

Different techniques have been employed to achieve diffusion bonds in predetermined localised regions of the metal sheet. One of these involves the use of stop-off material between the sheets in the selected areas where no bonding is required. The selection of stop-off materials depends on the alloy being formed and the process temperature. Common stop-off materials for titanium alloys are yttria (Y_2O_3) or boron nitride (BN).

2.1.5 Superplastic forming equipment and tools

The superplastic forming method is different from more conventional sheet forming processes. The forming environmental conditions are also different, which determine the selection of equipment and tooling materials.

2.1.5.1 Forming equipment

In the superplastic forming process there is a need to constrain the forming tools in order to counteract the forming gas pressure. Moreover, a seal is required at the interface between sheet and tool around the periphery to prevent forming gas leakage. A press is typically employed to fulfil these process requirements. Hydraulic presses and mechanical clamping systems have been employed in superplastic forming [16]. The hydraulic press can be loaded and unloaded rapidly, but it requires a significant capital investment. The mechanical clamping systems are cheaper, but slower to load

and unload. In higher volume manufacturing plants robotic systems are commonly used to aid the loading and unloading of parts, especially in high-temperature superplastic forming operations, such as titanium alloys. The heating system is tailored to the process temperature required and the allowable thermal gradients. In general electrical heating is employed, in which resistance heating elements are embedded in plates placed between the tooling and the press platens.

2.1.5.2 Tooling materials

Superplastic forming tooling is generally heated to the forming temperature, which is in the range 850°C - 950°C for Ti-6Al-4V, and subjected to internal gas pressure and pressing clamping loads. More crucial are the clamping loads and thermal stresses encountered during heat-up and cool-down and the environmental conditions at forming temperature. Thermal stresses can cause permanent distortions in the die, which are avoided by selection of good strength and creep resistance materials at high temperature. Low thermal expansion materials are preferred for high temperature processes. Furthermore, materials that do not show phase transformation during heating and cooling are desirable.

The environmental conditions during the superplastic forming of high-temperature metal sheets can be critical. Oxidation can alter tooling surface and affect the surface quality of formed parts. The compatibility between the superplastic sheet, the releasing agent and the tool is important as well. Chemical interactions can arise at the interface tooling/sheet, above all when working with reactive materials such as titanium alloys, resulting in degradation of tooling working surface and formed part. Generally, material with low solid solubility with the sheet are good candidates for compatibility.

A variety of materials have been employed for SPF tooling, including metals and alloys, ceramics and graphite [30]. Numerous metallic alloys have been developed over the years to be suitable to the SPF environment [31]. Metallic dies are generally part of the family Ni-Cr-Fe heat resistant cast steel. Die manufacturers, where the most recognised are *Aubert & Duval* (France), *Cronite* (UK) and *RTI International Metals* (USA), have carefully selected alloy composition in order to offer an optimal compromise between manufacturing, performance and cost. Crucial factors of the die composition design are the material castability, machinability and weldability [32]. Metal tools are preferred for large production quantities, such as 100 parts or more. Graphite tools are suitable for approximately 100 parts, although graphite involves cleanliness issues in workshops. Ceramics can be cast into the desired shape and are therefore inexpensive for a variety of large parts, although their brittle nature implies the use of ceramic tools for prototypes or small production quantities, usually in the order of 10 parts.

Ceramic dies For certain applications metallic dies suffer some limitations due to long lead times and high non-recurring costs. Various works have been conducted to develop SPF ceramic dies as a cheaper alternative to metallic dies for prototyping and for small series and low-rate production [7, 32]. Non-reinforced ceramic dies are employed in the field of SPF for medical and dental prostheses [33, 34, 35]. Reinforced ceramics have been developed for the shaping of titanium aeronautical parts. Two strategies have been developed for reinforced ceramics:

- Macro-scale reinforcement, and
- Micro-scale reinforcement.

Macro-scale reinforcement has been developed by the Boeing Company and it is obtained by adding high-strength fused silica rods, which are cast directly into the ceramic aggregate [7, 36]. The rods are placed in specific positions of the die, depending on its shape, in order to diminish twisting and deflection loads. The die life of such stand-alone dies is substantially increased with this technique [36].

Micro-scale reinforcement has been studied in the last fifteen years by several research groups. At the *Research Centre on Tools, Materials and Processes of Ecole des Mines d'Albi* a reinforced ceramic has been studied, where the addition of short metallic fibres improved the ceramic die ductility, which have been named fibre reinforced refractory castables (FRRC) [37, 6, 4, 8]. The inclusion of fibres on the ceramic matrix induce a quasi-ductile behaviour, in which the load is transferred to the fibres when brittle matrix cracks.

Different approaches have been developed to enhance ceramic ductility. However, little has been done in the past years to overcome the surface degradation of SPF ceramic tools. Boeing has developed a cordierite-based ceramic glaze coating that can be plasma sprayed onto the ceramic die surface to generate a protective shell [38], while Aurok Company is trying to develop suitable protective coatings for FRRC dies [32].

2.2 Surface wear of ceramic

In order to understand the wear mechanisms that take place at the die surface, this section discusses the surface wear of ceramic materials. Ceramic materials are inorganic, non-metallic materials. Ceramic materials can be crystalline or partially crystalline, and they exhibit high stiffness, high strength, especially under compression loads, and great chemical and thermal stability. On the other hand, due to the nature of the covalent chemical bonds in the material, ceramic materials are brittle, thus material strength is determined by initial crack concentration, which depends on the manufacturing process

[39]. Dislocation mobility is almost negligible in ceramics, which affects the poor plasticity of this class of material. Porosity created during the manufacturing process is the main cause of initial crack generation, which affects the mechanical performance [39].

Wear is the term referred to the erosion of material from the original position in a solid surface generated from the interaction with another surface [40]. The complex nature of wear can be divided into different mechanisms:

- Adhesive wear;
- Abrasive wear;
- Surface fatigue;
- Fretting wear; and
- Erosive wear.

The list is not exhaustive, as different wear mechanisms can be found in the literature, such as cavitation, corrosive and diffusive wear [41]. The listed wear mechanisms are not mutually exclusive, thus the overall surface wear can be the result of different wear mechanism contributions.

In SPF ceramic dies, the main contribution to the surface damage is due to adhesive wear, oxidation and chemical interaction between ceramic and titanium alloy blank [32]. During the SPF process the titanium sheet slides on the die surface, thus in the following sections adhesive wear during sliding will be discussed. In addition, attention will be paid to surface damage characterisation and diagnosis, and the last section focuses on friction properties of ceramic materials.

2.2.1 Sliding and adhesive wear

Sliding and adhesive wear refer to types of wear generated by the sliding of one solid surface along another surface. Adhesive wear is as ambiguously defined as is sliding wear, although the two are not synonymous. Adhesive wear denotes a wearing action in which no specific agent can be identified as the cause of wear [40]. The study of wear aims to identify and to define the specific wear modes in order to find ways to prolong the wear life of sliding systems. Each wear mechanism can be contrasted by proper choice of material, surface specifications, lubricant and method of operation.

When studying sliding surfaces, they are generally considered clean and dry. In the real world, such surfaces are far from perfectly clean, and even if they were cleaned before any operation, they become inevitably contaminated by the atmosphere. Standard conditions of work can be defined for the three classes of materials:

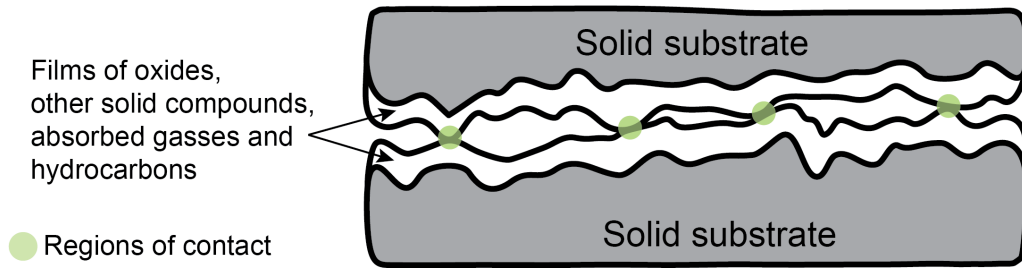


Figure (2.4) Schematic of two sliding solid surfaces with adsorbed films. When rough surface are put into contact, the actual contact occurs only in a few isolated regions [40].

- Metals will usually be covered with a oxide film and adsorbed gases and hydrocarbons;
- Polymer surfaces may contain absorbed water, mould release agents, adsorbed gases and hydrocarbons;
- Ceramics will be covered with absorbed gases, hydrocarbons and water; in addition, non-oxide ceramics may oxidise.

The thickness of the adsorbed layers is of the order of dozens of nanometers. The presence of these films may affect the bonding of sliding surfaces. Furthermore, variations in the thickness and properties of these films is one major reason for the very wide range of friction data reported for all materials [40]. When two surfaces slide against each other (cf. Figure 2.4), adsorbed films will be in contact and interact each other. If the contact pressure is high, a solid layer may fracture and expose substrate material. Small regions of both substrate materials may come into contact and bond together.

At the points of substrate-to-substrate contact, the bond strength depends on the materials. Identical metals bond together when the bond strength is near the strength of the metals. Dissimilar metals will bond with less strength at the beginning, but the bond strength will increase with time, according to Fick's diffusion laws [42]. Ceramic materials will bond very well if the atomic lattices are well aligned. The bond strength depends on the lattice dimension match. Oxides, sulphides and other compounds that are usually present in the adsorbed layers are generally ionic or covalent structures.

Conformity of contacting surface is also a factor to take into consideration when studying adhesion. Ductile materials conform somewhat via plastic deformation, unlike brittle materials that do not conform. Furthermore, sliding adds shear stress to any normal stress imposed, increasing the probability of plastic flow and fracture of materials

in the contact regions. The sliding generates a layer of mixed substances, some of which will fall out as wear debris, some others remains on one of the two sliding surface as a transfer film. The properties of the mixed film depend on the contacting bodies, the temperature, the chemical reactivity and many other parameters.

2.2.2 Surface damage

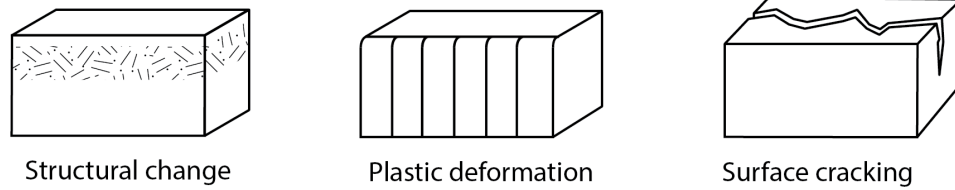
Surface damage can be defined as topographical or microstructural changes, or both, in a surface layer. Surface damage in tribosystems can be generated in many consecutive small steps, but several micromechanisms are active at the surface. The observed damage is then the cumulative effect on a macroscale of micromechanisms. The topographical approach is based on a direct classification of surface damage features rather than on the more traditional classification made considering wear mechanisms that are active producing the damage.

2.2.2.1 Surface damage types

Damages on a surface can be classified in different types (cf. Figure 2.5), and generally the pattern of the damage is a combination of them [43]. Therefore, the examination and interpretation may be difficult, but the classification illustrated in figure 2.5 is useful to explain surface wear and damages. The surface damage comprises damage without and with exchange of material. The surface damages that do not imply exchange of material arise when either a structural change, a plastic deformation or a surface cracking takes place. The surface can be damaged after structural changes, such as ageing, tempering, phase transformations or recrystallisation. Furthermore, plastic deformation can cause surface damage. When surface cracking takes place, the damage is caused by excessive local contact load or cyclic variations of thermally or mechanically induced strains. The surface damages that imply exchange of material can involve loss or gain of material. When loss of material takes place, material is removed from the surface behind wear scars of various shapes and sizes. Fundamental elements in the process of material removal can be shear fracture, extrusion, chip formation, brittle fracture, fatigue fracture, chemical dissolution and diffusion. When surface damage involves gain of material, particles are transferred on the surface from the countersurface.

Surface damages are normally a combination of different types of damage, which means that several mechanisms are involved simultaneously during wear. The overlapping mechanisms interact during surface operation, mutually increasing the effect of one another, as for example in high-temperature erosion where simultaneous corrosion and wear are involved. The oxidised layer is more prone to erosive wear, which in turn increases the oxidation rate by exposing new metallic surface to the atmosphere.

Surface damage without exchange of material



Surface damage exchanging material

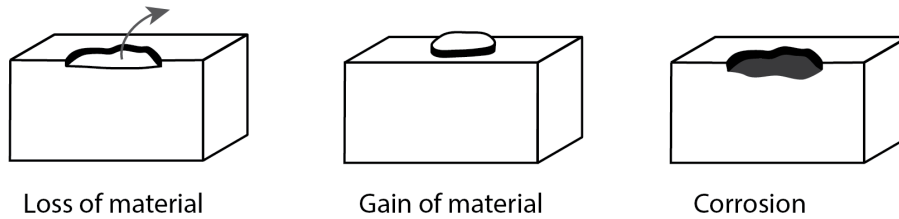


Figure (2.5) Classification of surface damage [43].

Occasionally the combined effect can result in a reduction of the damage effect. One example of such a counteractive interaction is the suppression of severe adhesive wear of metals in sliding contacts by the formation of an oxide layer the oxide layer reduces the adhesive forces between the sliding bodies, which diminishes the probability of shear fracture of the metal surfaces. In favourable cases, the friction is reduced and the adhesive metallic wear is replaced by a mild wear of the slowly growing oxide layer.

2.2.2.2 Diagnosis of surface damage

For a better understanding of surface damages, topographical study of the surface should be supplemented with microstructural studies on cross sections [40]. The structure and the composition of the damaged surface layer are often very different from those of the virgin surface.

Tribographical studies of a damaged surface can identify the type of damage which sets the life limit criterion. It is important to take into consideration the type of problem the damage is causing and the effect of a certain type of damage on the surface performance. In the next paragraphs the different surface damage modes of interest for ceramic materials will be discussed.

Damage dominated by brittle fracture. Hard and brittle materials such as ceramics, ceramic coatings, cemented carbides, cermets and hardened steels often shows

brittle fracture as a mode of surface failure. The crack is generally initiated in localised areas of the surface where the tensile stresses are concentrated and exceed the fracture stress limit of the surface material. The type of damage can vary from a relatively large scale fracture to fragmentation on the microscale [43]. Cracks can be generated by scratching of abrasive particles, which may come off the surface. In addition, brittle fracture is often associated with very high wear rates [43]. To prevent high tensile stress concentrations, high point loads should be avoided, and in sliding contact this can be achieved using smooth surfaces and rounded shapes. Furthermore, the presence of large abrasive particles should be avoided. Differently from ductile materials, once the surface of brittle materials has been damaged, the tribological response is most unlikely to be re-established, even reducing the load.

Damage dominated by fatigue fracture. Surface fatigue fracture is generated by repeated unidirectional or reciprocal sliding and it is often shown by the same types of materials that suffer brittle fracture [43]. Hardness, toughness and the coefficient of thermal expansion are the major material properties that have an effect on fatigue fracture. Fatigue fracture can be avoided in sliding surfaces by reducing the shear stresses using an efficient lubricant or by promoting friction-reducing layers at the surface.

Surface damage involving gain of material. Transfer of material from one surface to the other, during sliding, occurs frequently. Generally, the added material may:

- Clad to the surface;
- Become embedded in the surface; or
- Successively build up a layer on the surface.

Transferred material may be either detrimental or favourable to the overall performance of the sliding system. In some cases the added material acts as protection from wear of the working surface.

2.2.3 Friction and wear of ceramics

Ceramics, which are inert non-metallic materials, and cermets, which are metallic bonded ceramics, have been widely employed for tribological purposes although their high manufacturing costs have limited their applicability to special applications, such as high-temperature or corrosive environments. Ceramic products can be divided into two classes, depending on their application, properties and manufacturing process:

- Fired clays consisting primarily of small crystals of hydrated aluminosilicates; or

- Advanced ceramics which are pure dense oxides, nitrides, carbides and borides.

Ceramic dies are part of the class of fired clays. The high-tech products are used in tribological applications. Whereas the fired clays consist of a glassy matrix, while the high-tech ceramics are crystalline high density and high purity materials, with very little, if any, glassy binder. Traditional ceramics have 5 to 15% porosity, while high-tech ceramics present less than 0.5% porosity [44].

Ceramics can wear by chipping, due to their brittleness. Surface and subsurface cracks form small chips of material and a fine powder is produced as this wear debris grows up during the wear process. Ceramic materials are sensitive to any high contact stresses that contain tensile components. Ductile materials, like metals and plastics, can deform plastically to relieve high contact stresses before fracturing. Ceramic plastic deformation is very small, when compared with ductile materials.

Increasing the temperature of a ceramic material to about 0.6 times the melting point, T_m , increases the mobility of dislocations and increases the potential for plastic deformation. Strength reduction and increased creep rates also accompany the rise in temperature. However, the increase in plasticity with increase in temperature does not produce the ductility that is common in metals: either a brittle or semi-brittle behaviour persist [44].

During sliding of surfaces, brittle materials can show abrasion or erosion wear mechanisms. The wear behaviour is very different, but both these processes involve tensile components in the contact state of stress. For abrasive wear, the wear rate is proportional to the elastic modulus and inversely proportional to hardness and fracture toughness. However, it has been shown that alumina and silicon carbides also exhibit a sensitivity to microstructure during wear by scratch tests [45]. The grain size and properties of the intergranular material were found to influence wear.

Ceramic materials are sensitive to strain rate, exhibiting an increased tendency to crack when increasing the sliding velocity. In addition, ceramics are sensitive to impact, which makes them vulnerable to erosive wear. The relative hardness of ceramic and eroding material is crucial for the erosion mechanisms. When the eroding is softer or about the hardness of the ceramic, a small increase in the eroding hardness causes a large increase of erosive wear. When the eroding is much harder than the ceramic, microstructure and fracture roughness become more important to the rate of erosion [46]. Hard ceramics will resist particle erosion of soft eroding; when the eroding hardness become harder, then the erosion rate can be minimised by increasing ceramic toughness, through small grain size and minimising porosity.

2.3 Wear assessment

This section focuses on the state-of-the-art of available testing and characterisation techniques to assess wear of ceramic surfaces, preferably under SPF conditions. The purpose of this thesis is to select, or develop, a test method for the wear assessment of ceramic surfaces under SPF conditions.

The next section focuses on the different laboratory testing techniques that try to simulate wear conditions at high temperature and/or under sliding for metallic and/or ceramic materials. In addition, section 2.3.2 addresses the characterisation techniques that are usually employed to identify and study surface wear and damages. The last section summarises the findings and states the requirements of the test method that has been developed for this research purpose.

2.3.1 Laboratory testing

During the SPF process different interactions take place between the die and the metal sheet, such as adhesion, mechanical interaction of surface asperities, ploughing of one surface by asperities on the other, deformation and/or fracture of surface layers [47]. These interactions will usually occur simultaneously but they may arise in different areas of the die. In the superplastic forming process the sheet is clamped along the border of the die while the rest flows into the die cavity, driven by gas pressure. Considering the die working surface, we can identify three most significant regions of die-blank interaction, summarised in Figure 2.6:

- Sealing regions: wear is mostly denoted by adhesion of die-blank;
- Sliding regions: wear is characterised by the sliding on the die surface of the blank that is superplastically deforming; and
- Corner regions: wear is defined by both adhesion and mechanical interaction blank-die surface.

A multitude of tests have been developed to evaluate die-blank interaction in metal forming [47, 48, 49], although only a few of them have been applied to simulate hot forming processes such as SPF [50]. In fact, very little has been done on the wear assessment of ceramic dies during hot forming processes [51]. The outcomes of a systematic review of tests available, which have been applied, or can be applied, to evaluate ceramic die wear under hot forming conditions are summarised below.

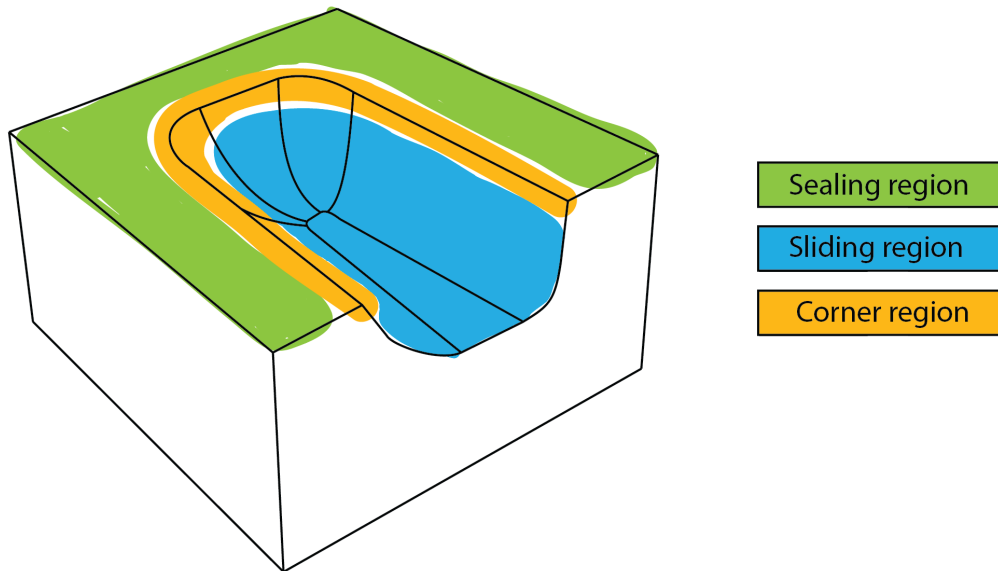


Figure (2.6) Schematic representation showing the interactions that dies undergo during the SPF process depending on the die area in consideration.

2.3.1.1 Strip drawing test

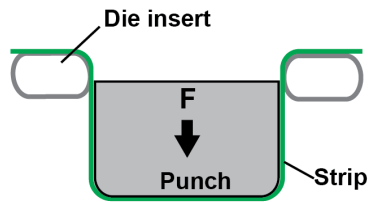
The strip drawing test, shown in Figure 2.7, is a tribology test employed in sheet metal forming to check friction conditions between two moving surfaces in contact. A sheet metal sample is pulled over a surface that simulates the geometry of the die. The test is usually performed to simulate the drawing process. It is usually performed to evaluate lubricant and coating for the contact area between tool and metal sheet at a deformation rate representative of the forming process [52, 53, 54, 55]. This type of test has been performed with varying strain rate, temperature and geometry of the contact surface and it is employed to study the effect of these parameters on the coefficient of friction for aluminium alloys at temperature up to 500°C [47].

This method's strengths are the stretching of the metal sheet during testing, the different geometries employable and the strain control. The strip drawing test is effective in simulating die's corner areas during a forming process, but its ability to simulate other die's areas is limited due to the test layout.

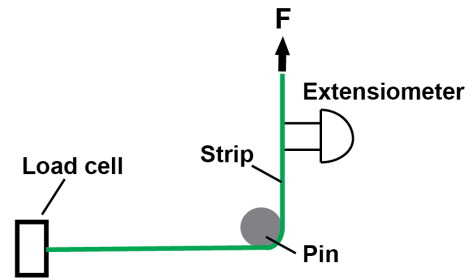
2.3.1.2 Draw bending test

Similar to strip drawing, the draw bending test is based on the drawing process of metal sheet. The draw bending test can be carried with several configurations, such as stretching strips of metal around pins [49, 53], stretching under bending (c.f.

Strip drawing test

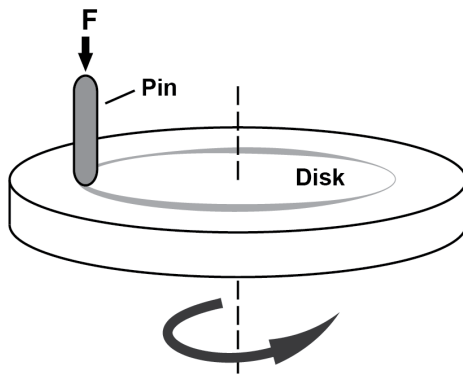


Draw bending test

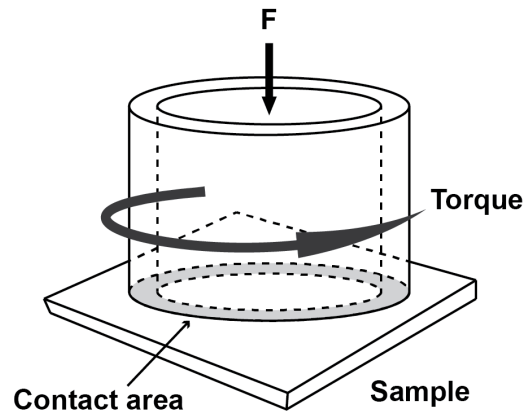


L-configuration

Pin-on-disk test



Twist-compression test



Ford test

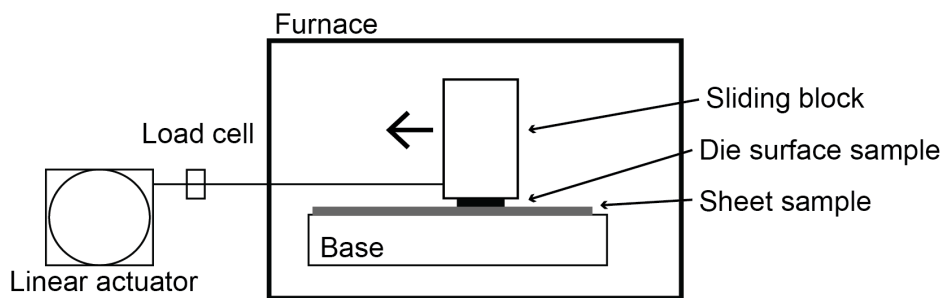


Figure (2.7) Schematic representation of the test techniques identified: strip drawing test, draw bending test, pin-on-disk, twist-compression test and Ford test.

Figure 2.7) [56] and bending under tension [48]. The test is employed to check friction between metallic dies and aluminium sheets [57]. In addition, all the tests in literature are conducted at room temperature, which is a weakness for our purpose.

2.3.1.3 Pin-on-disk test

This technique, shown in Figure 2.7, is widely employed for friction measurement of different materials. It consists on a rotating disc and a pin pushed onto the disc surface with a controlled load. Pressure of the pin and velocity of the disc are the controlled parameters. Pin-on-disk testers are available at operative temperature up to 1000°C [51, 58, 59, 60]. The apparatus allows acquisition of friction coefficient, and disk and pin analyses are employed for the evaluation of wear scars through SEM and profilometry.

With pin-on-disk it is possible to test wear of ceramic against metallic materials at temperature up to 1000°C, controlling the pressure and the rotation speed. In addition, the test gives information regarding friction coefficient and wear rate. A limitation of this method is that the superplastic alloy is not stretched during the test and sliding occurs repeatedly over the same location, which is not a proper representation of the SPF process.

2.3.1.4 Twist compression test

The twist compression test, shown in Figure 2.7, consists of a rotating hollow cylinder tool pressed against a fixed sheet metal specimen while pressure load and torque can be measured to extrapolate friction coefficient. The circular wear track left on the cylinder and on the metal specimen is used to determine wear rate. The twist compression test has been employed to measure die-part interface frictional response under cold forming operations [61, 62, 63, 50], but the torsion-compression state can be adapted to simulate the sliding of metal sheet on the die during SPF.

2.3.1.5 Ford test

Friedman et al. [64] developed at Ford Motor Company a method to evaluate coatings and lubricants performance for aluminium alloys SPF dies. The test is based on measuring the force required to pull a test block with a specific surface over a sheet sample. The system is placed in a furnace and a linear actuator, with a load cell, are placed outside the furnace and linked with the sliding block through a pull rod. This method is typically used for the estimation of friction coefficient. In addition wear traces can be studied on both the titanium and die samples.

Table (2.2) Summary of the identified test method employed to determine wear and friction in sheet metal forming.

Wear tests	Strip drawing	Draw bending	Pin-on-Disk	Twist compression	Ford test	Required test
General application	Wear and friction in deep drawing, quick plastic forming of Al alloys	Wear and friction in stretch forming, deep drawing of Al alloys	Tribology of surfaces during sliding against alumina or diamond	Lubricants performances	Friction between metallic die and sheet metal	SPF ceramic die surface wear
Testing temperature	Up to 500°C	25°C	Up to 1000°C	Up to 1000°C	500°C	Above 850°C
Testing atmosphere	Qir, nitrogen or argon	Air	Air (most common) or nitrogen	Air	Air	Air or argon
Plastic deformation of sample	Yes	Yes	No	No	Yes	Preferable
Sample displacement	Stretching and/or bending of sample	Stretching and/or bending of sample	Rotation against tool	Rotation against tool	Linear	Not relevant
Material of tools	Metal against metal	Metal against metal	Metal, ceramic or polymer against alumina or diamond	Metal against metal	Metal against aluminium alloys	Ceramic against titanium alloys
Geometry of tools	Strip surfaces	Pin or cylinder	Pin or sphere	Hollow cylinder	Flat	Flat

2.3.1.6 Test methods comparison

A number of standard methods for wear and friction measurement have been reviewed and their characteristics are summarised in table 2.2. These tests are employed to estimate wear and friction behaviour between surfaces. The identified standard tests have some drawbacks as they are often poorly correlated to true wear conditions that occurs during the SPF process of titanium alloys. These tests can take into consideration few parameters at a time, such as fixed or limited tool size or real surface contact situations (a strip, a pin or a ball). The scope of this research work is to implement a test method that is able to evaluate die-blank interaction under high-temperature SPF conditions.

Five testing techniques have been identified and described above. Table 2.3 summarises the pros and cons of each testing method considering the characteristics of the SPF process described in section 2.1.

Table (2.3) Summary of pros and cons of each laboratory test.

	Pros	Cons
Strip drawing	<ul style="list-style-type: none"> • Stretching of metal sheet • Different geometries • Strain rate control 	<ul style="list-style-type: none"> • Only friction measurement • Up to 500°C • Test only representative of corners • Test only metal against metal
Draw bending	<ul style="list-style-type: none"> • Stretching of metal sheet • Strain rate control 	<ul style="list-style-type: none"> • Test at room temperature • Test only metal against metal
Pin-on-disk	<ul style="list-style-type: none"> • Test ceramic against metallic • Pressure control • Rotation speed control • Friction measurement and wear characterisation 	<ul style="list-style-type: none"> • No stretching of metal sheet • For prolonged cycles • Not really representative of the stresses at the die-part that occurs under SPF process
Twist compression	<ul style="list-style-type: none"> • Pressure control • Rotation speed control • Friction measurement and wear characterisation 	<ul style="list-style-type: none"> • No stretching of metal sheet • Test at room temperature
Ford Test	<ul style="list-style-type: none"> • Friction measurement of sliding surfaces • Linear speed control 	<ul style="list-style-type: none"> • Limited pressure control

The table shows that most of the tests are poorly correlated with the real conditions experienced at the interface ceramic die-titanium part. None of the tests available is truly representative of the SPF process because they have been either employed at lower temperature or with metallic dies, or different part material. Starting from the pros and cons of the available tests, a new test should be developed to simulate the real SPF conditions at laboratory scale. The new test method should be able to investigate, and better understand, the interaction of ceramic die-titanium part under SPF conditions.

The test should be able to simulate the most significant regions of SPF die-part interaction: the sealing region; the sliding region and corners and edges. Ideally, the test should be able to assess wear of ceramic tools against titanium alloy samples at temperature of 900°C or higher, under a controlled strain rate. In addition, this laboratory test should be able to identify die surface damages in-situ, in order to be able to quickly identify ceramic die failure when transferring this technology into manufacturing. Furthermore, the test should be able to give more information about the friction

at the ceramic surface, which can be beneficial for finite element simulations.

2.3.2 Laboratory characterisation techniques

Many techniques for the measurement and characterisation of bulk materials and their surfaces have been applied for tribological and chemical interaction. Furthermore, specialised techniques have been developed in many cases to provide information of unique laboratory tests. The following sections discuss the most commonly used characterisation techniques of surface analysis. The purpose of this discussion is to give the reader a broad picture of available methods among the laboratory characterisation techniques that are employed to characterise wear and chemical interaction during sliding of two surfaces.

2.3.2.1 Surface texture

In order to study the interaction of two solid surfaces when sliding over each other, tribologists often measure and compare surface texture and roughness parameters, before and after the wear process, and at intermediate stages when possible. The study of the relation between wear properties and surface texture can lead to the specification of optimised surfaces depending on the various surface needs.

The term surface texture refers to the condition of a surface made of fine irregularities (peaks and valleys) produced on the surface by the forming process. Surface engineers, by convention, refer to the surface texture as the sum of two components: roughness and waviness. Roughness consists of the finer irregularities characteristic of the manufacturing process, while waviness is composed of more widely spaced irregularities that are often produced by vibration in the manufacturing process. However, the terms surface texture and roughness are normally used interchangeably [65].

There are two types of roughness measurements, depending on whether the surface topography measurement is made simply along a line (profile method) or over an area of interest (areal method). The profile roughness parameters are more common and are defined with an R , while the areal roughness parameters give more significant values and are defined with an S [65], but both are referred to surface roughness. Areal roughness parameters are becoming popular due to the ability of optical instruments to inspect the surface roughness over an area and they are defined by the standard ISO 25178 series [66].

In both types of techniques, surface roughness quantifies the vertical deviation of the real surface from its ideal form. The value of the deviation gives a quantitative analysis of the roughness grade of a surface. Roughness measurements are standardised and consistent methods among surface engineers [67] and typical amplitude roughness profile parameters are specified in Table 2.4.

Table (2.4) Roughness amplitude parameters description from BS EN ISO 4287:1998+A1:2009

Parameter	Description	Formula
R_a	Arithmetic average of absolute values of height calculated over the entire length	$R_a = \frac{1}{n} \sum_{i=1}^n z_i $
R_q	Root mean squared	$R_q = \sqrt{\frac{1}{n} \sum_{i=1}^n z_i^2}$
R_p	Maximum peak height	$R_p = \max(z_i)$
R_v	Maximum valley depth	$R_v = \min(z_i)$
R_z	Average distance between the highest peak, and lowest valley in each sampling length	
R_{sk}	Skewness of the heights distribution	$R_{sk} = \frac{1}{nR_q^3} \sum_{i=1}^n z_i^3$
R_{ku}	Kurtosis of the heights distribution	$R_{ku} = \frac{1}{nR_q^4} \sum_{i=1}^n z_i^4$

The amplitude parameters are incomplete in the characterisation of a surface morphology, as two surfaces (as in Figure 2.8) can present the same R_a parameters, but they are completely different in nature. To discern the two surfaces a set of parameters, called *R-k parameters*, are derived from a graphical construction on the Abbott-Firestone curve [68] as defined in the ISO 13565-2 [69].

The Abbott-Firestone curve, also called bearing curve, is widely employed to reveal tribological performance of surfaces. The bearing area curve is generated by simulating a virtual horizontal line that move from the top to the bottom of the profile, evaluating the percentage of contact the line would make with the surface at each level. The resulting curve gives the percentage of the profile points at each height (cf. Figure 2.9).

Abbott and Firestone initiated the employment of the bearing curve in 1933, with which they extracted three important parameters for the surface characterisation. The *peak* roughness, Rpk , has been defined as the range of heights in between 2-25%, the *core* roughness, Rk , in the range 25-75% and the *valley* roughness, Rvk , covers the range 75-98% of the bearing curve [68]. The parameters calculated from the Abbott curve are summarised in Table 2.5.

From the bearing curve it is also possible to extrapolate volume parameters, in order to evaluate the volume of material and void in the peaks and valleys respectively. The volume parameters are interesting for the evaluation of the amount of peaks and valleys and their distribution in the analysed surface. According to *Michigan Metrology, LLC*

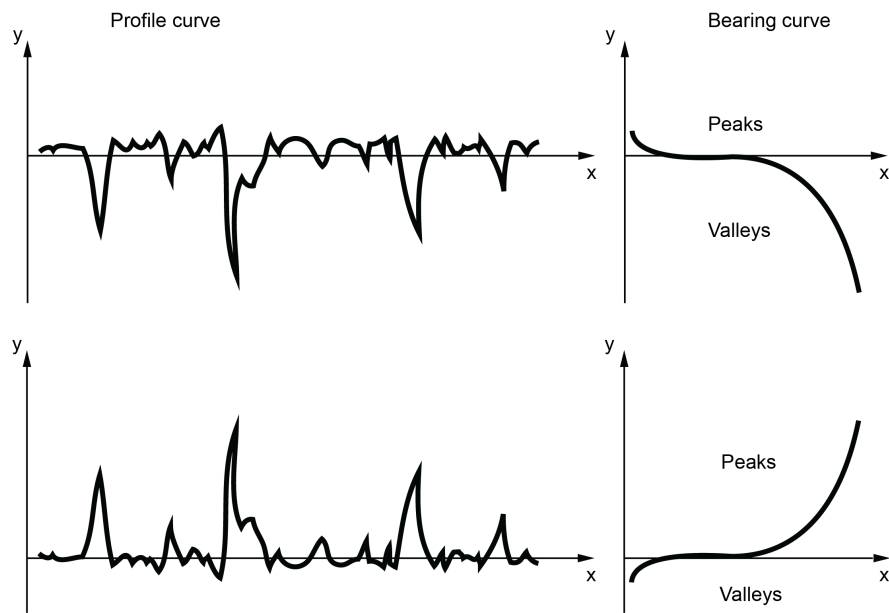


Figure (2.8) On the left two surface profiles with the same R_a parameter, but different in nature. On the right, the Abbott-Firestone curve reveals the different surfaces nature.

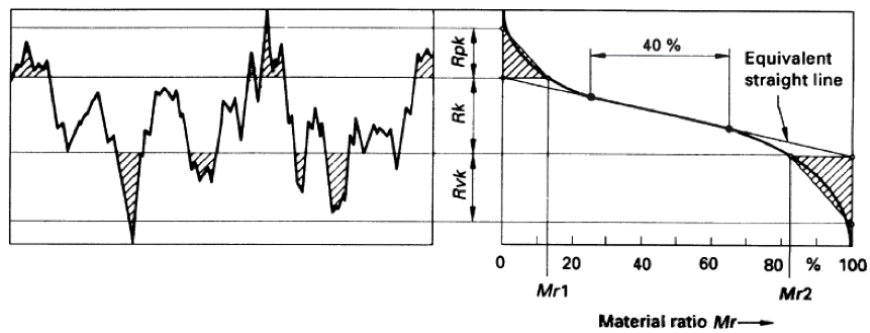


Figure (2.9) Calculation of the surface parameters from the Abbott-Firestone curve as from ISO 13565-2 [69].

Table (2.5) R-k parameters from the Abbott-Firestone curve.

Parameter	Description
R_k	Core roughness, the depth of the roughness core profile
R_{pk}	Reduced peak height, the average height of the protruding peaks above the roughness core profile
R_{vk}	Reduced valley depth, the average depth of the profile valleys projecting through the roughness core profile
R_{mr1}	The material portion $mr1$ is determined by the intersecting line, which separates the protruding peaks from the roughness core profile (expressed in %)
R_{mr2}	The material portion $mr2$ is determined by the intersecting line, which separates the valleys from the roughness core profile (expressed in %)

[70], the volume parameters are defined as follows in reference to Figure 2.9, where the material ratio $Mr1$ is defined by the peak roughness Rpk and the material ratio $Mr2$ is calculated by the valley roughness Rvk :

- V_{mp} the Peak Material Volume is the volume of material comprising the surface from the height corresponding to a material ratio level $Mr1$ to the highest peak;
- V_{mc} the Core Material Volume is the volume of material comprising the texture between heights corresponding to the material ratio $Mr1$ to $Mr2$;
- V_{vc} the Core Void Volume is the volume of void in the same interval calculated for the V_{mc} ; and
- V_{vv} the Valley Void Volume is the volume of void comprising the surface from the height corresponding to a material ratio level $Mr2$ to the deepest valley.

The material volume parameters are useful to understand the amount of material that may be worn away and how much material is available to support the load once the peaks are worn away. The void volume parameters are employed for considering fluid flow, coating applications and debris entrapment. The Core Void Volume, V_{vc} , may be useful to establish how much core space is void once a surface has been run-in resulting

in decreased peak heights. Furthermore, the Valley Void Volume, V_{vv} , indicates the potential remaining volume after significant wear of a surface has resulted.

2.3.2.2 Confocal infinite focus microscope

Confocal microscopy is one of the possible non-contact available techniques for surface topography imaging that is applied in characterising worn and damaged surfaces. A confocal scanning optical microscope is able to produce optical images that maintain a clear focus over a large depth of field. Quantitative measurements of surface topography can be obtained; surface roughness can be measured in opaque samples and substructures can be characterised in optically translucent samples.

The term confocal means "single focus". Confocal microscopy relies on obtaining confocality through a pinhole optic that prevents out-of-focus light reaching the image plane. As Figure 2.10 shows, the sample is illuminated through an objective lens with a pinpoint of light and a pinhole aperture is placed in the reflected light path. Due to the pinhole, reflected light from other regions of the sample is blocked. An image of the sample is created by moving either the sample or the light source along a scan pattern [71].

Confocal images allow three-dimensional reconstruction and sectioning of surfaces [72]. Confocal microscopy is good for imaging and analysis of surfaces with large differences in height, which are difficult to study with conventional light microscopy. Confocal images have very good resolution and sharp contrast levels; light reflected from sample features away from the focal plane of the objective lens is blocked, so that out-of-focus regions remain dark without deteriorating the image resolution.

Confocal images offer the possibility to study worn and abraded surfaces. Surface damage can be characterised visually and quantitatively without physically contacting the surface, avoiding the risk of creating additional damage during the measurement. Confocal microscopy is commonly used in semiconductor surface analysis, biological samples, and other material applications [73]. In contrast to electron microscopy (c.f. Section 2.3.2.3), samples do not need to be electrically conductive and vacuum compatible.

Specimen requirements and limitations. Confocal microscopy is an optical technique, thus specimen requirements are minimal:

- Samples do not need to be electrically conductive or vacuum compatible;
- Opacity of the sample determines which features can be studied, but both opaque and translucent samples can be analysed;

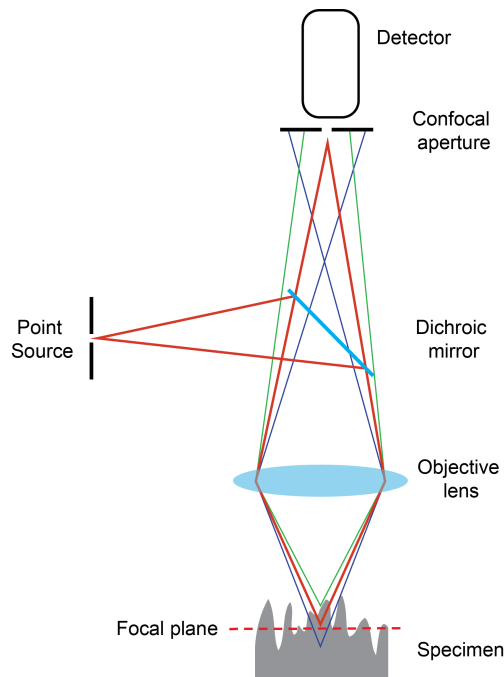


Figure (2.10) Confocal microscopy.

- In opaque samples quantitative surface roughness can be measured, but subsurface defects cannot be imaged;
- Features in opaque samples that are obscured from line-of-sight view cannot be studied because the light is not able to reach them;
- In translucent samples subsurfaces can be analysed, but the reflectivity of the internal surface determine how well that surface will be visible in the optical section; and
- Features with nearly vertical sides, such as cracks where the depth is much larger than the width, are very difficult to resolve in confocal microscopy because the light from these features is often not reflected back to the objective lens.

A limitation of confocal microscopy is the availability of objective lenses that have the optimum magnification power to view features of interest in the specimen. The objective lenses affects the three-dimensional resolution of the microscope; critical objective lens characteristics are the focus distance, the field of view and the numerical aperture.

2.3.2.3 Electron microscopy

Scanning electron microscopy, commonly known as SEM, is a well established analytical technique and its basic principles and instrument design are extensively de-

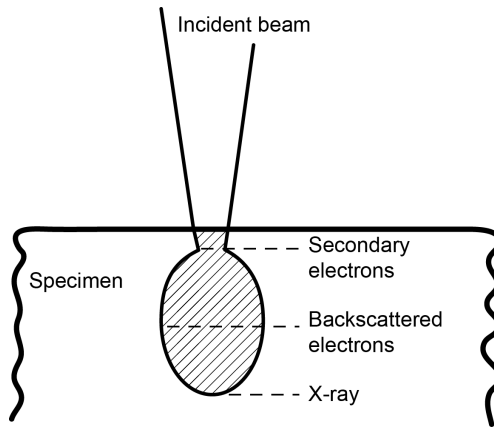


Figure (2.11) Electron-sample interaction.

scribed by Bowen [74] and Goldstein [75]. The SEM offers high resolution images (up to 10 nm) and chemical composition analysis of the sample with the same instrument. Interaction of the electron beam with the sample causes several quantum-physical interactions which include: secondary electron emission (< 50 eV), backscattered electrons (> 50 eV), cathodoluminescent, Auger electrons and characteristic X-rays emission (cf. Figure 2.11). For the characterisation of the surface secondary electron emission, backscattered electron emission and X-ray emission are of interest, thus the following discussion will focus on these emission mechanisms.

Secondary electron emission. Secondary electron signal, which falls in the energy range below 50 eV, is the primary source for surface topography with the SEM. The secondary electron signal is generated throughout the interaction volume (cf. Figure 2.11). Due to the low energy involved, the detected signal comes from the first layers of the specimen surface and it is strongly influenced by surface orientation. The maximum escape depth is in the order of 1 to 10 nanometers, depending on the sample density [76]. An element that is inclined to the beam appears brighter than one normal to the electron beam. Brightness is enhanced at fine-scale roughness because of the larger area from which secondary electrons can escape the sample surface. Electron beam penetration depth can be enhanced employing higher accelerating voltages (15 - 20 kV) [76].

Imaging of solid samples under the electron beam requires contrast between the various features. The contrast depends of several factors, such as atomic number differences, crystallinity and surface potential [75]. In general, secondary electron emission is insensitive to the atomic number, Z , although secondary electrons are also generated by backscattered electrons that are sensitive to Z . Therefore, secondary electron emission is indirectly affected by Z ; for this reason phases with different average atomic num-

bers can be distinguished in secondary electron images. Similarly, crystallinity does not affect directly secondary electron emission, but backscattered electron emission is sensitive to crystal degree and orientation of the sample, thus crystallinity influences indirectly secondary electron emission as well.

Backscattered electron emission. Backscattered electrons are the electrons that leave the specimen with energies greater than 50 eV and have a component of direction of the velocity vector opposite to that of the incident beam. This includes inelastically scattered electrons and, at high energy, primary electrons that elastically collided the specimen with almost no loss of energy. Backscattered electrons normally have energies from 0.5 to 0.9 of the incident beam energy.

The efficiency with which backscattered electrons are generated depends on the atomic number involved. Heavy atoms are less efficiently backscattered than lighter elements. The distribution of backscattered electrons is also dependent on the beam orientation with respect to the sample surface. Because of these dependencies, backscattered electron signals contain both topographic and compositional information.

Backscattered electron signal intensity is strongly affected by crystallinity of the sample: the electron channelling is the ability of electron waves to propagate on a crystal for long distances with negligible loss of energy [77]. This results in a variation in contrast that distinguishes grain of different orientation at the surface of a carefully polished polycrystalline sample.

X-ray emission. Specimen composition can be analysed using X-ray emission signal. A small interaction volume ($\sim 1 \mu m^3$) enables the SEM, equipped with the proper detector, to achieve compositional microanalysis. The X-ray emission can occur if the incident electron energy is high enough to activate fluorescence of the atoms on the specimen surface. The energy needed depends on the atomic number and the available energy levels of the elements.

Two types of X-ray spectrometers exist. The wavelength-dispersive spectrometer (WDS) separates the emitted X-rays according to wavelength. X-rays that enter the spectrometer are Bragg diffracted by an appropriate single crystal, and the intensity is measured by means of a proportional counter. By appropriately rotating and moving the diffracting crystal and the counter, the spectrum of emitted X-rays can be scanned in serial fashion. The minimum concentration of an element that can be detected can be as low as 0.01% under favourable conditions.

The energy dispersive spectrometer (EDS) separates the emitted X-rays according to energy. The energy selected by a semiconductor diode, which gives an electric signal with intensity dependent of the X-ray energy distribution. The acquisition process is

faster than in WDS, but EDS resolution is significantly poorer (~ 150 eV for EDS and ~ 20 eV for WDS).

The EDS detector needs to be cooled at approximately liquid nitrogen temperature in a high vacuum. Protection from the sample chamber is normally provided with a beryllium window, but polymers or diamond films can be employed as well. Absorption of the window decreases the sensitivity of the detector at low energies. EDS systems are simpler and cheaper than WDS systems. Both WDS and EDS systems use computers for control and data acquisition. Accurate X-ray emission results require a smooth and homogeneous surface of the sample. The data analysis may be semiquantitative (without reference standards) or quantitative (with standards). In the case of quantitative analysis, prior collection of spectra from reference specimens with known concentration of each element present in the sample is required. In addition, the X-ray signal can be employed to generate maps showing the distribution of elements over a scanned area of the sample surface.

2.4 Coating materials and release agents for SPF ceramic dies

A suitable surface treatment can introduce important benefits to the working surface of ceramic dies, protecting the interface die-part from wear, and preventing the formation of cracks [38, 7, 32]. This section focuses on coatings and release agents that have previously been studied or employed on SPF ceramic dies.

2.4.1 Cordierite

Cordierite is a magnesium aluminium cyclosilicate; stoichiometric cordierite is a composition of magnesium oxide, aluminium oxide and silicon oxide in ratio 2:2:5 ($2MgO - 2Al_2O_3 - 5SiO_2$). Cordierite is a refractory material and it has been studied as a coating for ceramic materials for hot forming applications [78, 7]. A cordierite coating has been studied (and patented) at the Boeing Company (US 6,692,844 [38]) as a protective coating for SPF ceramic die. Cordierite has three different crystalline forms:

- μ -cordierite, often referred to *quartz_{ss}*, which is metastable;
- Indialite
- α -cordierite

Where each crystalline form has different physical properties, including coefficient of thermal expansion (CTE) and glass-transition temperature (T_g). The deposition

of the coating has been tailored in order to match the CTE between the cordierite coating and the substrate (silica based concrete). Amorphous cordierite coating showed a greater CTE than crystalline ones. Cordierite glasses crystallise into a metastable hexagonal low temperature phase, which resembles quartz, hence the name quartz solid solution (quartz_{ss}). At higher temperature, the metastable μ -cordierite transforms to either hexagonal phase (indialite) or orthorhombic phase (α -cordierite) [79]. Weaver, et al. [78] investigated the effect of the crystalline phases and titanium oxide addition effects on the final CTE. Titanium oxide is a nucleating agent that decreases T_g and stabilises the μ -cordierite phase. Furthermore, the titanium oxide content affects the CTE, thus the coating CTE can be tailored through the titanium oxide concentration on the ceramic-glass.

Cordierite coatings have been deposited via air plasma spray, and the deposition process can be summarised in the following steps:

1. Raw material sieving and mixing;
2. Sintering of the mixture in order to obtain crystalline cordierite;
3. Milling of the crystals and resizing of the powder to sprayable size; and
4. Air plasma deposition.

2.4.2 Release agents

Boron nitride (BN) is typically employed in SPF for both metallic and ceramic dies as a releasing agent. Blohowiak and Newquist in their patent [80] dissuaded the use of boron nitride on ceramic dies for temperatures above 800°C, suggesting instead to use cerium oxide (CeO_2). Ceramic dies present high porosity, compared to metallic dies, where porosity is a source of oxygen that oxidise boron nitride to boron oxide (B_2O_3) that bonds to the high reactive titanium alloys surface. Cerium oxide is thermochemically stable at SPF operational temperature and it forms neither compounds nor eutectic compositions with either the titanium part or the ceramic die constituents. Furthermore, cerium oxide does not sinter and remain in powder form up to 800°C. Moreover, cerium oxide powder is red-brown; its natural colour is different from ceramic dies and titanium part, which makes it easy to identify on the die surface. Cerium oxide is usually used as a final polishing material in the glass optics manufacturing, so it is readily available, and it is not considered a hazardous or toxic material.

2.5 Conclusion

Superplastic forming (SPF) is employed to form high-value advanced alloys for aerospace applications. Superplasticity of materials is observed at elevated tempera-

ture when the material grain size is finer than 10 μm , under a controlled strain rate. Nowadays, only a limited number of alloys available in the market exhibit superplasticity, such as Ti-6Al-4V, which has been extensively employed in manufacturing of aircraft components. Several SPF processes have been developed and different tooling materials have been employed. For this research work, the author focused on SPF of single Ti-6Al-4V sheet blow formed with ceramic dies.

Ceramic materials are brittle and strength is determined by initial crack concentration. Under SPF conditions, the main contribution to the surface damage of ceramic die is due to adhesive wear and chemical interaction between the die and the titanium alloy forming part. Ceramic wear resistance is affected by chemical reactions, which occur at the ceramic surface with the environment. Furthermore, brittle materials are much prone to early failure due to cyclic stressing. The type and extent of failure of a surface depends strongly on the process used to form and prepare the surface.

From manufacturers experience [7, 32, 81], surface damages observed on SPF ceramic dies is dominated by brittle fracture that generates surface cracking and gain or removal of material from the surface. Sliding, abrasion and erosion can take place on ceramic surfaces. The grain size and properties of the intergranular material in the ceramic influence the wear and the relative hardness of ceramic and eroding material properties are crucial for the erosion mechanisms. In fact, the removal of hard particles from ceramic surface increases the cyclic wear rate.

A review of the available laboratory test methods has been conducted, in order to identify a suitable test able to assess the wear of ceramic dies under SPF conditions. A multitude of tests have been discussed although they all present some limitations to simulate surface condition of ceramic dies under titanium alloys superplastic forming conditions.

A test method is needed to investigate and better understand the interaction of ceramic die-metallic part under SPF conditions. The test should be able to assess wear of ceramic tools against titanium alloy samples at temperature above 850°C, under a controlled strain rate. In addition, this laboratory test should be able to identify die surface damages in-situ, while giving information about friction coefficient. Cordierite is the only material that has been already studied as protective coating for SPF ceramic dies. Different release agents have been employed on SPF ceramic dies, such as boron nitride (more common) and cerium oxide.

The literature review gives the background knowledge required to understand this research work, making aware the reader of the forming process, the employed tooling materials and the problems and limitations involved.

2.6 Summary

The literature review is divided into four main topics. The first part discusses about the theory of superplasticity, superplastic materials and the superplastic forming. In the second part are discussed the surface wear mechanisms of ceramic materials. Then, the wear assessment methods are showed in the third section. Finally, the chapter concludes with a review of available coatings for superplastic forming ceramic dies.

Chapter 3

Research methodology

The literature review revealed a lack of test methods to investigate the die-part interactions under controlled conditions that can simulate the SPF process. This chapter discusses the research strategy employed by the author to fill this knowledge gap existing in surface wear testing of ceramic materials under SPF process conditions.

3.1 Motivation of the research

In the last ten years researchers have been working on new reinforcing technologies to improve ceramic die design to increase their lifespan [1, 7, 37, 6, 4, 8]. Ceramic brittle fracture is becoming a secondary issue, while surface wear and spalling is still a poorly-defined problem in SPF, which reduces both die life and part quality and, thus, increases the process costs. The considered forming process is a high-value/low-volume manufacturing process, where the study of the interactions during the process is difficult and expensive. Furthermore, the previous chapter showed that there is a lack of understanding regarding the interactions that occur at the die-part interface during the high-temperature forming process.

The reason for this knowledge gap, despite the interest of manufacturers, lies in the absence of a significant laboratory test capable of simulating the SPF process. Such a test would be helpful to understand the chemical and physical interactions and to generate a wear mechanism model.

The Advanced Forming Research Centre (AFRC), with its industrial sponsors, has put great effort on the employment of low-cost ceramic materials in SPF dies and they are interested in the characterisation of the wear mechanisms of ceramic die surfaces that take place during SPF processes.

This research interest is focused on developing knowledge regarding possible surface treatments and coating solutions that protect the ceramic die surface from crack generation and prevent excessive wear at high temperature. To support these aims, the

research targets here can be summarised as follows:

- Create a standardised laboratory test for ceramic wear analysis under SPF conditions;
- Generate knowledge on the chemical and physical interaction at the die-part interface during the SPF process; and
- Evaluate the effect of surface treatments/coating solutions on die surface degradation.

The research outcome will be a test protocol for the characterisation of the interaction at the die-part interface under SPF conditions. The test protocol proposed in this work is focused on ceramic die materials and coatings, however, the test protocol can be extended to metallic die materials as well. The author contribution to the test protocol development lies on the data analysis methodology and results interpretation in relation to the selected key metrics indicators, rather than on the development of the test rig, which was already available at the time this research work started.

3.2 Research question

The literature review shows that a number of standard methods to characterise wear and friction of surfaces have been put in place to assess either metallic or ceramic materials. However, they have some drawbacks as they are often poorly correlated to true wear conditions of the SPF process (cf. table 2.3). These tests can take into consideration few parameters at a time, and they are often run at temperatures far below the typical SPF temperature of titanium alloys. With this work, the author wants to answer to the following (main) research question:

How can we evaluate the interaction at the die-part interface under SPF conditions?

A test method should be developed to be able to answer the research question. The literature review gives information on the requirements for the test method; it should be able to represent the conditions of the forming process in order to analyse the die wear and friction against part.

This work is an engineering-oriented research, based on technology. As with all engineering-oriented research, this work is driven by the need for performance [82] and it focuses on the application of suitable technologies. This study wants to develop a test method that is able to recreate the SPF conditions at a laboratory scale. The test

method will be employed to characterise wear of ceramic materials currently employed as SPF dies; it will assess other technical ceramics that could be employed in SPF; and it will evaluate possible protective coatings for SPF ceramic dies. The implementation of such a test method will answer the research question stated before. In addition, the test method will answer further (secondary) questions, which are:

- Would it be possible to assess the effectiveness of a protective coating for SPF ceramic dies? and,
- Would it be possible to identify a suitable coating able to improve ceramic die life-time?

Research can be distinguished into two categories: pure research and applied research. Pure research contributes to a deep theoretical understanding and for a more abstract formulation of the phenomena, while applied research contributes for making human intervention in real world environments more effective [83]. This work falls in the category of applied research, and it focuses on the employment of a technology into a process and often it is problem-oriented. This type of research describes a problem and it tries to identify adequate techniques to solve it [84].

Technology readiness levels (TRL) have been created by the National Aeronautics and Space Administration (NASA) in 1989 to define the maturity of emerging technologies and then adopted in several specialised areas, such as software, biomedical and manufacturing. TRL comprises nine levels (cf. Figure 3.1), from pure research to full rate production demonstration. When considering the TRL for manufacturing, this work ranks in the interval 3-5, in between research to prove feasibility and technology development.

The outcomes of this research will give a better understanding of the wear mechanisms of ceramic dies under SPF conditions, producing knowledge in a laboratory environment, and it will enable further research to study possible protective coatings to be employed in ceramic dies.

3.3 Research strategy

The previous chapter described the available laboratory tests employed to study wear of sliding surfaces. All these tests are often poorly correlated with the ceramic die SPF conditions because they have been either employed at lower temperature or with metallic dies, or different part material. The discussed laboratory tests are the starting point for the development of a suitable test method.

This work addresses the problem of identification and characterisation of surface wear of ceramic materials, with or without protective coatings, during high-temperature

Technology Readiness Levels (TRLs)

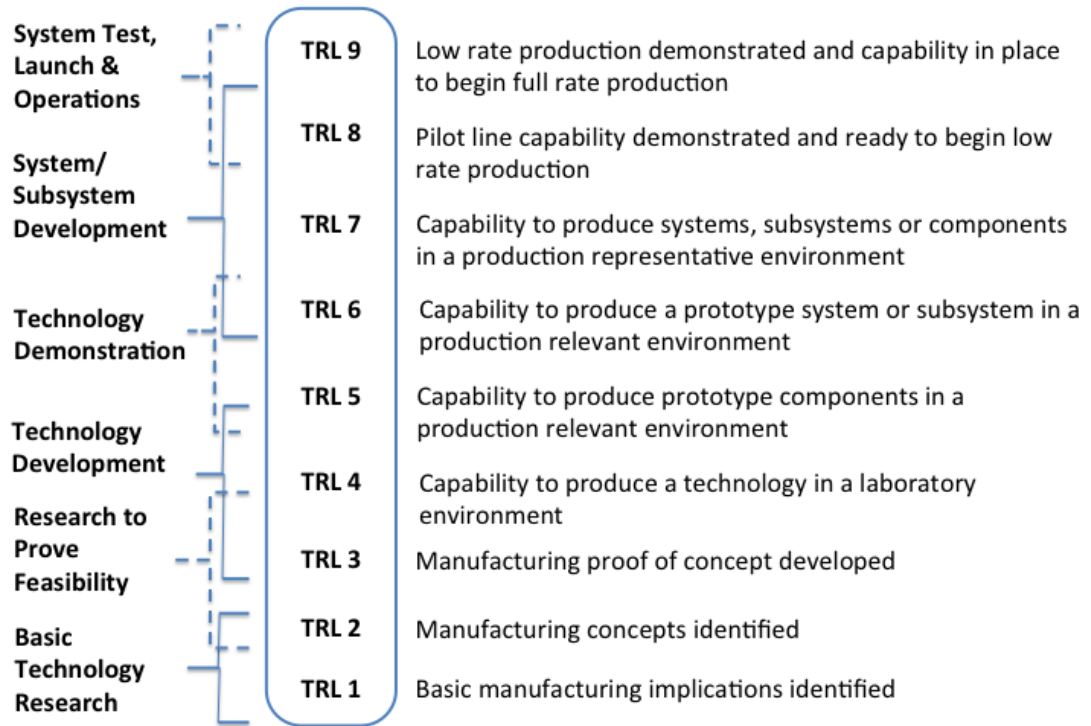


Figure (3.1) Technology readiness levels (TRL) for manufacturing [85].

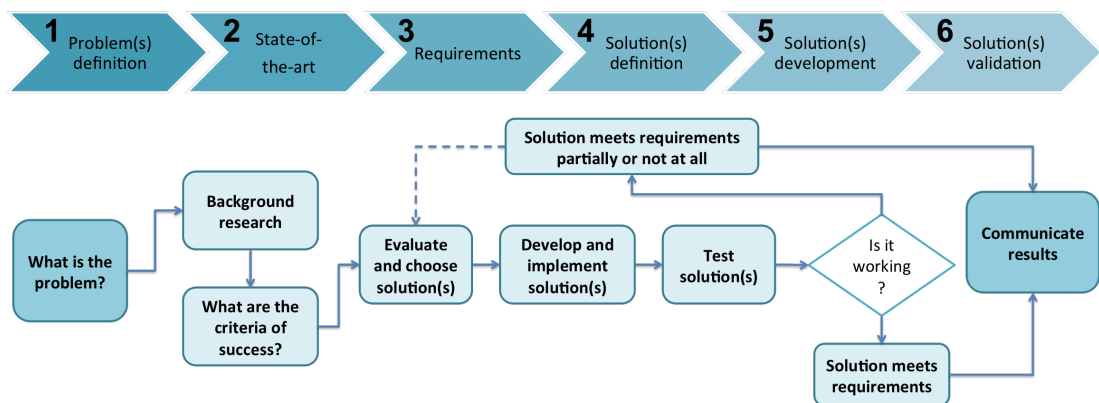


Figure (3.2) Research strategy diagram.

forming processes. The strategy applied by the author to answer to the research question is based on six steps, as showed in Figure 3.2.

1. Define the problem;
2. Background research;
3. Specify requirements;
4. Evaluate and choose solution(s);
5. Develop and prototype solution(s); and
6. Test solution(s).

The previous chapters defined the problem and presented the state-of-the-art of surface wear assessment methods. The overall objective of this research is to understand the wear mechanisms of SPF ceramic dies and to study protective coating solutions; therefore, the following chapter will introduce the test method developed to answer the research questions.

Chapter 4

Equipment and materials

In the previous chapter the state-of-the-art on SPF in wear assessment has been described and the requirements of the SPF process have been defined. As part of the research strategy, this chapter considers a solution definition, in order to develop a suitable test method. The test method is able to simulate the ceramic die-titanium sheet interface at superplastic forming conditions has been developed and it will be described in this chapter. Characterisation methods and the materials employed will be discussed as well, clarifying the selection process for coating materials, in order to answer to secondary research questions stated in the previous chapter.

4.1 The wear assessment method

4.1.1 The test selection

Different tests have been developed to evaluate die-blank interaction in metal forming [47, 48, 49, 50], although only four of them have been applied to simulate similar forming processes to SPF for titanium alloys. In fact, very little has been done on the wear assessment of ceramic dies during hot forming processes [51]. The literature review in Chapter 2 reveals the possible test methods that have been already employed, or could be applied, to evaluate ceramic die wear under high-temperature forming conditions.

When considering SPF of titanium alloys, the critical parameters for test selection include the ability to test at temperatures above 850°C and strain rates in the range from 0.001 to 0.1 s^{-1} [26] or even slower. Ideally, in light of what it has been discussed in chapter 2, with such a test we should be able to:

- Impose a pressure between a ceramic die and a titanium alloy part in the pressure range applied in SPF process (cf. chapter 2);
- Testing at the titanium alloy's superplastic temperature range (above 850°C);

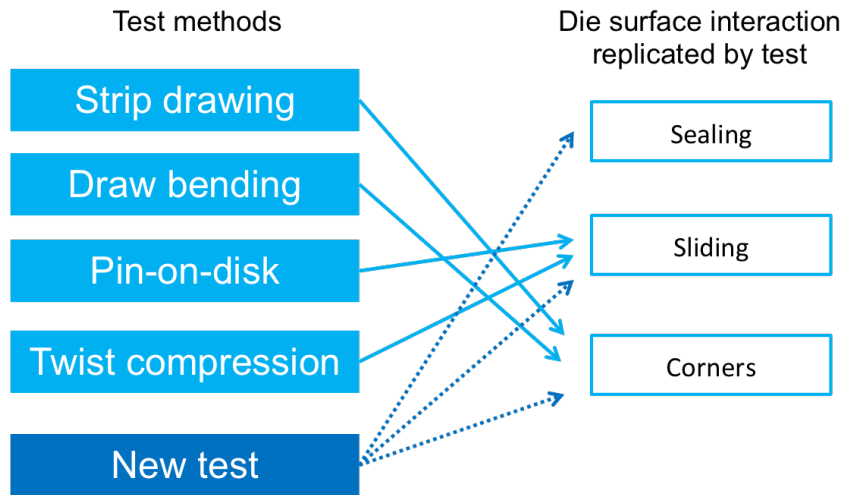


Figure (4.1) Test methods limitation in terms of capability to simulate die-part interface interactions during the SPF process. The new test method should be capable of simulating all the interactions that take place at the die surface during SPF.

- Simulate the sliding that occurs during SPF of titanium parts against ceramic dies, imposing shearing at the die-part interface (through plastic deformation or rotation of the titanium sample);
- Identify die surface wear in-situ;
- Extrapolate a friction coefficient that could be used in finite element simulations.

An evaluation of the available test methods has been undertaken by the author, which is summarised in table 2.2 in chapter 2, in order to develop a test method that fulfil the SPF requirements. Figure 4.1 shows the major limitation of the test methods discussed in chapter 2, which relies on the ability to simulate a proper die-part interface interaction. Each available test method is able to simulate only one of the conditions that take places at the die surface during SPF, while the new test method should be able to simulate multiple conditions.

The author identified at the Advanced Forming Research Centre a testing equipment available to generate testing condition similar to the one described by Friedman et al. [64] for the Ford test. The identified test rig has a rotational geometry, differently from the linear geometry of the Ford test. In addition, the test rig have been designed to carry out experiment under titanium alloys forming conditions. The following sections focus on the test rig employed and the design of suitable tools to develop the new laboratory test to assess SPF ceramic die wear.

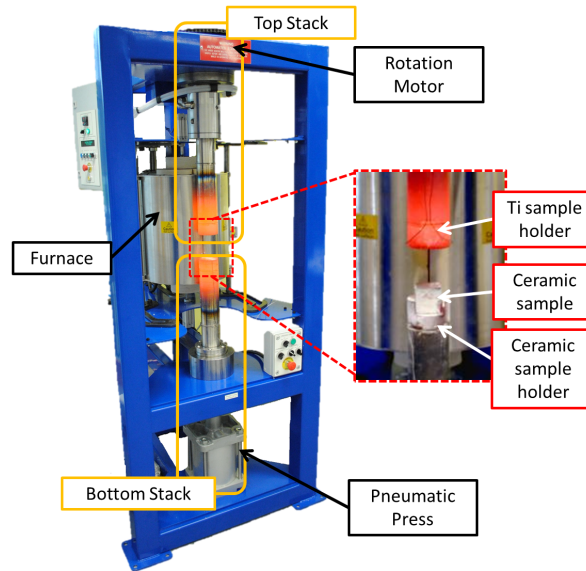


Figure (4.2) The test rig employed to simulate the superplastic forming process at laboratory scale. It comprises two stacks and a cylindrical furnace. Each extremity of the stack has an interchangeable tool, which can be either the sample holder or the metallic/ceramic tool. The rig is able to apply pressure and rotation to the tested sample, controlling applied load, rotation speed and temperature.

4.1.2 The test rig

The available experimental apparatus showed in Figure 4.2 has been previously designed by researchers at the AFRC [86] to test the interaction between metallic die materials and titanium alloys under SPF process conditions. The test rig is a unique piece of equipment in which the SPF process can be simulated at a laboratory scale.

The rig is equipped with a cylindrical furnace, which wraps around both the stacks when in operation. The furnace is able to achieve operating temperatures up to 1000°C.

The rig is composed of two stacks. The bottom stack introduces a static load in the range from 1 to 20 kN over a variable surface up to $2.0 \cdot 10^{-2} \text{ m}^2$, that simulates the gas pressure in the SPF chamber. The top stack is linked to a rotation motor, where rotation speed ranges from 0.001 rpm to 0.1 rpm, and each extremity of the stack has an interchangeable tool set.

The rig is connected to a control unit, which records temperature, applied normal force variation, rotation speed and torque.

4.1.3 Tool design

Part of the author contribution to the experimental apparatus comprises the design of the tools that enable the rig showed in section 4.1.2 to test ceramic materials. The test

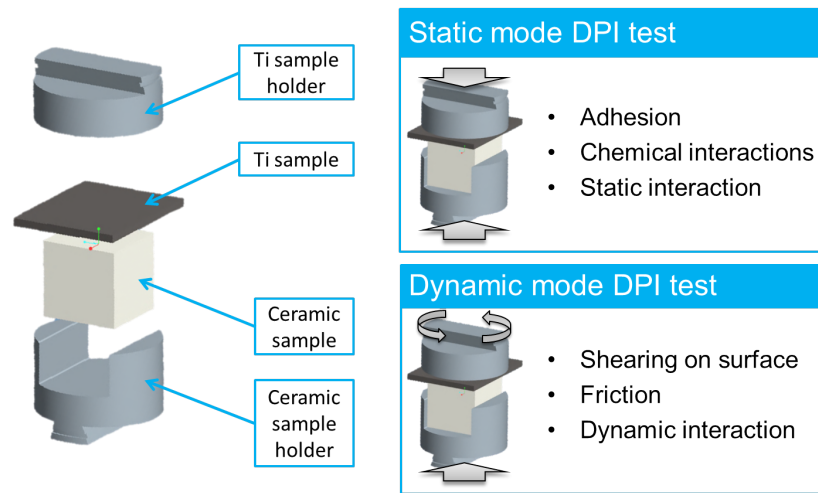


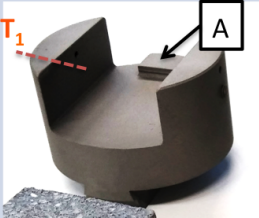
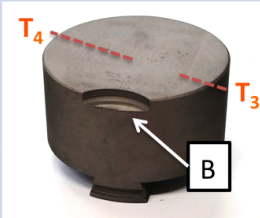
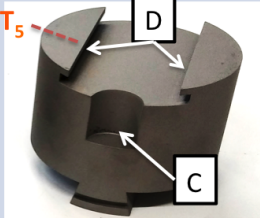
Figure (4.3) Schematic representation of the end tools of the rig employed for the two test modes: a static mode test (compression), where pressure is applied to ceramic sample and metal sheet specimen; a dynamic mode test (compression + rotation), where pressure is applied to the ceramic sample and torque is applied at the metal sheet sample to obtain shearing at the interface ceramic-titanium alloy.

rig is employed to carry die-part interface (DPI) experiments. The DPI test comprises two experimental configurations (cf. Figure 4.3): a static mode (compression) to test adhesion wear; a dynamic mode (rotation and compression) to simulate sliding of metal sheet on die surface. The static mode test simulates the conditions of the sealing area on a ceramic die (cf. Figure 2.6), while the dynamic mode test simulates corners and sliding areas.

Two sets of end tools have been designed by the author and made at the AFRC (cf. figure 4.4). A comprehensive discussion of the tool set design has been conducted by the author in a previous work [87] and it is summarised in table 4.1. The tool design takes into consideration applied load, operational temperature, time at operational temperature, atmosphere and geometric restrictions. Three tools have been designed by the author to enable the testing of ceramic materials: One lower tool has been designed to hold the ceramic sample in position and two upper tools have been designed for the static and dynamic test respectively. The tools have been made of stainless steel 316L grade, and thermal expansion considerations have been taken into account during the design process. The thermocouples have been placed on the tools in order to control temperature during the test in different region of the samples. Thermocouple positions are showed in table 4.1.

Depending on the selected DPI test mode, a different end tool set is assembled into the rig. Figures 4.4.a and b show the end tools for static and dynamic test respectively.

Table (4.1) Specification of the tools design.

	Lower tool	Upper tool Static mode	Upper tool Dynamic mode
			
Purpose	To hold ceramic sample in position	To compress Ti sample against ceramic sample	To compress Ti sample and to transfer rotation from upper tool to Ti sample in order to get sliding of Ti sample against ceramic surface
Material	Stainless steel 316L	Stainless steel 316L	Stainless steel 316L
Design considerations	Thermal expansion $dL = (\alpha_{SS316L} - \alpha_{ceramic})L_0\Delta T$		Thermal expansion $dL = (\alpha_{SS316L} - \alpha_{Ti64})L_0\Delta T$
Dimensions	\varnothing 80 mm h 50 mm	\varnothing 80 mm h 50 mm	\varnothing 80 mm h 50 mm
Additional features	A: Ceramic sample stopper	B: Hole to easy remove Ti sample when it sticks to the upper tool	C: Hole to easy remove Ti sample D: Ti sample holders to keep sample in position and transfer rotation
Temperature control	T ₁ : thermocouple in contact on the side of ceramic sample (distant 20 mm from testing surface) T ₂ : thermocouple in contact on the side of ceramic sample (distant 5 mm from testing surface)	T ₃ : thermocouple inside upper tool 5 mm deep in the tool diameter and distant 5 mm from testing surface T ₄ : thermocouple inside upper tool 40 mm deep in the tool diameter and distant 5 mm from testing surface	T ₅ : thermocouple in contact with Ti sample (distant 5 mm from testing surface)

The end tools (cf. figure 4.4.c) are placed at the extremities of the bottom and top stacks in the test rig, and comprise a bottom tool, which is a ceramic sample and its holder, and a top tool, that is a titanium sample holder.

4.1.4 Correlation between strain rate and rotation

The DPI test involves a rotational sliding of a non-deforming titanium sample against a ceramic surface at SPF temperature. Figure 4.5 summarises the concept behind the selection of the proper rotational velocity to simulate the sliding of a titanium blank onto the die surface during SPF. Considering the one-dimensional problem of discrete elongation of the titanium blank during SPF, and constant elongation rate along the considered time, the sliding velocity can be defined as:

$$v_{sliding} = \frac{L_f - L_0}{t_f - t_0} = \frac{\Delta L}{\Delta t} \quad (4.1)$$

where L_f is the length of the bar at the time t_f . Depending on the strain rate and the die geometry, the titanium sheet will take a certain amount of time to completely deform into the die. If the imposed pressure is constant, the sliding velocity of the titanium blank on the die surface can be assumed to be constant.

The DPI rig can simulate the sliding velocity by imposing the rotation of the titanium sample on the ceramic sample surface. The rotational velocity of the titanium sample can be controlled in the DPI rig. The author assumed, to ease the calculation, that the contact area between the ceramic sample on the bottom tool and the titanium sample on the upper tool is a circle inscribed into the area of the ceramic sample. Once the sliding velocity $v_{sliding}$ is obtained from die geometry and SPF simulation, the angular velocity on the DPI rig can be calculated as:

$$\omega = \frac{v_{sliding}}{r} \quad (4.2)$$

where r is the radius of the area of contact.

The correlation between sliding of blank material onto the die surface during the SPF process and the rotational sliding of titanium sample against the ceramic surface in the DPI rig does not take into account the plastic deformation of the titanium that occurs during SPF. The absence of plastic deformation of the titanium sample in the DPI rig is a limitation of the experiment, which leads to a lower chemical interaction at the die-part interface [9, 41].

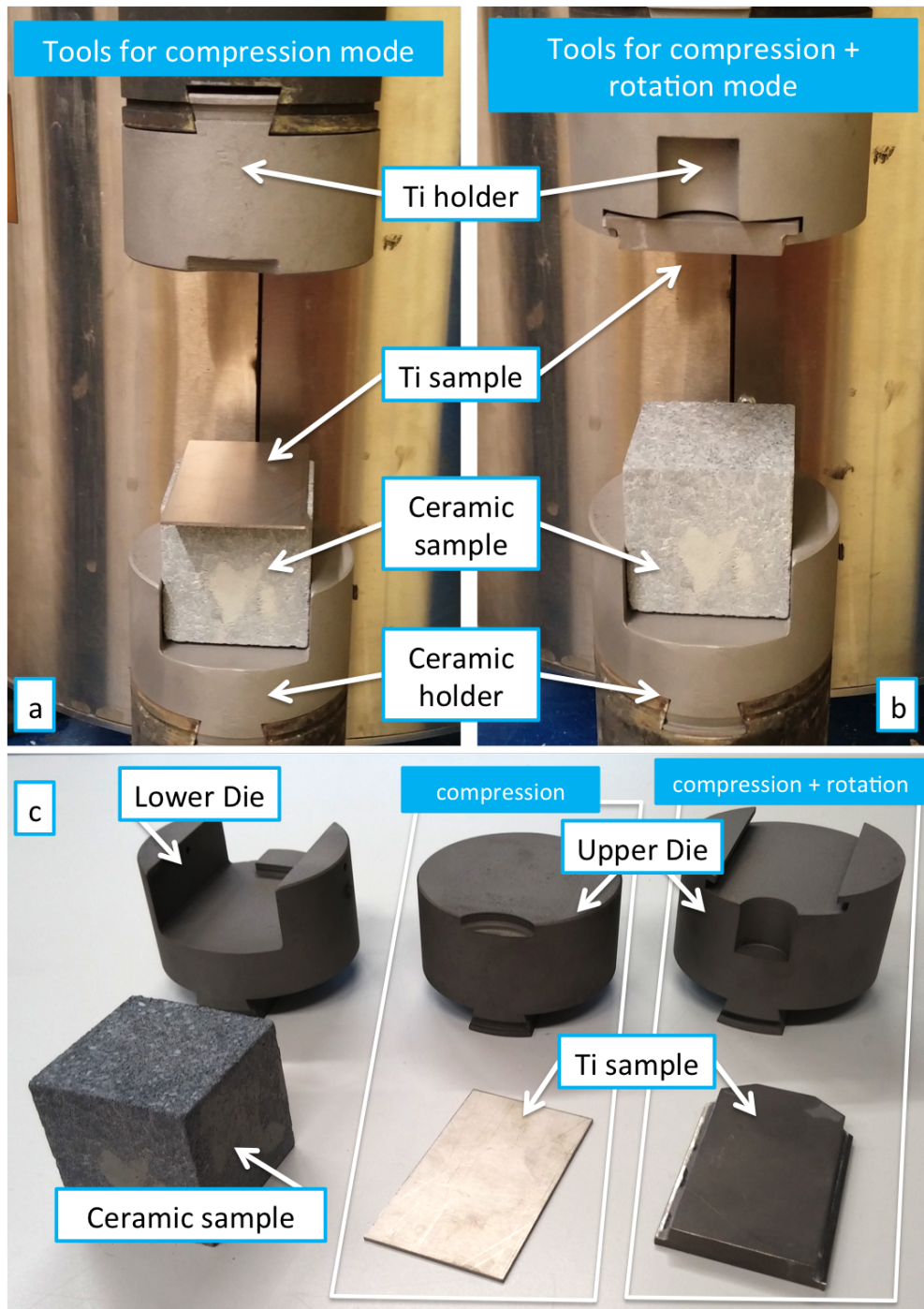


Figure (4.4) The end tools manufactured for the two DPI experiment modes. The static mode configuration (a) is composed of a ceramic sample holder and a ceramic cube sample, where a thin titanium sample is held on top. The dynamic mode configuration (b) is composed of a different top tool, where a thick titanium sample - with T shape in section - is held on the top in order to induce the rotation of the titanium sample onto the ceramic die surface. The disassembled end tools are shown in (c).

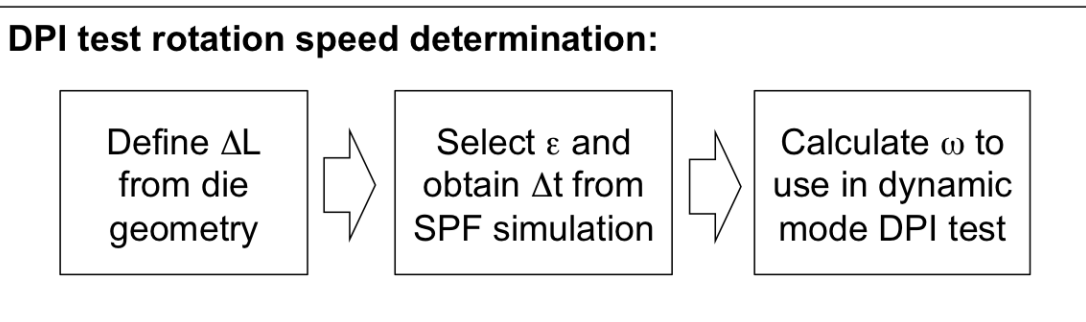
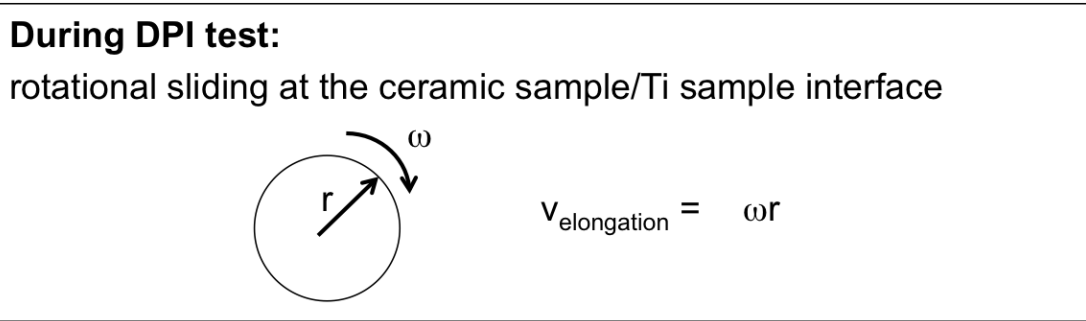
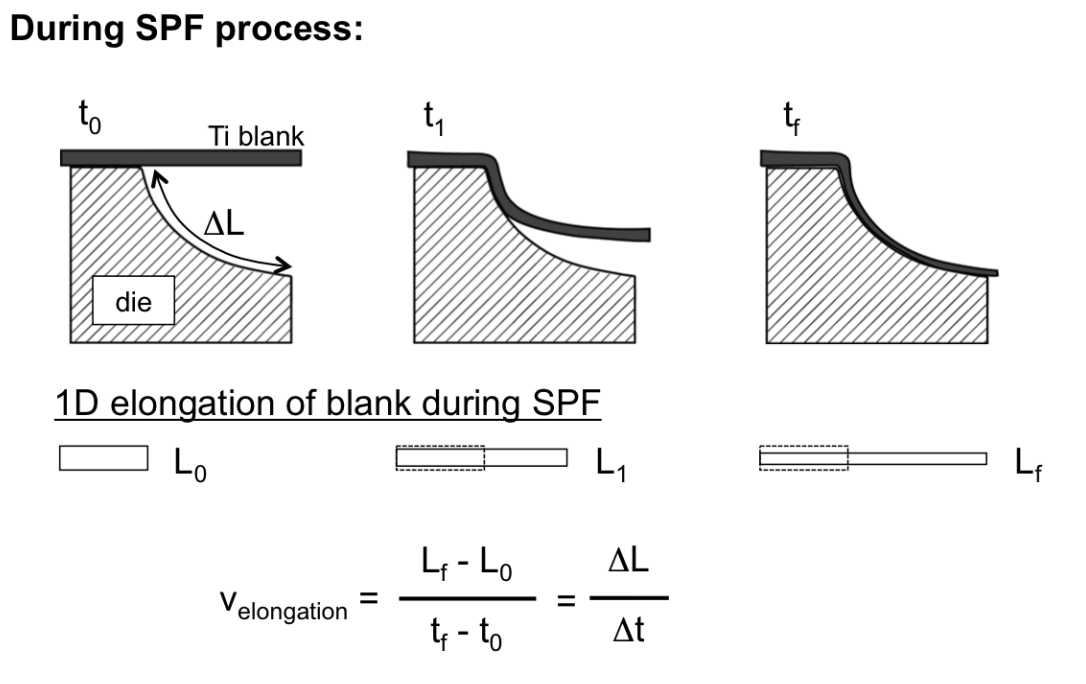


Figure (4.5) Correlation between strain rate and rotation.

Table (4.2) Summary of the key metrics evaluated for the different die-part interface experiment mode.

DPI test modes	Hot cracking		Surface degradation		Scale accumulation	Chemical inspection	Friction
	Surface thopography	Thermal images	Surface thopography	Thermal images			
Static mode	✓	✓	✓	✓	✓	✓	
Dynamic mode	✓	✓	✓	✓			✓

4.2 Characterisation methods

The aim of the DPI experiment is to evaluate the resistance to thermo-mechanical cycles of coated and uncoated working surface under SPF conditions. The author proposed four key metrics to evaluate coating performance:

- Die resistance and surface degradation;
- titanium part scale accumulation;
- chemical interaction; and
- friction.

The key metrics are evaluate depending on the DPI test mode in use, as shown in Table 4.2.

4.2.1 Die resistance and surface degradation

Die resistance and surface degradation are investigated by visual and quantitative measurement of 3D surface topography changes before and after the experiment. Imaging confocal microscopy is employed to record the surface degradation of the die, acquiring the surface topography and areal surface roughness - $Sa(Die)$ - before and after each experiment.

An Alicona InFineFocus confocal microscope is used for the acquisition of a sequence of confocal images through the depth of focus of the objective; 5x magnification is employed for the measurement, with 400 nm and 55.99 μm as vertical and lateral resolution respectively.

Thermal imaging has been widely employed in hot-forming to evaluate in-situ die degradation [34]. Such a technique enables the identification in-situ of the surface

damages or material accumulation during the unloading of titanium sample from the die. A Land Instruments FTI-E 1000 thermal imaging camera has been installed to monitor the die condition in-situ. Thermal images are recorded to monitor the ceramic surface degradation during the loading and unloading of titanium sheet specimens.

4.2.2 Titanium part scale accumulation

Imaging confocal microscopy is employed as well to monitor the titanium part scale accumulation after each testing cycle. Visualisation of the surface area is a powerful tool when associated to topographic surface analysis. Significant information can be extrapolated directly from the plot of the surface, while quantitative data can be calculated from surface roughness parameters; for instance, peaks are important when considering friction and wear properties, as the interaction between surfaces concentrates around them, while valleys are important for the retention of lubrication [88].

For both qualitative as well as for quantitative characterisation, 3-D analysis is a powerful tool which can give greater information compared with conventional 2-D methods. 3-D analysis, or areal analysis, can give several parameters that helps recognise different wear mechanisms [89].

Single parameters, which are inherently synthetic, cannot completely describe the complex reality of a surface. Each parameter can only give information about some specific features of the microgeometrical texture, and this requires interpretation [88]. As discussed in section 2.3.2.1, the Ra parameter (or Sa when referring to areal analysis) on its own does not describe the functional behaviour of the surface, and many existing surfaces can be characterised by the same Ra value but are really different with respect to functionality (cf. Figure 2.8). The Sa parameter has been employed by the author as a process control parameter in the characterisation of the DPI test outcomes, since changes in Sa value may indicate that some surface conditions have changed. Each titanium sample $Sa(Ti)$ is measured and it is employed to detect major changes on the testing surface of titanium samples. However, Sa parameter does not give any information about the functionality of the surface, thus 3-D roughness parameters have been employed to characterise wear mechanisms. The volume of asperities $Vmp(Ti)$ and voids $Vvv(Ti)$ on the titanium surface, together with visual examination of the die surface topography, are employed in this work by the author to identify and characterise the wear mechanisms involved.

Surface roughness parameters have been extrapolated using a dedicated commercial software (IF-MeasureSuite v4.1) provided by the confocal microscopy manufacturer (Alicona Imaging GmbH). A comprehensive discussion of data acquisition and analysis procedure is given in appendix B This characterisation technique enables a quantitative analysis on the surface degradation of the die through the study of the surface roughness

Table (4.3) SEM sample preparation procedure for coated and uncoated ceramics.
NOTE: the sample preparation procedure has been optimised by the author starting from the suggested procedure in the Buehler catalog [90].

Surface	Abrasive/size	Load [N]	Base speed [rpm]	Relative rotation	Time
Diamond Grinding Disk (like Buehler Apex DGD)	75 μ m Diamond water cooled	35	300	Same	Until plane
TexMet P	15 μ m Diamond	25	150	Inverted	6:00
VerduTex	6 μ m Diamond	25	150	Same	4:00
VerduTex	3 μ m Diamond	25	150	Inverted	4:00

change during the die lifetime.

4.2.3 Chemical interaction

A Quanta FEI scanning electron microscope (SEM) is employed for visual and chemical inspection of samples' surface and fractography for failure analysis. In addition, chemical interactions are studied with energy dispersive X-ray (EDX) spectroscopy available with the SEM in use.

Ceramic materials are extremely hard and brittle and may contain pores. Sectioning of ceramic samples has been performed using a diamond blade. For coated ceramic samples, the orientation of the sample during sectioning has been chosen keeping the coating in compressive state. Deformation of the sample is not a problem for ceramic materials, however, during preparation care must be taken in order to avoid break out of grains or cracking of the sample.

Vacuum infiltration of low-viscosity castable epoxy is employed for sample mounting. Pullouts of material is the major problem that arises during SEM sample preparation of ceramic samples. To avoid this problem, mechanical preparation of samples has been conducted with rigid grinding discs and hard cloths [90]. The sample preparation procedure is showed in table 4.3. Care has been taken during grinding of coated samples: to be sure that cracks on the coating have not been generated during sectioning, the first grinding step has been conducted up to three times, checking with optical microscope every time if new cracks arise. After preparation, samples have been dried under vacuum for at least 48 hours before introducing into the SEM chamber for inspection.

4.2.4 Coefficient of friction

In the dynamic mode DPI test a rectangular rotating titanium specimen is pressed against a fixed ceramic sample with the surface shape of a square. During the test the applied pressure from bottom stack and torque from rotation of the top stack are monitored. In figure 4.6 is showed the die-part interface interaction during the DPI test, where the square indicates the ceramic cube surface in contact with the titanium sample. For the calculation of the coefficient of friction (COF) the contact area is assumed to be the circle inscribed into the square, with radius R equal half the length L of the square. Assuming the pressure is constant and uniform over the considered surface, the coefficient of friction μ at the point P can be written as:

$$\mu = \frac{\tau}{p} \quad (4.3)$$

where τ is the shear stress and p the pressure at point P . Assuming the coefficient of friction to be constant over the considered surface, the torque T produced by the rotation of a titanium sample on a circular contact area A with radius R is calculated as:

$$T = \int_A \tau r dA = \int_0^R \int_0^{2\pi} \tau r^2 dr d\theta = \frac{2\pi R^3}{3} = \frac{2}{3} A R \quad (4.4)$$

Thus the COF can be calculated as:

$$\mu = \frac{3T}{2\pi R^3 p} = \frac{3T}{2ApR} \quad (4.5)$$

The COF measure is useful for the evaluation of different surface treatments and coatings in terms of physical and chemical interactions at the die-part interface. High COF indicates strong chemical and/or physical interaction during the sliding. Moreover, due to the assumptions made, the measured COF is an underestimate of the real one, but it is an useful output for comparison between different surfaces and coating employing the same test conditions.

4.3 Limitations of the test

The DPI rig has been selected for the development of a test protocol that enables the characterisation of the interface die-part under SPF conditions. The DPI rig design has some constrains which limit some of the test potentials. Three limitations have been identified, which are:

- Lack of stretching of titanium sample during the test;
- Maximum angle of rotation θ , and

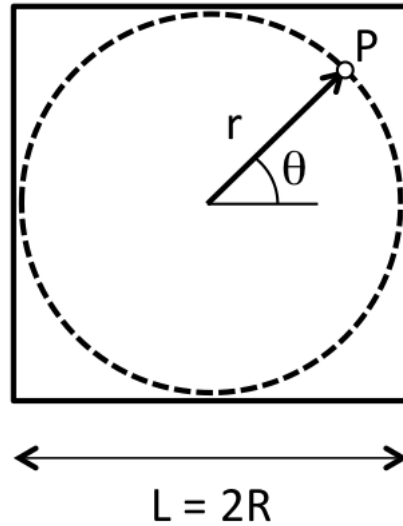


Figure (4.6) Schematic representation of sliding during DPI test.

- COF underestimation.

The main limitation of the DPI experiment is due to the absence of titanium sample plastic deformation during the test, which has been taken into account during the chemical interaction analysis at the die-part interface. During SPF process the titanium blank undergoes to plastic deformation while sliding on the die surface, exposing new non-oxidised titanium surface on the die surface [91]. The absence of titanium stretching while sliding on the die surface during the DPI experiment leads to the absence of generation of new non-oxidised surface, resulting in underestimation of chemical interaction and friction at the die-part interface.

The second limitation of the test, due by a DPI rig design constrain, is the maximum angle of rotation θ equal to 270° . Due to the geometry of the samples, the angle of rotation constrain limits the testing sliding distance up to 117.8 mm. The rotation speed ω is limited in the range of 0.001 - 1 rpm, which is not a constrain limits for the test purpose, as the testing sliding time can be up to 12 hours for θ equal to its maximum value and ω equal to 0.001 rpm.

Finally, the calculated COF value during the DPI test is underestimated, due by two factors: a geometric factor (as the area of contact between ceramic die and titanium sample during rotation is greater than the one assumed in section) and a chemical factor (the absence of stretching of the titanium sample causes a less chemical interaction with the die surface as explained earlier) 4.2.4.

4.4 Substrate, coating and metal sheet materials

In the present work the ceramic substrate employed for the experiments is a commercial castable refractory ceramic powder (Ceradyne ThermoSil[®] 220), which has already been employed for SPF dies by Boeing [1], thus selected by the author as a baseline material to assess surface wear. The powder is composed of fused silica reinforced with silicon carbide particles. A study has been carried out to evaluate the ceramic performance under SPF conditions with the use of the DPI test. Chapter 5 will focus on the evaluation of the Ceradyne under different SPF conditions. In addition, a comparison with another refractory material is carried out in order to evaluate the materials performance for the selection of the suitable substrate material for the protective coating study.

The ceramic samples employed for the DPI test are cast in cubes of 50.0 mm per side following ceramic powder supplier's instruction. Care is taken on the top and bottom surface parallelism, which is within ± 0.2 mm tolerance in order to have a uniform load distribution during the experiment. Top average surface roughness (Sa) of uncoated ceramic is also controlled to be below 10.0 μm .

Part of this research work focuses on the investigation and assessment of protective coatings for SPF ceramic dies. In terms of coatings, there are many possible combinations and the evaluation of their effectiveness is related to the operating conditions of the forming process. There has been limited use of ceramic dies in SPF at industrial scale and, as a result, there is limited availability of protective coatings for such application in the market. Thus, protective coating investigation for SPF application is a relatively new area of research.

In order to select a suitable coating solution, it is important to highlight the requirements imposed by the operating conditions of the SPF process for titanium alloys:

- The coating should sustain high temperatures (above 850°C);
- The coating should sustain thermo-mechanical cycles;
- The coating should adhere to the ceramic substrate;
- The coating coefficient of thermal expansion (CTE) should match the substrate CTE;
- The coating should be chemically inert with Ti-6Al-4V in all the range of operating temperatures.

Considering the forming condition restrictions, very few coatings have been already used in ceramic SPF dies (cf. section 2.4), and more have been identified from similar

applications (cf. appendix A). In addition, regarding the only coating that has been developed for SPF ceramic dies [38], there are no published results of its effectiveness under SPF conditions (probably due to a lack of laboratory testing methods).

Coating selection is based on weighting its temperature operability and CTE, which should be similar to the substrate's CTE. Moreover, availability in the market is another important factor to take into consideration during the selection of the coating material. All the tested coatings are already available in the market as frit for glasses or as raw materials for clay. The identified coatings are composed of a mix of aluminosilicate powders with a specified composition, or they are ceramic glazes already available in the market.

The metal sheet samples are made of commercial SPF grade Ti-6Al-4V alloy with dimensions 40.0 x 60.0 x 1.2 mm for the static mode DPI test and 40.0 x 60.0 x 9.0 mm for the dynamic mode DPI test. In the following chapters the metal sheet sample, Ti-6Al-4V, will be referred with its alloy name or as titanium alloy or simply as titanium specimen. In every test boron nitride (BN) suspension (Kenametal, WJMB grade) is sprayed on each face of the Ti-6Al-4V sample as a release agent. A precision scale (accuracy ± 0.001 g) is used to apply a constant amount of release agent to each face of the Ti-6Al-4V sample.

4.5 Summary

This chapter defines the solution to be implemented to assess surface wear of ceramic materials under SPF conditions. The chapter evaluated the following topics:

- The wear assessment method: several test methods have been identified in the literature and the evaluation of their characteristics compared with the specifications of the SPF process of titanium alloys showed that a new test method should be required to better simulate the die-part interactions that take place during the forming process.
- The new test method will be conducted with an experimental apparatus that is discussed in the chapter. The test rig is able to simulate SPF conditions at a laboratory scale.
- In order to be able to test ceramic materials under different SPF conditions, two sets of tools have been designed and manufactured. The new test method, or die-part interface (DPI) test, has two working modes: static and dynamic, where each mode recreates the contact and sliding interactions respectively.
- The DPI test's key metrics to evaluate wear are: the resistance to thermo-mechanical

cycles, the die surface degradation and titanium scale accumulation. In addition, chemical interaction and friction are considered as well.

- Ceramic substrate, coating and metal sheet materials that are employed for the wear assessment are described.

The following chapters will discuss three studies where the DPI test is employed for the assessment of surface wear under SPF conditions. In chapter 5 a comparative study of two ceramic materials will be conducted. In chapter 6 the same coating material is deposited employing two different deposition methods, and the DPI test is employed to assess coating performance. In chapter 7 several coating materials undergo to the DPI test to assess their performance under SPF conditions.

Chapter 5

Comparison of different ceramic die materials and validation of the DPI test

This chapter is divided into two main sections: in the first section the DPI experiment is employed to compare wear of two possible SPF die ceramic materials. The uncoated ceramic materials are tested in both static and dynamic mode and the results are crucial for the selection of the ceramic substrate to be employed in the protective coatings study. The second section focuses on the comparison of the DPI test outcomes with a SPF forming trial carried out at the Advanced Forming Research Centre. Part of this work has been presented at the EuroSPF 2016 conference [92] and it has been published in the *Materialwissenschaft und Werkstofftechnik* journal [93].

5.1 Comparison of different ceramic die materials

5.1.1 Materials

In this chapter, within the ceramic die materials employed in SPF [28, 7, 4, 94], two commercial materials, Ceradyne ThermoSil[®] 220 and Horizon Chrome infiltrated, have been selected for the DPI experiment. Ceradyne ThermoSil[®] 220 is a fused silica castable with addition of silicon carbide reinforcing particles and calcium aluminate binder. The cast material has bulk density of 2109 kg/m³ and CTE equal to $1.7 \cdot 10^{-6} / ^\circ\text{C}$ [95]. In this study the author refers to the particle-reinforced ceramic material as *Ceramic CT*. The Horizon-Chrome infiltrated (*Ceramic HC*) is a commercial freeze cast refractory material made of fused silica infiltrated with chrome oxide through a treatment with chromic acid solution. The chrome oxide infiltration increases mechanical properties of the bulk material. The resulting bulk density is 1830 kg/m³ and CTE

equal to $1.9 \cdot 10^{-6} / ^\circ\text{C}$ [28].

The ceramic samples have cubic geometry (50.0 x 50.0 x 50.0 mm) and have a testing surface of 2500 mm². Each sample is dried for 50 hours before testing. The metal sheet samples, as discussed in section 4.4, are made of commercial SPF grade Ti-6Al-4V alloy with dimensions 40.0 x 60.0 mm. Thickness of the samples depends on the selected DPI test mode: 1.2 mm thick samples are employed for static mode test and 9.0 mm thick samples are employed for dynamic mode test. All titanium samples are sprayed with boron nitride (BN) suspension (Kenametal, WJMB grade). The starting roughness of Ti-6Al-4V samples has been measured with confocal microscope technique. All the Ti-6Al-4V samples employed for the DPI experiment have a starting surface roughness, $Sa_0(\text{Ti})$, below 3.0 μm .

5.1.2 Design of experiment

The DPI test is employed to assess the surface wear behaviour of different ceramic materials when exposed to representative SPF conditions. The test rig discussed in section 4.1.2 has been used for the experiments. As showed in figure 2.6, the static mode DPI test evaluates the die surface degradation typical of the adhesion areas, while the dynamic mode DPI test gives information regarding friction and surface degradation of sliding and corner areas.

5.1.2.1 The static mode DPI experiment

The static mode DPI test is carried out employing the static mode end tool set (cf. figure 4.3 and 4.4). The experiment consists on a series of thermo-mechanical cycle loads at standard SPF conditions as shown in figure 5.1. Two experiments have been conducted on each ceramic material: low pressure (LP) and high pressure (HP) static mode DPI test. Testing parameters are summarised in table 5.1. The temperature is kept at 900°C, while the duration of the cycle depends on the applied pressure and it is extrapolated from FEA of a SPF pressure cycle required to form a Ti-6Al-4V sheet onto a die geometry discussed in section 5.2 regarding SPF trials validation.

The static mode DPI test procedure is showed in figure 5.1 and comprises the following points:

1. During the setup of the rig the ceramic sample is inserted in the dedicated holder tool. Once the ceramic sample is stable at temperature, the furnace is opened in order to introduce the first titanium sample.
2. A non-tested Ti-6Al-4V specimen is loaded onto the ceramic sample. A certain amount of time is needed to let the system reach again the testing temperature.

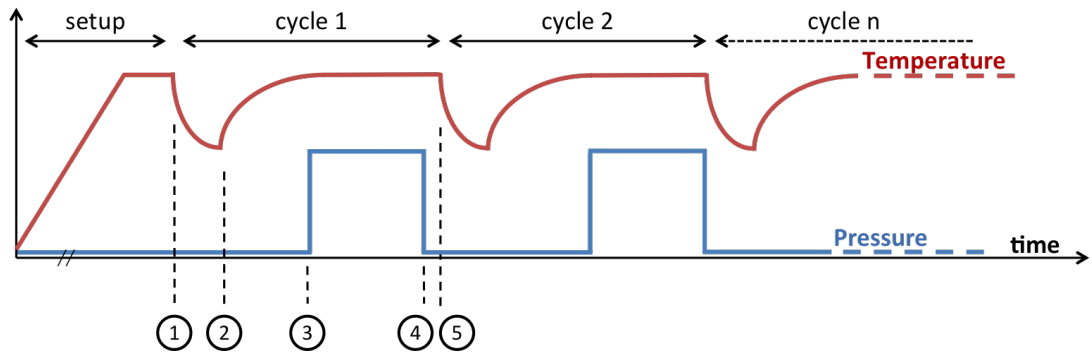


Figure (5.1) Schematic representation of temperature and pressure during the static mode DPI test.

Table (5.1) Test parameters of static mode DPI test.

Parameters	Low Pressure – LP DPI static mode	High Pressure – HP DPI static mode
Temperature [°C]	900	
Contact area [m ²]	2.5 x10 ⁻³	
Pressure [MPa]	1.2	2.0
Load [kN]	3	5
Time under pressure [min]	105	60

3. Once the system (including ceramic sample and Ti-6Al-4V specimen) is at temperature, the test rig applies a pressure between the ceramic and the titanium samples. The applied pressure depends on the selected pressure mode (LP or HP) and is kept for a certain amount of time, which is representative for a SPF production cycle. At this stage, the ceramic and Ti-6Al-4V are at testing temperature under pressure for a determined amount of time.
4. Pressure is released;
5. The cylindrical furnace is opened; the tested Ti-6Al-4V specimen is removed; thermal images of the tested ceramic sample are recorded; a new Ti-6Al-4V specimen is loaded and the rig is ready for a new cycle.
6. Operations from point 2 are repeated until the last Ti-6Al-4V specimen to be tested.

5.1.2.2 The dynamic mode DPI experiment

During the dynamic mode DPI test, the proper end tool set is assembled on the test rig (cf. figure 4.3 and figure 4.4). The titanium sample is pressed and it rotates against the ceramic surface. The transmitted torque due to the rotation is recorded and the estimated coefficient of friction (COF) is extrapolated as discussed in section 4.2.4. In addition, the resistance to thermal cycles is studied through comparison of surface morphology of the ceramic sample before and after the test.

The dynamic mode DPI test comprises three runs. For each run one new untested ceramic sample is employed. All samples test surfaces are polished before the dynamic mode DPI experiment in order to get a surface roughness below $10.0 \mu\text{m}$. The testing parameters are showed in table 5.2. Temperature is kept at 900°C , while the duration of the cycle depends on the applied pressure and it is extrapolated from FEA of a SPF pressure cycle required to form a Ti-6Al-4V sheet onto a die geometry discussed in section 5.2 regarding SPF trials validation. Three pressure levels have been tested, corresponding to three cycle duration. Considering the geometry of the ceramic die employed for SPF validation trials, which is discussed later in this chapter (cf. section 5.2), the sliding surface length L is highlighted along the plane xz in figure 5.10 and it is 12 cm. Due to die symmetry. This length L is used to calculate the angle of rotation needed on the DPI rig to simulate such sliding. As explained in section 4.1.4, with a rotation angle of 270 degrees, which is the maximum angle allowable on the DPI rig, the total length of sliding of the titanium sample on the ceramic surface under the DPI rig is 11.78 cm ¹. Thus, the angle of rotation is kept at 270 degrees for all the runs, while the rotation speed is calculated from the cycle duration as:

$$\bar{\omega} = \frac{\Delta\theta}{\Delta t} \quad (5.1)$$

The dynamic mode DPI test procedure is showed in figure 5.2 and comprises the following points:

1. During the setup of the rig the ceramic sample is inserted in the dedicated holder tool. Once the ceramic sample is stable at temperature, the furnace is opened in order to introduce the titanium sample.
2. A non-tested Ti-6Al-4V specimen is loaded on the upper tool into the DPI rig. A certain amount of time is needed to let the system reach again the testing temperature.

¹The length of sliding in the DPI rig is calculated as the length of the circular arc $L = \frac{2\pi r \theta}{360}$, where $r = 2.5 \text{ cm}$ and $\theta = 270 \text{ degrees}$.

Table (5.2) Test parameters of dynamic mode DPI test.

Parameters	Run 1	Run 2	Run 3
Temperature [°C]	900		
Pressure [MPa]	1.2	1.6	2.0
Rotation angle [°]	270		
Rotation speed [rpm]	0.007	0.009	0.013
Time [min]	105	80	60

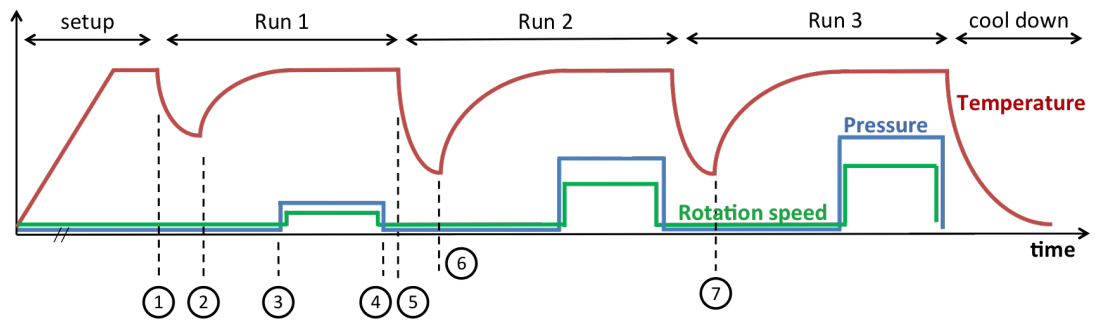


Figure (5.2) Schematic representation of temperature, pressure and rotation speed during the dynamic mode DPI test.

3. Once the system is stable at temperature, pressure and rotation are applied at the ceramic-Ti-6Al-4V interface. Pressure, rotation speed and time depend on the selected run as showed in table 5.2.
4. Pressure is released, rotation is arrested.
5. The cylindrical furnace is opened; the tested Ti-6Al-4V specimen is removed; thermal images of the tested ceramic sample are recorded; the tested ceramic sample is removed and a new ceramic sample is inserted into the ceramic holder; a new Ti-6Al-4V specimen is loaded on the upper tool.
6. Once the system reached the testing temperature, the rig is ready for run 2.
7. Operations of points 5 and 6 are repeated to carry out run 3.

5.1.3 Results

5.1.3.1 Ceramic die hot cracking and surface degradation

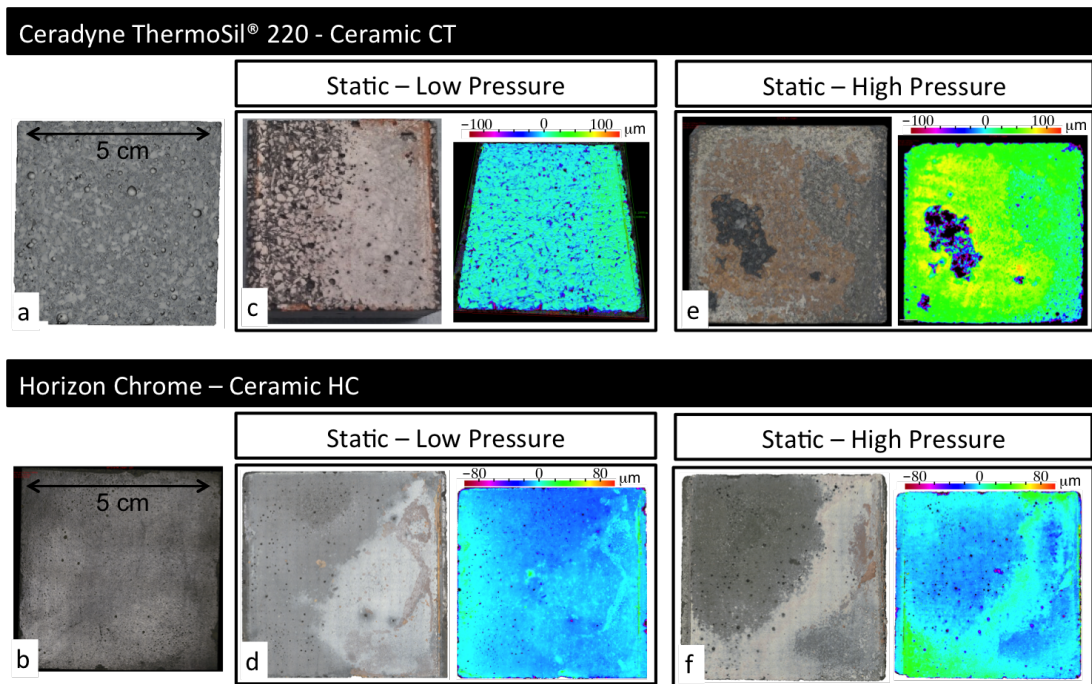


Figure (5.3) Ceramic CT (a) and ceramic HC (b) sample surfaces before the experiment. Ceramic CT (c) and ceramic HC (d) sample surfaces after static mode low-pressure DPI test. Ceramic CT (e) and ceramic HC (f) sample surfaces after static mode high-pressure DPI test. Every image is composed of a visual image and a pseudo-coloured 3D topography of the surface, where red indicates peaks and violet indicates valleys.

Static mode DPI test. Figure 5.3 presents the ceramic samples surfaces before and after the static mode DPI test. Figures 5.3.a and 5.3.b show the surfaces before the test of ceramic CT and ceramic HC. Figures 5.3.c and 5.3.d show the resulting ceramic surface wear under low-pressure conditions, while figures 5.3.e and 5.3.f are the resulting surface under high-pressure static mode DPI test. The surface images are complemented with the 3D topography obtained with the confocal microscope imaging technique described in section 4.2. The following observations can be made:

- Ceramic CT as cast is not dense and it shows surface porosity, while ceramic HC shows very little porosity. The porosity in ceramic CT is due to bubble formation during the manufacturing process of the ceramic due to gas produced by chemical reactions. The measured surface roughness before the experiment ($Sa_i(Die)$) is $(8.37 \pm 0.65) \mu\text{m}$ for ceramic CT and $(5.96 \pm 0.39) \mu\text{m}$ for ceramic HC batches respectively.
- At low-pressure conditions neither ceramic material shows any drastic wear. The post-test surface is characterised by deposition of release agent (white) and oxides (red) from the titanium sample to the ceramic surface. The change of ce-

ramic surface roughness during the test is an indication of the magnitude of wear. The measured surface roughness of the die after the experiment ($Sa_f(Die)$) is $(5.91 \pm 0.67) \mu\text{m}$ for ceramic CT and $(4.53 \pm 0.33) \mu\text{m}$ for ceramic HC respectively, indicating low surface wear.

- Evidence of hot cracking is found in ceramic CT when tested under high-pressure conditions. Cracks arise during the unload of titanium samples and they grow at each cycle, where ceramic matrix particles are removed from the surface. On the other hand, ceramic HC does not show any critical wear under high-pressure conditions. The measured surface roughness of the die after the experiment ($Sa_f(Die)$) is $(22.8 \pm 1.5) \mu\text{m}$ for ceramic CT and $(6.81 \pm 0.52) \mu\text{m}$ for ceramic HC respectively.

The images in figure 5.3 are complemented with thermal images in figure 5.4 recorded during the unloading of Ti-6Al-4V sample. Thermal images are recorded in gray scale, where white represents the hotter area and black the colder area.

Figures 5.4.a and 5.4.b show the surface of ceramic CT before test and figures 5.4.c and 5.4.d present the resulting ceramic CT surface wear under low-pressure and high-pressure static mode DPI test conditions respectively. Under low-pressure conditions fifteen cycles are carried out and a small amount of wear is observed, which is characterised by a layer of oxides deposited on the ceramic surface. At high-pressure condition ten cycles are carried out, and clear wear is identified from thermal images. The surface is damaged due to adhesion of Ti-6Al-4V samples to the die. The fracture has been recorded during the unloading of the third titanium sample.

Figures 5.4.e and 5.4.f show the surface of ceramic HC before test and figure 5.4.g and 5.4.h are the results of ceramic HC wear under low-pressure and high-pressure static mode DPI test conditions respectively. Thermal images recorded after eight cycles for both low-pressure and high-pressure static mode DPI tests show no evidence of surface damage, only the deposition of release agent layer from the titanium samples is observed. The use of thermal images can help to identify surface wear after removal of Ti-6Al-4V parts in-situ. This technology can be implemented into manufacturing SPF press to monitor surface condition of ceramic dies in production.

Dynamic mode DPI test. The dynamic mode DPI test is useful to understand the material response under shearing of a titanium sample onto die surface at SPF conditions. Three runs have been conducted, where for each run a ceramic sample is tested against a Ti-6Al-4V specimen as described in section 5.1.2.2. Figure 5.5 shows the results obtained under Run 3 conditions. Thermal images before (figure 5.5.a) and after (figure 5.5.b) test highlight the transfer of boron nitride to the ceramic surface,

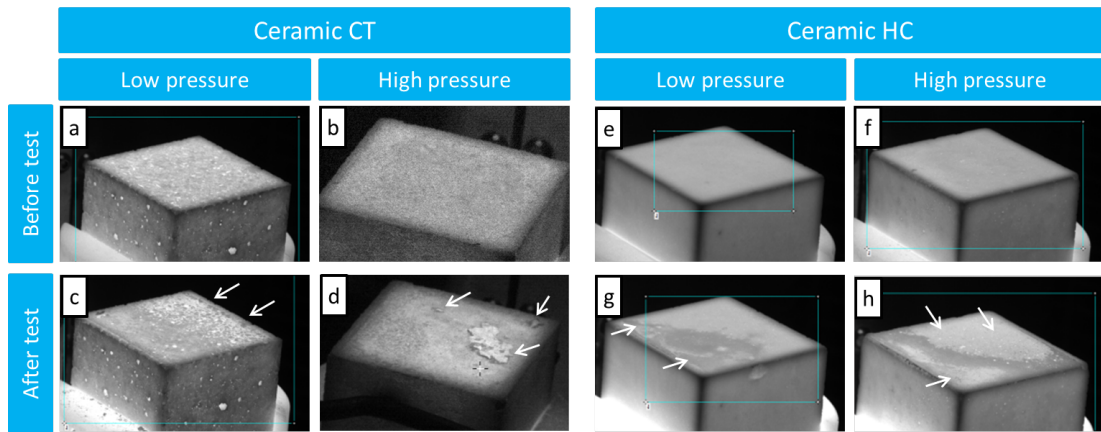


Figure (5.4) Thermal images of the ceramic CT surface before test (a,b) and after DPI static low-pressure test (c) and DPI static high-pressure test (d). Thermal images of the ceramic HC surface before test (e,f) and after DPI static low-pressure test (g) and DPI static high-pressure test (h).

with a circular track due to the rotation of the titanium sample. This is evident also in the ceramic 3D surface topography (figure 5.5.c). The titanium samples employed for the dynamic mode test show a circular track on the boron nitride layer, but no evident track on the titanium (figure 5.5.d), indicating absence of erosion under the testing conditions.

Ceramic HC, under dynamic mode DPI test, suffers from the shear stress imposed by the titanium sample which rotate on its top surface, resulting in cracking of one corner of the cube under Run 3 conditions. Figure 5.6 shows the recorded thermal image before (figure 5.6.a) and after test (figure 5.6.b) and the resulting 3D topography (figure 5.6.c), where damage is visible on one corner of the ceramic cube. Run 3 have been interrupted once an audible noise of the ceramic crack has been heard during the test. In addition, the titanium samples show a track of the rotation in both the boron nitride layer and the titanium surface; part of the titanium material has been engraved by the ceramic particles released during the cracking (figure 5.6.d).

5.1.3.2 Titanium part surface degradation

The degradation of the ceramic die surface cannot be analysed after each SPF cycle, thus the change in roughness of each Ti-6Al-4V sample is analysed as a parameter of the die wear. Due to the temperature and pressure, the titanium samples surface will mirror the die surface wear during the SPF process. The titanium part surface degradation is measured as a function of the titanium sample roughness change during the static mode DPI test.

The areal roughness parameter, $Sa_i(Ti)$, of each titanium sample as a function of

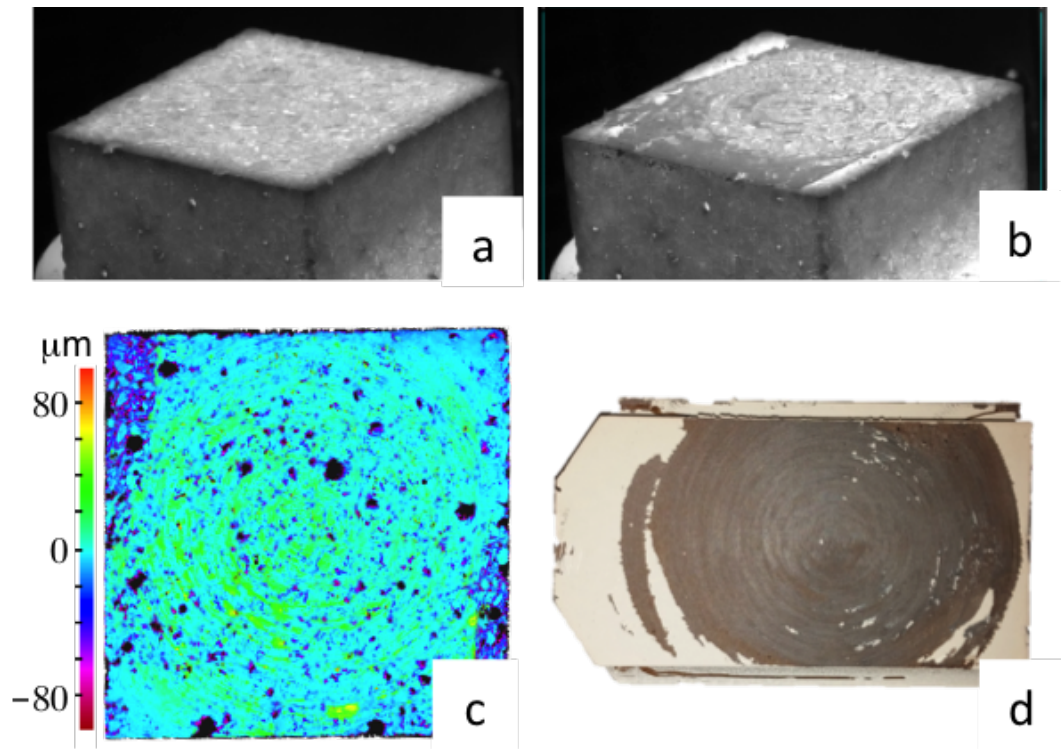


Figure (5.5) Ceramic CT surface under dynamic mode DPI test. Thermal images of ceramic CT surface before (a) and after (b) test. The ceramic CT surface topography after test in pseudo-colour (c). A titanium sample employed for the dynamic mode DPI test (d).

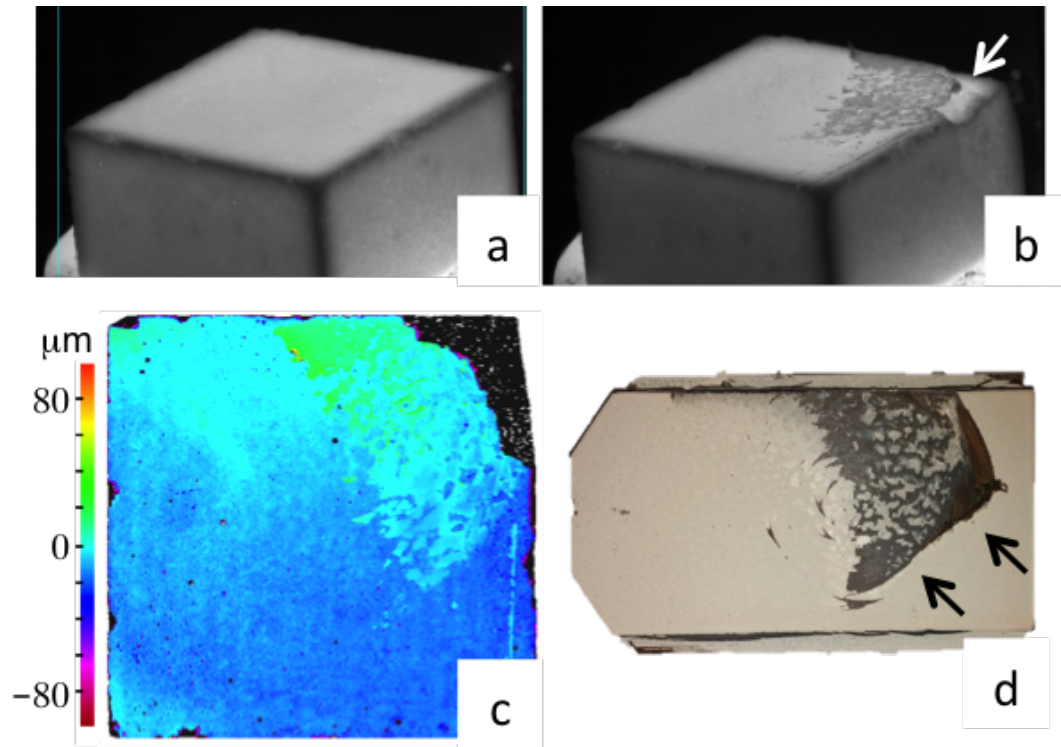


Figure (5.6) Ceramic HC surface under dynamic mode DPI test. Thermal images of ceramic HC surface before (a) and after (b) test. The ceramic HC surface topography after test in pseudo-colour (c). A titanium sample employed for the dynamic mode DPI test (d).

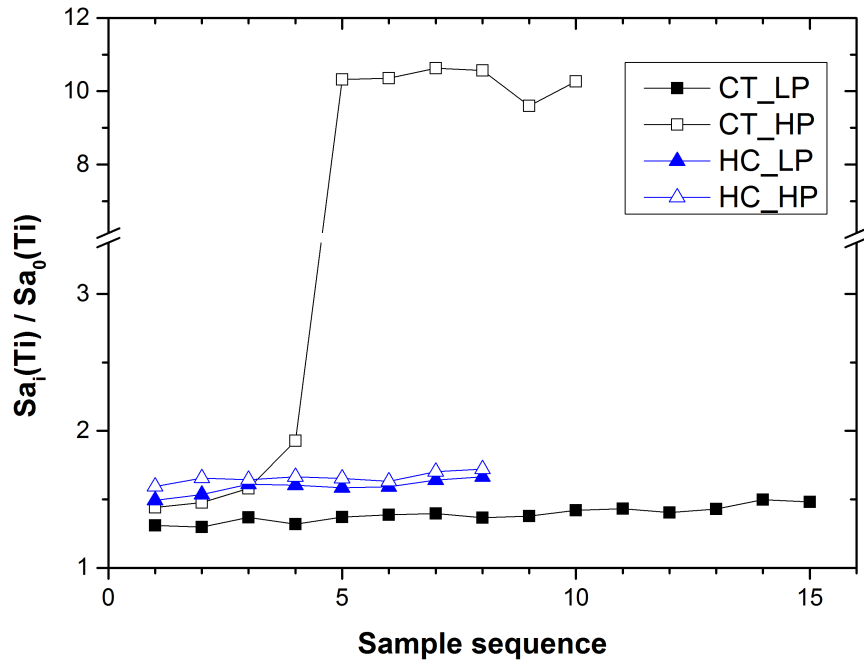


Figure (5.7) In static DPI test, titanium samples roughness normalised by their initial roughness. In black square are represented the ceramic CT surface degradation for low-pressure condition (LP, full square) and high-pressure condition (HP, empty square). In blue triangle are represented the ceramic HC surface degradation for low-pressure condition (LP, full triangle) and high-pressure condition (HP, empty triangle).

the cycle sequence has been studied. $Sa_i(Ti)$ is normalised with the roughness of the same sample before test, $Sa_0(Ti)$. The graph in figure 5.7 shows the trend of titanium surface degradation depending on the titanium sample number, which gives an idea of the die surface degradation. In figure 5.7, in black is represented the ceramic CT surface degradation under low-pressure condition (LP, full square) and high-pressure condition (HP, empty square). In the same graph, in blue is represented the ceramic HC surface degradation under low-pressure condition (LP, full triangle) and high-pressure condition (HP, empty triangle).

Ceramic CT shows low surface degradation for low-pressure condition, while the high-pressure test reveals a drastic increase in surface degradation starting from the third SPF cycle; this data confirm the damage discussed in the previous section. Ceramic HC has a similar trend for both low-pressure and high-pressure conditions, but the low-pressure condition trend is always below the one measured for the high-pressure condition.

The roughness value of a surface gives an incomplete interpretation of the surface

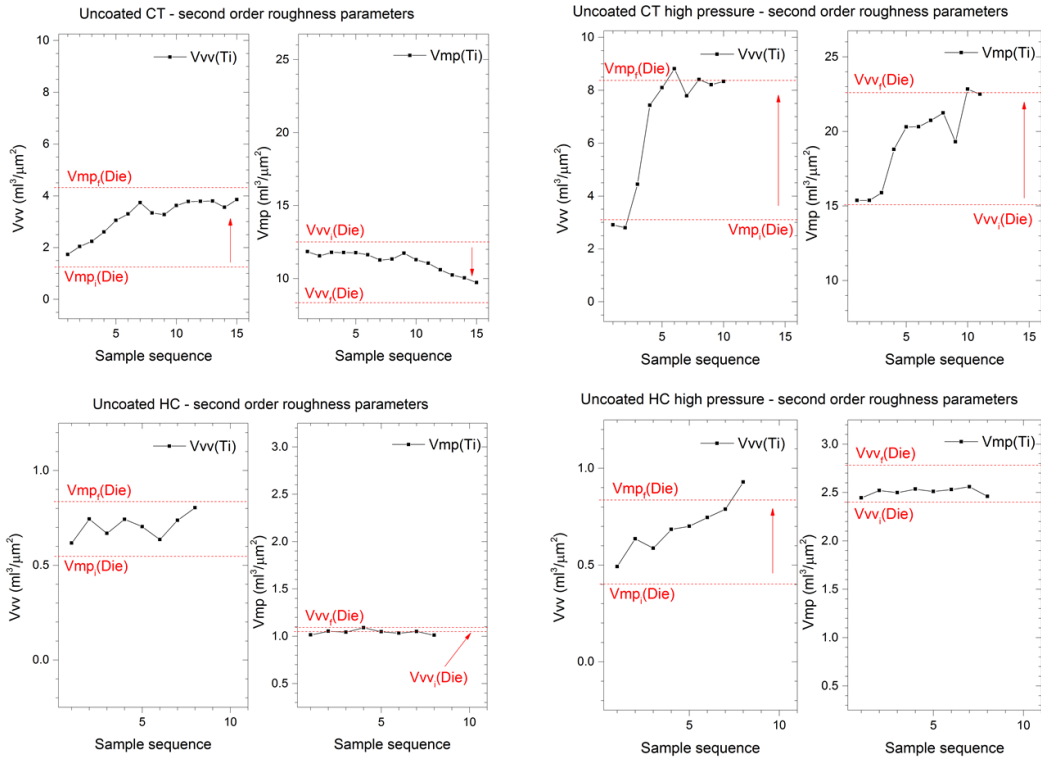


Figure (5.8) In static DPI test, the measured material peak volume per unit area, V_{mp} , and the void valley volume per unit area, V_{vv} , measured for uncoated CT ceramic tested with low-pressure (top, left) and high-pressure (top-right), and for uncoated HC ceramic tested with low-pressure (bottom, left) and high-pressure (bottom-right). For each ceramic sample the void valley volume measured on the titanium samples, $V_{vv}(Ti)$, is evaluated with the material peak volume measured on the ceramic before ($V_{mp_i}(Die)$) and after ($V_{mp_f}(Die)$) the DPI test; the material peak volume measured on the titanium sample, $V_{mp}(Ti)$, is evaluated with the void valley volume measured on the ceramic before ($V_{vv_i}(Die)$) and after ($V_{vv_f}(Die)$) the DPI test.

morphology, as two surface can present the same roughness value, Sa , being completely different in nature, as discussed in section 2.3.2.1. From the 3D surface topography it is possible to extrapolate the material volume of the surface and the void volume enclosed in the interface area of the material through the Abbott-Firestone curve [68]. The peak material volume per unit area, Vmp , and the valley void volume per unit area, Vvv , are not independent functions and are employed to get information related to the wear mechanism of the tested surface conditions. The parameters $Vmp(Ti)$ and $Vvv(Ti)$ have been measured for each titanium sample tested and for the ceramic surface before, $Vmp_i(Die)$ and $Vvv_i(Die)$, and after test, $Vmp_f(Die)$ and $Vvv_f(Die)$ (where i stands for initial and f for final values). During the DPI test the titanium sample surface is expected to mirror the die surface roughness due to superplasticity. For that reason the Vmp values of the titanium sample are compared with the Vvv values of the ceramic surface, and the Vvv titanium sample values are compared with the Vmp values of the ceramic surface.

Ceramic CT Vvv and Vmp trends are showed in figure 5.8. The ceramic material peak volume, $Vmp(Die)$, increase from 1.32 to 4.42 $\text{ml}^3/\mu\text{m}^2$ during the low-pressure static mode DPI test, which indicates transfer of material (oxides from titanium samples) on the top surface. The equivalent titanium samples Vvv values increase gradually until a saturation value after ten cycles, indicating that the wear on the ceramic surface is characterised by a sequential accumulation of material transferred from the titanium sample (where voids volume increase) into the ceramic surface (where peaks volume increase). The ceramic void valley volume, $Vvv(Die)$, decrease from 12.53 to 8.37 $\text{ml}^3/\mu\text{m}^2$ during the low-pressure DPI test, indicating that the wear mechanism is characterised by accumulation of material from the titanium sample to the ceramic surface, which goes to fill the voids on the surface. Peaks and valley distribution have been commonly used for tribological behaviour of surfaces. Vmp indicates how much material may be worn away for a given depth of the bearing curve, while Vvv may be useful when considering fluid flow or debris entrapment [96, 97, 98, 99, 100]. Under high-pressure conditions, the wear mechanism is different. The ceramic material peak volume, $Vmp(Die)$, increase together with the void valley volume, $Vvv(Die)$. The wear is characterised by accumulation of material on the top surface and generation of high volume of void valleys where the crack arises. In addition, the titanium samples values indicates that the crack on the ceramic surface arises starting from the third cycle.

Ceramic HC shows small changes in Vvv and Vmp values, validating the small wear seen in the previous section. The only considerable change is the increase of peak material volume, $Vmp(Die)$, under high-pressure conditions, due to the accumulation of material on the top surface.

5.1.3.3 Friction

The dynamic mode DPI test gives information regarding the COF between the ceramic material and the titanium sample under SPF conditions. In figure 5.9 are presented the resulting estimated coefficient of friction measured for ceramic CT (white) and ceramic HC (striped blue) depending on the testing condition. The error bars are measured as the standard deviation of the average. From the analysis of variance (ANOVA) of the means values of COF for each run, considering a significance level of 0.05 (thus a confidence level of 95%), results that the uncoated ceramic HC has a lower COF value than ceramic CT for the test conditions in Run 1 and Run 2, while there is no significant difference between the means values of COF in Run 3. Observations can be made from the results in figure 5.9:

- In Run 1 the resulting COF are 0.59 ± 0.08 and 0.27 ± 0.07 for Ceramic CT and Ceramic HC respectively;
- In Run 2 the resulting COF are 0.70 ± 0.09 and 0.44 ± 0.11 for Ceramic CT and Ceramic HC respectively;
- In Run 3 the resulting COF are 0.94 ± 0.13 and 0.89 ± 0.29 for Ceramic CT and Ceramic HC respectively;
- For lower pressure and speed (Run 1), both ceramic materials have lower COF than during the experimental conditions of Run 2 and Run 3; and
- Ceramic HC has lower COF than ceramic CT for Run 1 and Run 2, while the COF is comparable for Run 3;
- Ceramic HC COF during COF is affected by a high error bar, due to the breakage of the block during the experiment.

The COF gives an idea of the interaction at SPF temperature between the ceramic surface and the titanium sample. In addition, this data could be employed in finite element modelling for a more accurate simulation of the SPF process with ceramic materials.

5.2 Experimental validation

The validation of the DPI test is based on a parallel study that have been conducted at the AFRC [101, 102, 103, 104] at the time the author started his experimental work on uncoated ceramic materials. The objective of this research project was to provide a comprehensive overview of the process of producing a low-cost ceramic tool

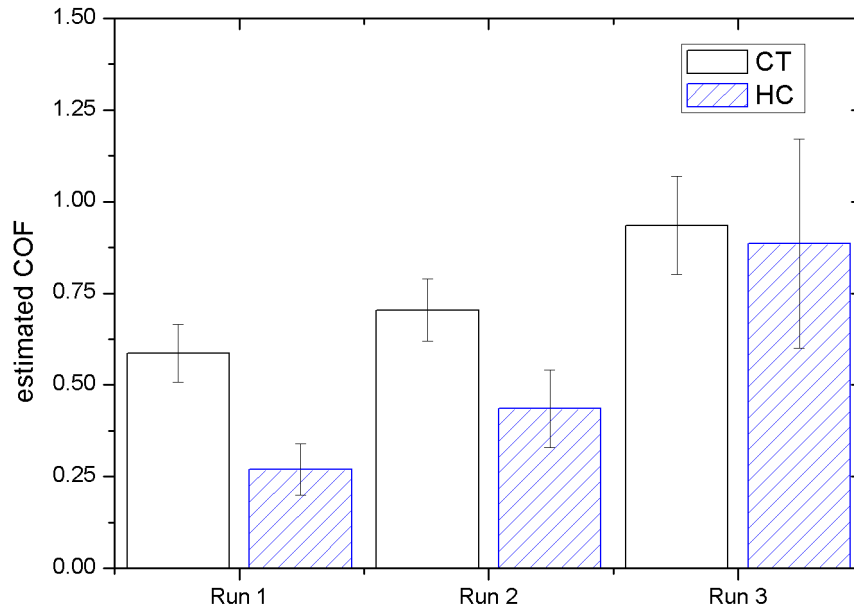


Figure (5.9) Coefficient of friction (COF) measured during the dynamic mode DPI test in each set of SPF conditions (run) for both ceramic materials.

for use in SPF including ceramic material selection, design of reinforcements using FEA, automatic generation of the pressure cycle for single sheet forming of Ti-6Al-4V material, manufacture of the die, SPF forming trials and subsequent analysis of the tool and validation of FEA with the produced parts [104]. Deliverables of the research are not in the public domain, and the author has not the right to share it, thus, in the following section only the details regarding the validation of the DPI test at a manufacturing scale are presented.

In the following sections an overview of the ceramic die design is provided. Furthermore, the design of experiment of SPF trials is presented and the analysis of ceramic surface wear is carried and compared with the outcomes from the DPI test.

5.2.1 Ceramic die design

Ceradyne Thermo-Sil 220 Castable has been down-selected as the ceramic material for SPF trials [101]. As the ultimate tensile strength of a brittle material is the stress at which the material loaded in tension cracks, when the material reaches this limit the die has therefore failed. Thus, the die design is the result of an iterative design process to produce a reinforced ceramic die with a maximum tensile stress below the material

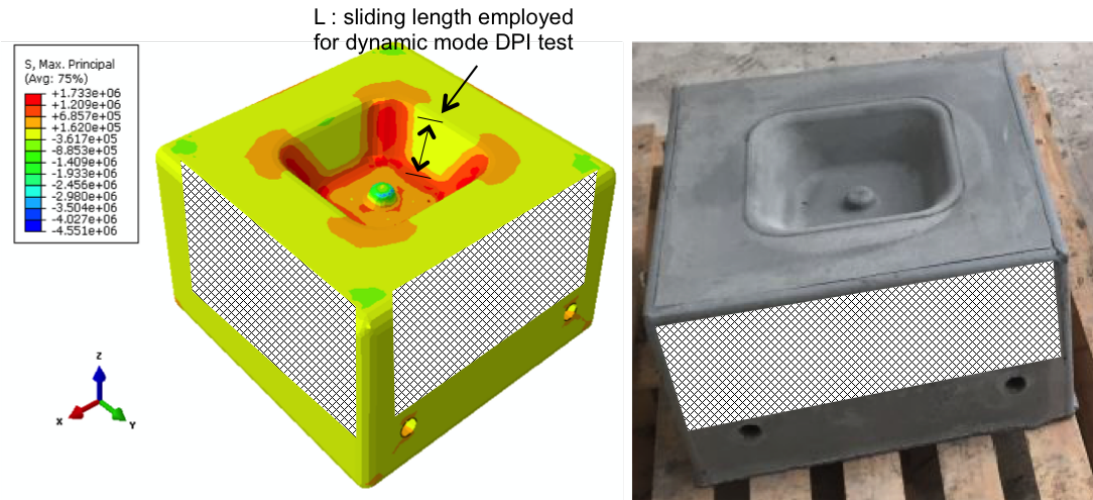


Figure (5.10) Ceramic die design for validation test from [104]: maximum principal stress in ceramic die design with applied pressure cycle (Pascal) using quartz rods as reinforcement on the left; manufactured ceramic die on the right. The reinforcement quartz rods has been omitted from in order to not infringe intellectual property. Figures from [104].

limit of 2 MPa [104]. The ceramic die geometry is presented in figure 5.10

5.2.2 Superplastic forming trials

The ceramic die has been employed to form 2.0 mm thick titanium sheet for SPF trials into a manufacturing scale 200 ton SPF press available at the AFRC. FEA has been carried from researchers at the AFRC [104] to generate the pressure cycle required to form a single sheet of Ti-6Al-4V to meet a target maximum strain rate of $3 \times 10^{-4} \text{ s}^{-1}$. The pressure profile is then applied in the models to assess the level of forming of the sheet into the die cavity and the stress distribution in the die to ensure this is below the allowable level. The SPF trials are conducted on nine Ti-6Al-4V parts at 900°C . The author cannot provide the detailed pressure curve, but the main parameters are as follow:

Pre-forming stage: from 0 to 1.2 MPa in 30 minutes;

Forming stage: hold at 1.2 MPa for 105 minutes.

The pressure value of 1.2 MPa has been employed in the low-pressure DPI static mode test. Table 5.3 shows the ceramic die working surface roughness parameters that have been measured by the author with the confocal microscope using replica method, due to the die dimensions of the die. The starting roughness of the ceramic die is comparable with the surface roughness of the ceramic samples employed during the

Table (5.3) Ceramic die roughness parameters. More details on the parameters significance can be found in section 2.3.2.1

Sa [μm]	Sq [μm]	Sk [μm]	Spk [μm]	Svk [μm]
12.15	55.41	11.21	25.66	81.76



Figure (5.11) Ceramic die after SPF trials. Figure from [104].

DPI test. Forming surface of the die and parts have been spray coated with boron nitride suspension (Kenametal, WJMB grade).

5.2.3 Results

During the SPF trials into the 200 ton SPF press adhesion between part and die caused surface ceramic material to be removed during part unloading phase. This resulted in warping of part during extraction already after the first formed part and critical ceramic die surface degradation. In addition, the die surface degradation reduced the ability to create an appropriate part-die seal on the following cycles, limiting the production run. The SPF trials have been stopped after only three cycles. Figure 5.11 shows the resulting ceramic die surface at the end of the SPF trial.

5.2.3.1 SEM inspection and comparison with the laboratory test

Figure 5.12 shows the resulting SEM images of the top surface of the uncoated ceramic substrate after low-pressure static mode DPI test. From visual inspection, the area with greater material accumulation have been selected for SEM investigation,

which is highlighted in (a). The SEM images of the top surface recorded with secondary electron detector (b) and backscattered electron detector (c) have been acquired. In addition, EDX maps of titanium (d), aluminium (e) and silicon (f) elements have been recorded. The titanium EDX map shows small amount of titanium transferred to the ceramic surface during the low pressure static mode DPI test.

Figure 5.13 shows the resulting SEM images of the top surface of the uncoated ceramic substrate after high-pressure static mode DPI test. The damaged area have been selected for SEM inspection, which is highlighted in (a). The SEM images of the top surface recorded with secondary electron detector (b) and backscattered electron detector (c) have been acquired. In addition, EDX maps of aluminium (d), silicon (e) and titanium (f) elements have been recorded. The titanium EDX map highlight a the multilayer structure of the titanium transferred during each cycle during the DPI test.

After the SPF trials a fragment of the die working surface (cf. figure 5.11) have been collected for SEM analysis. Figure 5.14 shows the resulting SEM image (a) from a sample removed from the top surface of the validation trial ceramic die after test. The SEM inspection have been carried out with the help of EDX maps of aluminium (b), silicon (c) and titanium (d) to verify the titanium transfer to the working surface of the die during SPF trials. A titanium-rich layer is visible in the SEM image and EDX titanium map, which indicates the transfer from part to working surface of the ceramic die during SPF trials. This phenomenon have been seen during DPI tests as well.

The selection of experimental parameters for static and dynamic DPI tests have been selected based on the SPF trial parameters. Under static mode DPI test two pressure levels have been chosen: during low-pressure test the pressure have been kept the same as during the forming stage of SPF forming trial, which is 1.2 MPa; while during high-pressure test a 2.0 MPa have been selected to simulate a faster SPF forming trial. The dynamic mode DPI test parameters have been defined by the ceramic die geometry employed for SPF forming trial.

The drastic wear of the ceramic die showed during SPF forming trial highlight the main limitation of the laboratory DPI test. During DPI test there is no superplastic deformation of the titanium sample onto the ceramic surface. This limitation turn out to show greater chemical interaction (adhesion) between die and part during SPF forming trial when compared to DPI test.

The SEM inspection shows deposition of titanium oxide onto the die surface during SPF trial and DPI tests. The low-pressure DPI test shows a smaller titanium oxide deposition compared to high-pressure DPI test. The latter shows a similar situation of the ceramic die surface after SPF forming trial, which suggests that the underestimation of chemical interaction of the DPI test due to the lack of superplastic deformation could be somehow corrected increasing the pressure under DPI test.

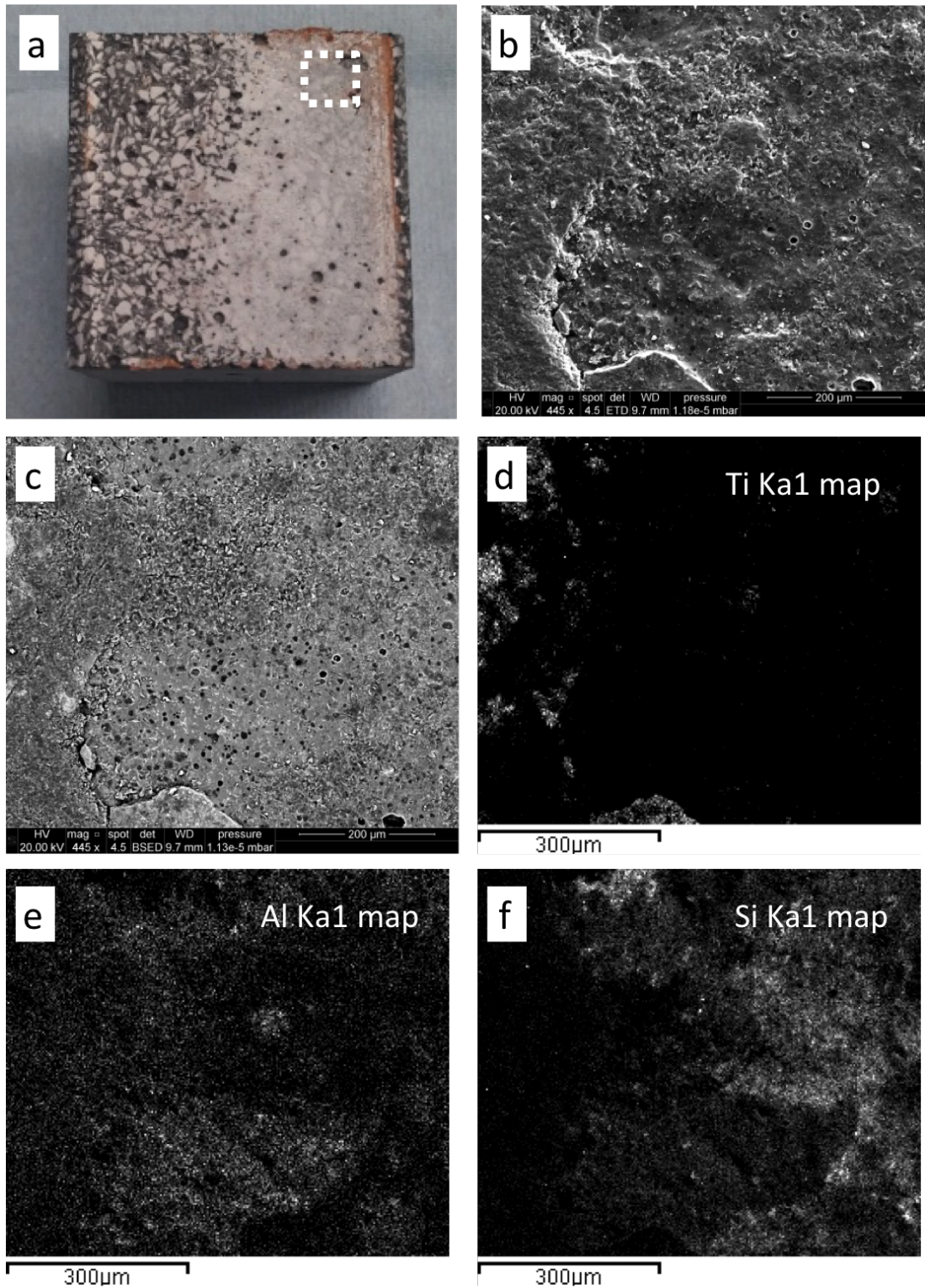


Figure (5.12) Uncoated ceramic CT after low-pressure static mode DPI test (a). The white rectangle highlights the area of interest for SEM inspection with secondary electron detector (b) and backscattered electron detector (c). EDX maps of titanium (d), aluminium (e) and silicon (f) have been recorded.

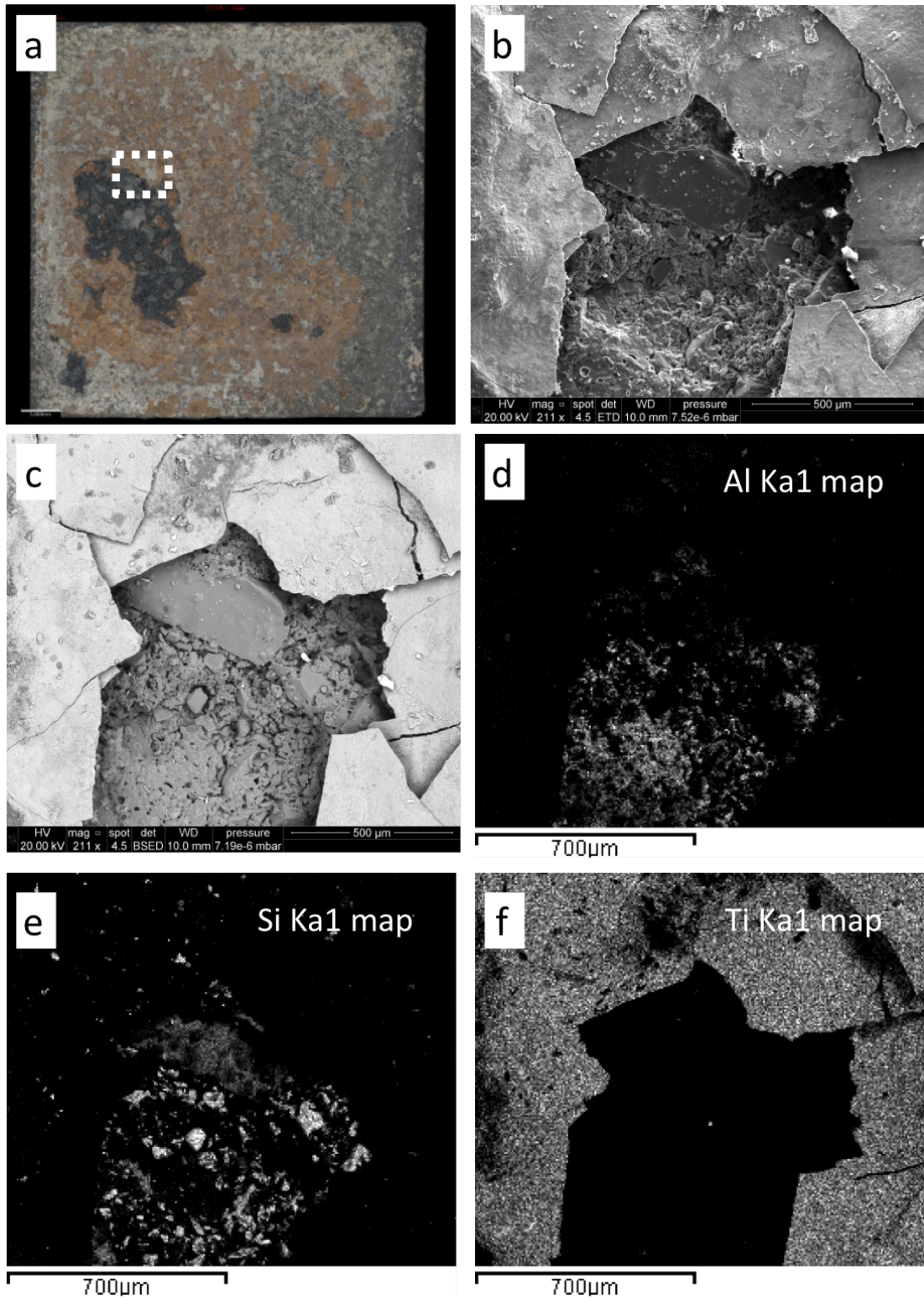


Figure (5.13) Uncoated ceramic CT after high-pressure static mode DPI test (a). The white rectangle highlights the area of interest for SEM inspection with secondary electron detector (b) and backscattered electron detector (c). EDX maps of aluminium (d), silicon (e) and titanium (f) have been recorded.

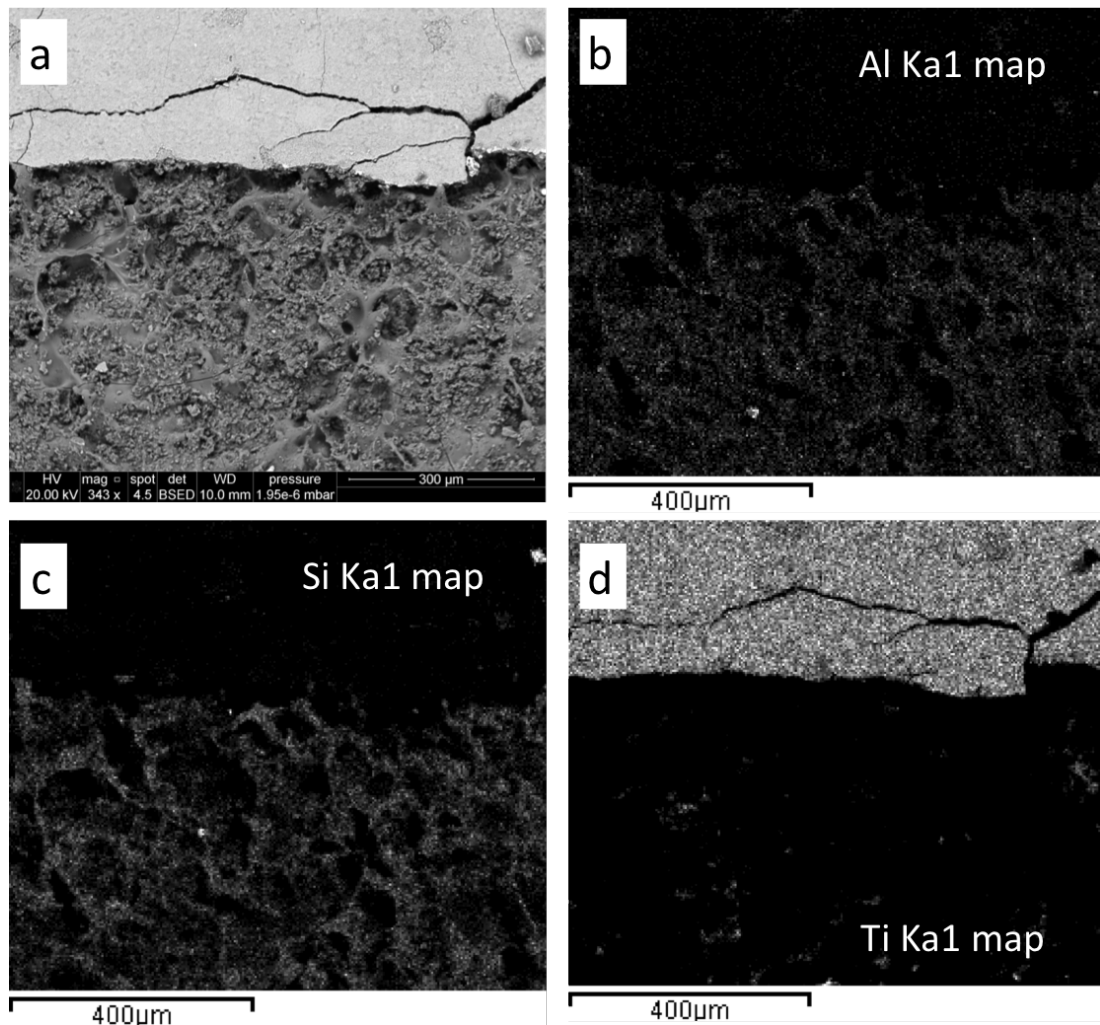


Figure (5.14) SEM image of ceramic die working surface after SPF trials (a). EDX maps of aluminium (b), silicon (c) and titanium (d) have been acquired.

The DPI test results, when compared with the SPF trial, shows similar outcomes when analysing the chemical interaction that takes place at the die-part interface, which is useful when studying the effectiveness of ceramic die protective coatings.

5.3 Conclusion

Two ceramic material have been tested to compare die material performance under SPF conditions. The current study has investigated ceramic material surface wear under SPF conditions with the DPI test, employing both static and dynamic test modes. The results of ceramic performance are important in the selection of eligible materials for SPF process applications, and for the following stages of this research project.

Under static mode DPI test, two conditions have been tested: low-pressure and

high-pressure. At low pressure, both ceramic materials show good resistance to thermal cycling and hot cracking has not been found. Under high-pressure conditions, drastic wear arise at the ceramic CT surface after only three cycles, while ceramic HC withstand the high-pressure conditions without showing any severe wear. The poor performance at high pressure are due to high porosity of the cast ceramic CT.

Under dynamic mode DPI test, three conditions have been tested in order to simulate different strain rate situations of the SPF process. In this case, ceramic CT withstand all the tested conditions with no critical wear at the surface: transfer of boron nitride from the part to the die is detected.

On the other hand, the ceramic HC sample broke during the dynamic mode test in a brittle manner. For this reason the ceramic HC has been withdrawn from further investigation on surface wear under SPF conditions. The ceramic CT material has been selected for the study on protective coatings to be employed on SPF ceramic dies, where a suitable coating should fill the surface ceramic CT porosities in order to enhance surface wear resistance. The aim of the study is to improve the ceramic CT properties under high-pressure conditions.

The results discussed in this chapter show that the DPI experiment is able to assess surface wear of ceramic materials under SPF conditions. The outcomes from the DPI experiment of ceramic CT (Ceradyne ThermoSil[®] 220) generate a wear surface baseline that will be employed for comparative studies during the protective coating investigation.

5.4 Summary

The current chapter showed the use of the DPI experiment to assess and compare the performance of two different ceramic materials under SPF conditions. The test is used to compare the key properties of two possible SPF die ceramic materials. The chapter outcomes can be summarised as follows:

- Particle-reinforced fused silica (Ceradyne ThermoSil[®] 220), ceramic CT, and infiltrated chrome silica (Horizon Chrome), ceramic HC, have been selected as ceramic die materials to be tested uncoated under the DPI test. Both static and dynamic modes have been employed in this study to assess the ceramic performance under multiple SPF conditions.
- The static mode test is composed of two level of testing pressure. Ceramic CT is wear resistant under low-pressure static condition, but cracks arise under high-pressure static condition.

- Ceramic HC shows good wear resistance under low- and high-pressure static condition.
- Dynamic mode DPI test reveals that ceramic HC integrity is drastically affected by shear stress induced by the titanium sample on the working surface, while ceramic CT does not show any critical damage.
- From 3D surface topography of ceramic and titanium sample it is possible to extrapolate material and void volume useful to understand the wear mechanisms that take place. The outcomes of the static mode DPI test in this study reveal that:
 - Wear of ceramic CT under low-pressure conditions is characterised by transfer of material from the titanium sample to the ceramic surface. This transferred material goes to fill voids on the ceramic surface.
 - Wear of ceramic CT under high-pressure conditions is characterised by accumulation of material on the die surface and generation of high volume of void valleys where cracks arise.
 - Ceramic HC under low-pressure conditions shows small changes of volume parameters, reflecting a neglecting wear on the ceramic surface.
 - Wear of ceramic HC under high-pressure conditions is characterised by a small accumulation of material on the die surface.
- Ceramic CT results have been compared with the outcomes of a SPF forming trial carried at the AFRC under a 200 ton SPF press employing the same ceramic material.

Chapter 6

Coating deposition optimisation

In this chapter petalite has been selected as a protective coating candidate for SPF ceramic dies. Two firing procedures have been investigated and the resulting coatings are tested with the DPI test. Ceradyne ThermoSil[®] 220 has been selected from previous chapter as substrate ceramic die material. Two firing procedures (firing A and firing B) have been used, which differ in terms of temperature and time. The DPI test helps to evaluate the ideal firing procedure. Part of this work has been presented at the EuroSPF 2016 conference [105] and it has been published in the *Materialwissenschaft und Werkstofftechnik* journal [106].

6.1 Introduction

The following study aims to evaluate two firing procedures for a protective coating material that have been selected and investigated by the author at the Advanced Forming Research Centre (AFRC) for SPF ceramic dies [107, 108, 109, 110]. The substrate ceramic material is made of Ceradyne ThermoSi[®] 220 and the coating is a low CTE aluminosilicate: petalite. Outcomes from the literature review in chapter 2 show that limited work has been conducted on protective coatings for SPF dies, in particular for ceramic dies. In addition, limited coating solutions are available in the market to fulfil the restrictions of the SPF process (thermodynamically stable at high temperature, chemically inert with titanium alloys, thermal shock resistant and low CTE). A protective coating for SPF ceramic die have been developed and patented from the Boeing Company in collaboration with the University of Missouri-Rolla [111, 78, 112, 38]. The protective coating is made of cordierite; the coating developed is a low thermal expansion ceramic glaze deposited via thermal spray. Cordierite is a ternary system composed of magnesium oxide, aluminium oxide and silicon oxide.

Due to the lack of information available, an extended coating material review has been conducted and it is available in appendix A, where coatings employed in application

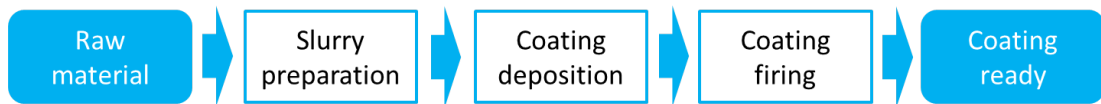


Figure (6.1) Flow chart of the coating deposition procedure.

similar to SPF that could be of interest for this study, are discussed.

For the research work conducted in this chapter, the author has proposed to select a low thermal expansion ceramic glaze similar to cordierite, which is petalite. Petalite is a ternary system composed of lithium oxide, aluminium oxide and silicon oxide. Further details about petalite can be found in section A.2.2. Petalite coating has similar property as cordierite, but it has not been tested (or patented) for SPF applications and the deposition technique employed by the author (dip coating) does not require capital investments.

The first part of this study focuses on the coating deposition technique: the variables involved in the deposition and the difference between the two procedures. The second part of the chapter focuses on the use of the DPI test to compare the resulting coatings obtained with different deposition parameters. Results will show the effectiveness of the DPI test to evaluate the same protective coating material performance, depending on the deposition procedure employed. The results show how effective the DPI test can be making strategic decisions on the selection of coating deposition parameters.

6.2 Coating deposition procedure

Once the protective coating material has been selected, a coating deposition procedure is generated (see figure 6.1). The deposition comprises three main steps:

1. Optimisation and preparation of the slurry (heterogeneous mixture of the solid coating powder dissolved in a liquid phase);
2. Deposition of the slurry on the ceramic substrate;
3. Thermal treatment (firing) of the deposited coating in order to achieve sintering of solid particles within the coating phase and between the coating and the ceramic substrate.

The coating raw material is supplied by MinChem Ltd (UK) as a white powder 325 mesh ($-75 \mu\text{m}$) milled and tray-dried white powder with average particle size of $5 \mu\text{m}$. The particle size distribution has been measured (cf. figure 6.2) with a laser diffraction particle size analyser (Malvern Mastersizer 2000), which shows a bimodal distribution

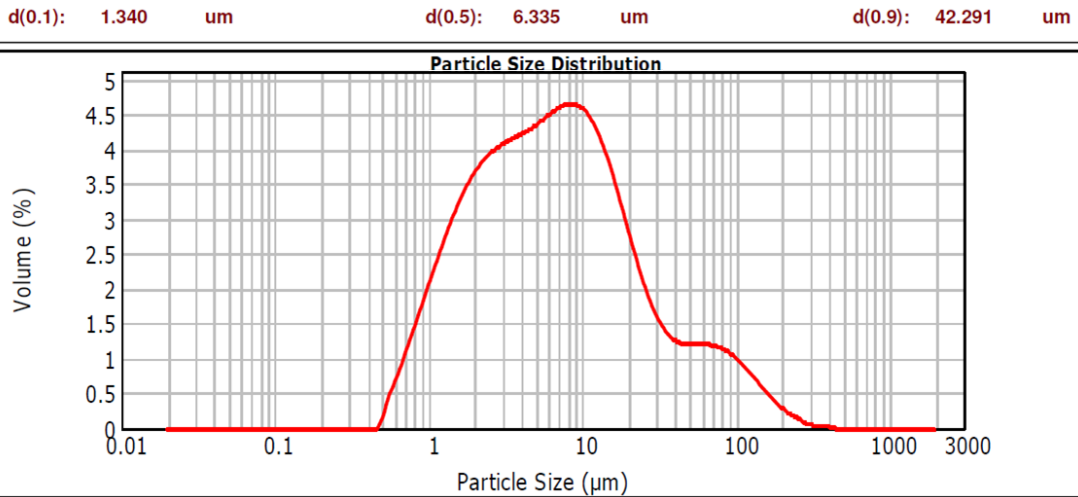


Figure (6.2) Particle size distribution of the powder raw material.

where the average particle size is around 5 μm and a larger particles size is centred around 50 μm .

A solubility study has been conducted by the author [109, 110] on the coating powder to determine solvent type and optimal concentration of the slurry for the deposition, where results showed that the optimised slurry is a 30% wt of coating powder dissolved in water. The solubility study described in [109] has been carried out to determine suitable solvent(s) for the dip coating deposition technique. The solubility test has been carried out by pouring 100 mL of solvent in a beaker then adding 1 mg of petalite powder at a time, mixing and comparing slurry rheology on a smooth plate inclined 30°. The viscosity of the slurry have been calculated as the time employed to run a distance of 5.0 cm on the inclined plate. Solvents employed were distilled water, ethanol, isopropyl alcohol, acetone and methanol. The second step is a wettability test, checking the contact angle between a ceramic sample and a drop of the slurry purred on it. Tests have been conducted at 20°C and atmospheric pressure.

The coating is deposited via dip-coating technique and deposition parameters have been studied and optimised in a previous work by the author [109]. Once the slurry concentration has been selected, a deposition procedure has been developed. Small ceramic samples (surface 1.0 x 2.5 cm) of Ceradyne ThermoSil[®] 220 have been employed for deposition trials. On each sample, a mask have been applied on part of the surface to coat, in order to have a coating step for thickness control. In order to achieve a target thickness of 300 μm with standard deviation below 10 μm the deposition procedure is the following:

1. Prepare the slurry;

2. Dip the ceramic sample into the slurry and keep it for 30 seconds;
3. Remove the ceramic sample from the slurry without turning it. Allow the excess of slurry to drip from the ceramic surface for 30 seconds, and then turn the sample;
4. Leave the sample to dry in air for at least 24 hours.

After deposition of the slurry, the coating is left to dry in air before the final step of the deposition. The firing step is a thermal treatment where solid state sintering occurs. This step is necessary to sinter the coating particles with each other and with the substrate, in order to obtain low porosity and good adhesion to the ceramic substrate. The firing cycle has been developed by the author in previous works [109, 110] and it comprises three stages (cf. figure 6.3):

Stage 1: The ceramic substrate with the dried slurry is introduced into the furnace and they are heated up to the firing temperature and left for a certain amount of time. During this stage solid state sintering of the coating particles occurs.

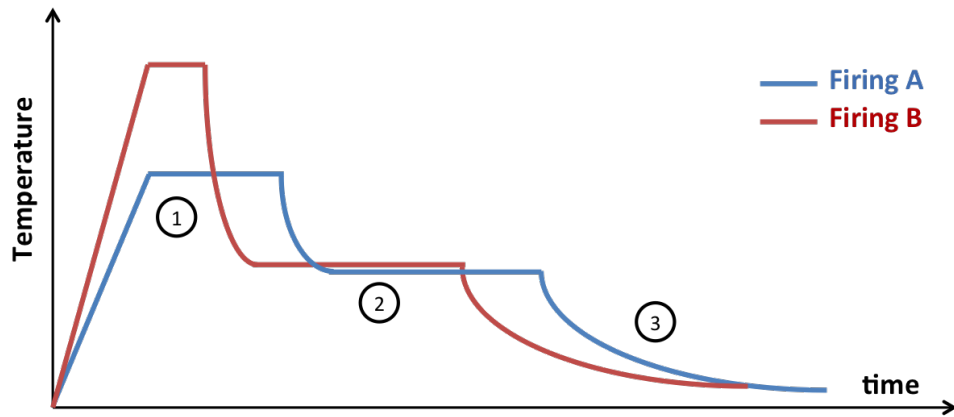
Stage 2: The temperature is dropped to 500°C and kept for 120 minutes. This stage helps the coating to release internal thermal stresses to avoid cracking caused by thermal shocks.

Stage 3: The furnace is turned off and the coated sample left inside to cool down.

In this investigation two procedures have been developed: firing A and firing B. The slurry preparation and coating deposition are kept the same, while the firing cycle is slightly different. In the firing process, temperature of firing and time are the factors that affect the sintering of the coating, which has been optimised in [109], while temperature and time for thermal stress releasing are kept the same for both the firing procedures. The temperature of firing A is lower than the temperature of firing B, but it has longer firing time.

The crystallography of the coatings obtained with firing A and firing B is investigated with a X-Ray diffractometer (Bruker D8 Advance XRD). The XRD uses the $\text{CuK}\alpha$ radiation (1.5418 Å) with a Ni filter and source potential and current of 40 kV and 40 mA respectively. XRD patterns of coating powders as received and after thermal treatment with firing A and firing B respectively have been obtained by step scanning from 10° to 65° 2θ in steps of 0.040° and counting time of 2 s per step.

The resulting XRD profiles are shown in figure 6.4; the XRD pattern of the raw material shows a high degree of crystallinity, because of the absence of the typical amorphous signal at small angles. The raw material shows high content of crystallised petalite (the main element of the selected coating material) and some of its derived



Parameters	Firing A	Firing B
Firing temperature [°C]	1100	1350
Firing time [min]	60	10
Releasing temperature [°C]	500	
Releasing time [min]	120	

Figure (6.3) Firing cycles and parameters.

oxides (α -spodumene and β -quartz). The XRD pattern of powder resulting from firing A indicate an high degree of crystallinity of β -spodumene, (the desired crystallographic form because of its CTE) with some trace of β -quartz, while firing B results in a totality of β -spodumene. The XRD shows that the thermal treatment, in addition to solid sintering of coating particles, causes a crystallographic transformation of the coating material from petalite to β -quartz and β -spodumene. The XRD pattern of firing A, compared with the one of firing B, indicates that the crystallographic transformation is not complete, as β -quartz peaks are recorded, while the firing B XRD pattern shows no trace of it.

6.3 Experimental conditions

The ceramic substrates are cubes (50.0 x 50.0 x 50.0 mm) refractory materials made of ceramic CT (studied in chapter 5), which is known in the market as Ceradyne ThermoSil® 220. The coating deposition procedure and the resulting coatings from firing procedures A and B are showed in figure 6.5. The resulting coating from firing A, named coating PET-A, is a white, opaque and dense layer that presents good adhesion to the ceramic substrate. The coating obtained with firing B is a translucent and dark

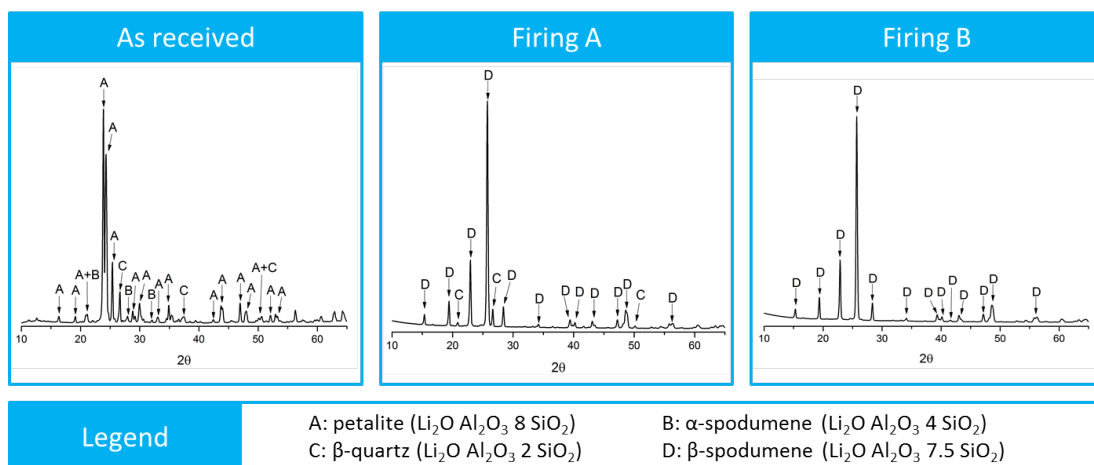


Figure (6.4) XRD pattern of coating raw material as received, after thermal treatment with firing A and firing B respectively.

well-adhered coating, which is labelled coating PET-B.

The starting surface roughness of the ceramic samples as received is $(8.12 \pm 0.44) \mu\text{m}$, thus rough enough to enable adhesion of the slurry to the ceramic surface during the deposition process. The measured roughness of the ceramic coating surface after firing is $(31.76 \pm 0.88) \mu\text{m}$ for firing A and $(59.2 \pm 1.7) \mu\text{m}$ for firing B respectively, thus further surface finishing would be needed if the coating will be introduced into production.

As in section 4.4, the metal sheet samples are made of commercial SPF grade Ti-6Al-4V alloy with dimensions 40.0 x 60.0 x 1.2 mm, which are cleaned and sprayed with BN (Kenametal, WJMB grade) suspension before the DPI test.

In this study the static mode DPI test is employed, and, as discussed in section 5.1.2.1, the trials consist on a series of thermo-mechanical cycle loads at standard SPF conditions. Time, temperature and applied load are the low-pressure condition static mode DPI test (cf. figure 5.1 and table 5.1). The rationale behind the decision to employ low-pressure experimental conditions is to keep a conservative approach to test the protective coating performance. The use of high-pressure conditions could make difficult to interpret the coating performance: if the coating fails, it would be difficult to explain if it failed because of the substrate failure or because of intrinsic failure mechanisms of the coating.

6.4 Results

6.4.1 Coating hot cracking and surface degradation

Figure 6.6 shows the resulting surface of coating PET-A after firing (figure 6.6.a), after unloading of the titanium sample under static mode DPI cycles (figures 6.6.b and

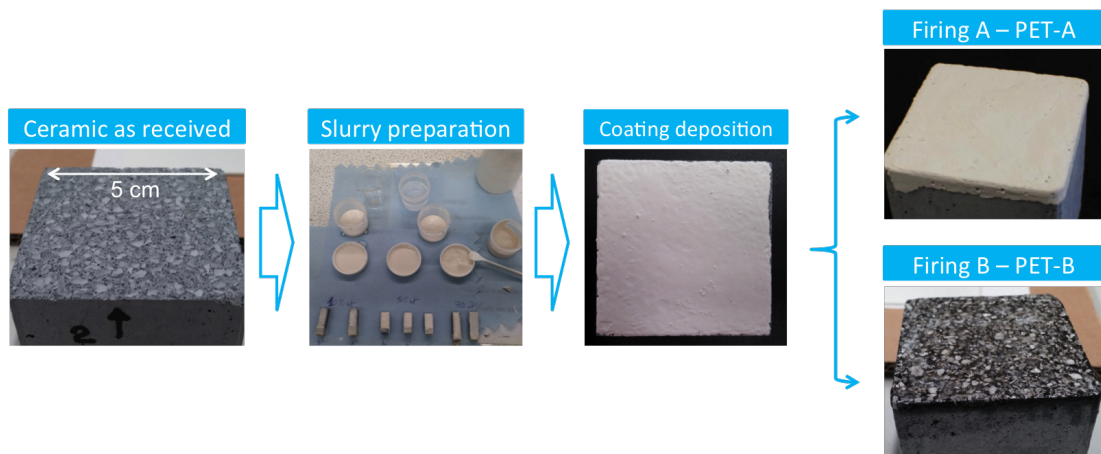


Figure (6.5) Coating deposition flow chart: the ceramic material is cast in cubes; the coating slurry is prepared with appropriate concentration; the coating is deposited by dipping and then fired. Two firing procedures have been studied.

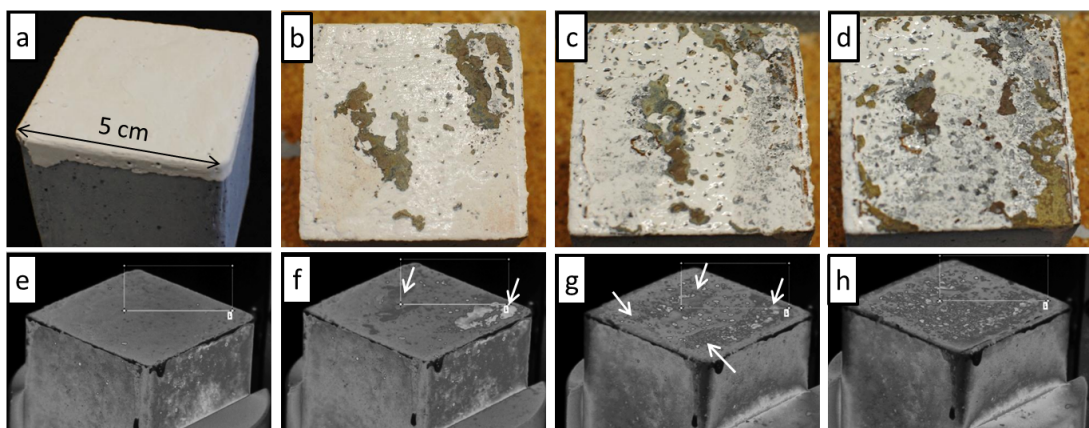


Figure (6.6) Coating PET-A before low-pressure static mode DPI test (a) and after one cycle (b), four cycles (c) and seven cycles (d). The test has been interrupted after seven cycles. Thermal images of coating PET-A before test (e), after one cycle (f), four cycles (g) and seven cycles (h) are presented.

6.6.c), and at the end of the experiment (figure 6.6.d). The coating is characterised by a white and opaque phase.

Thermal images of the coated ceramic sample (cf. figures 6.6.e - 6.6.h) revealed that the coating material has a very low emissivity compared with the substrate ceramic material, which results in a high contrast image when the surface starts to deteriorate. Wear is visible in thermal images, but it is not possible to distinguish between wear mechanisms.

Figure 6.7 presents the coating PET-B surface before and after the low-pressure static mode DPI test. The coating PET-B pseudo-colour and true-colour surfaces are

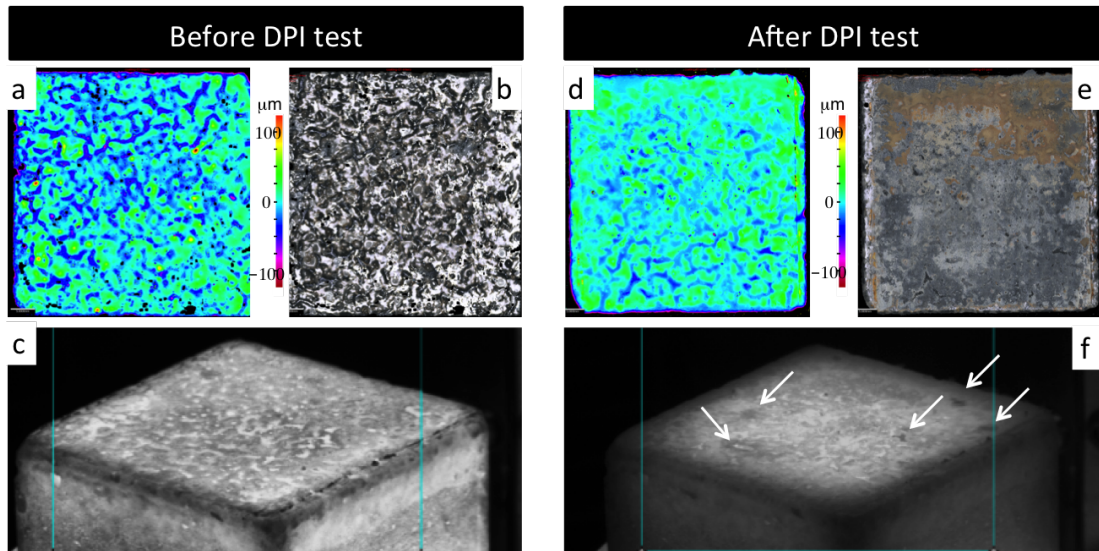


Figure (6.7) The coating PET-B surface before test is showed in pseudo-colour (a), true-colour (b) and the corresponding thermal images (c). The same surface after 10 cycles with low-pressure static mode DPI test is presented in pseudo-colour (d), true-colour (e) and thermal image (f).

presented in figure 6.7.a and 6.7.b respectively. In addition, the acquired thermal image (figure 6.7.c) is recorded to complete the picture of the surface condition of coating PET-B before DPI test. The coating exhibits remarkable waviness due to nucleation of the coating during the firing process. This aspect is absent in coating PET-A due to the different firing procedure.

After test the coating has been analysed with microscope confocal imaging technique and the resulting pseudo-colour and true-colour surface topographies are presented in figures 6.7.d and 6.7.e respectively. The pseudo-colour image shows that the coating kept part of its waviness during the test. True-colour and thermal images (cf. figure 6.7.f) of the coating surface recorded after the tenth cycle show localised accumulation of scale built-up on the surface.

6.4.2 Titanium part surface degradation

Due to the high temperature employed in the DPI test of titanium alloys, the degradation of the ceramic die surface with confocal microscope imaging cannot be analysed after each DPI test cycle, thus the change in roughness of each Ti-6Al-4V sample is investigated as a parameter of the die wear. The titanium samples, due to their superplasticity, after the static mode DPI test, reflect the die surface asperities. The roughness parameters of the titanium samples have been studied as a function of the cycle number, and normalised with their starting roughness, $Sa_0(Ti)$. Figure 6.8 shows the

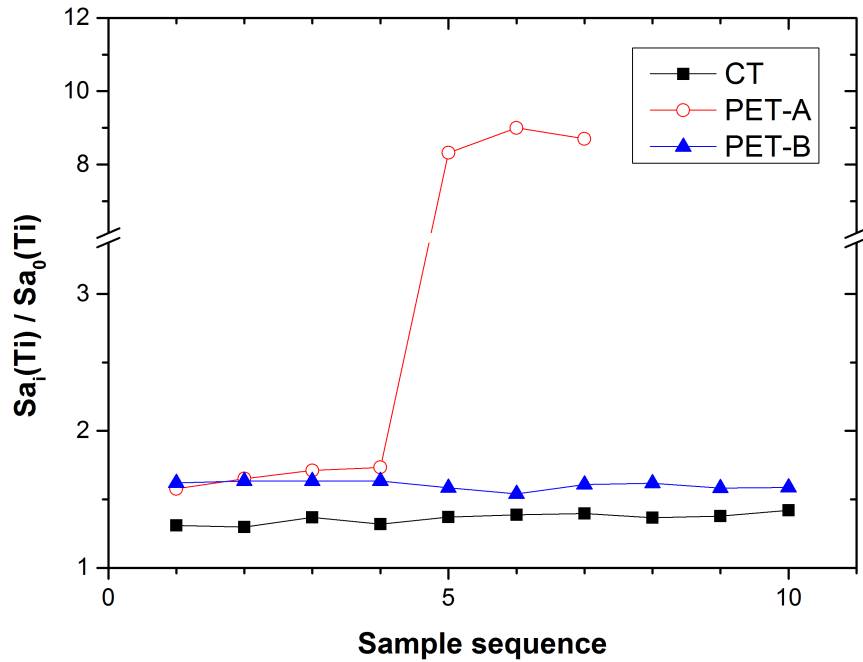


Figure (6.8) Titanium samples roughness normalised by their initial roughness. Black squares represent the ceramic CT surface degradation for low-pressure condition. Red circles represent the ceramic CT with coating PET-A surface degradation. Blue triangles represent the ceramic CT with coating PET-A surface degradation. All the samples have been tested in low-pressure static mode DPI test conditions.

resulting normalised values of the titanium surface roughness trends, $Sa_i(Ti)/Sa_0(Ti)$, from the low-pressure static mode DPI test for the uncoated ceramic (as reference) in full black squares, the coating PET-A in empty red circles and the coating PET-B in full blue triangles.

For coating PET-A, the titanium sample normalised surface roughness starts from a value of 1.5, similar to coating PET-B, but the trend suddenly changes and the value increases almost one order of magnitude after four cycles, indicating wear of the coating. With coating PET-B, the titanium sample normalised surface roughness is higher than samples tested with the uncoated ceramic, but the trend is almost flat with small fluctuations around the value of 1.6. The results indicate that coating PET-A is affected by drastic wear after four titanium samples, while coating PET-B shows a steady wear condition. In addition, coating PET-B wear is greater than wear of the uncoated surface (ceramic CT).

As discussed at page 70 the Vmp values of the titanium sample are compared with the Vvv values of the coating, and the Vvv titanium sample values are compared with

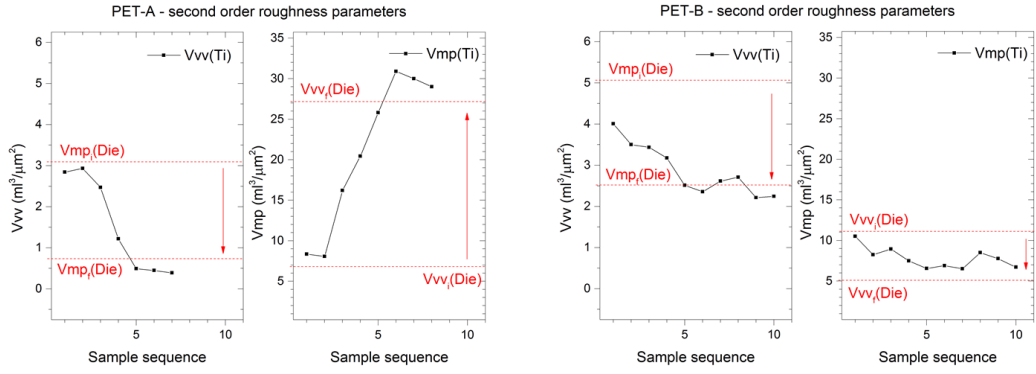


Figure (6.9) The measured material peak volume per unit area, Vmp , and the void valley volume per unit area, Vvv , are shown for coating PET-A and PET-B. For each coating the void valley volume measured on the titanium samples, $Vvv(Ti)$, is evaluated with the material peak volume measured on the coating before ($Vmp_i(Die)$) and after ($Vmp_f(Die)$) the DPI test; the material peak volume measured on the titanium sample, $Vmp(Ti)$, is evaluated with the void valley volume measured on the coating before ($Vvv_i(Die)$) and after ($Vvv_f(Die)$) the DPI test.

the Vmp values of the coating.

Coating PET-A Vvv and Vmp trend (cf. figure 6.9) shows that the coating's material peak volume, $Vmp(Die)$, decreases, while the coating's void valley volume, $Vvv(Die)$, increases during the DPI test. This trend denotes erosion of material from the asperities, thus a decrease of the die's Vmp value, and removal of material from the coating generating new (or bigger) voids and/or porosities. The values measured on the titanium sample shows that wear starts after only two cycles.

Coating PET-B Vvv and Vmp trends are both decreasing during the DPI test. The coating material peak volume, $Vmp(Die)$, decreases from 5.07 to $2.52 \text{ ml}^3/\mu\text{m}^2$ during the DPI test. The equivalent titanium sample Vvv values decrease gradually, indicating that the wear on the coating is denoted by a sequential erosion of coating asperities. The coating void valley volume, $Vvv(Die)$, decreases from 11.23 to $5.27 \text{ ml}^3/\mu\text{m}^2$ during the DPI test. The equivalent titanium sample Vmp values decrease gradually, indicating a sequential filling of porosities on the coating surface. In addition, the coating PET-B $Vvv(Die)$ change during the DPI test is smaller than the change seen in coating PET-A, denoting that wear rate is higher for coating PET-A than coating PET-B.

6.4.3 Chemical interactions

During the SPF process scale builds up on the die surface. Cross section and top surface SEM images are taken to investigate the chemical interaction at the die-part interface. Ceramic samples have been prepared for SEM investigation as explained in

section 4.2.3.

The coating PET-A after test is showed in figure 6.10.a; a top view surface area (X) and a cross section area (Y) have been prepared and inspected with SEM. The cross section of the coating after low-pressure static mode DPI test is showed in figure 6.10.b. The coating shows multiple cracks parallel to the substrate surface, which are due to weak intra-coating bonding, causing spallation. In order to avoid cracks generation during sample sectioning, the sample have been mounted in epoxy resin before cutting the cross section. In addition, sample grinding have been repeated multiple time to avoid artefacts (cf. section 4.2.3). The top view area in figure 6.10.c and EDX maps relative to titanium (d), aluminium (e) and silicon (f) show the titanium accumulation on the ceramic surface after the DPI test.

Figure 6.11.a shows the resulting coating PET-B cross section after firing B, which exhibits some porosity. The coating-substrate interface is not clearly identifiable: the coating is composed of an external layer of about $200\ \mu\text{m}$, and a $200\ \mu\text{m}$ intermix layer fused with the ceramic substrate. The external porosity may act as a crack starting point, but the intermix layer indicates a good adhesion of the coating to the substrate. The intermix layer is composed of ceramic substrate matrix and melted coating. Figure 6.11.b shows the coating PET-B cross section after low-pressure static mode DPI test. The cross section area reveals a $50\ \mu\text{m}$ oxide layer built-up on top of the coating, were titanium have been transferred from the Ti-6Al-4V during the simulated SPF cycles. The titanium presence have been identified through EDX spectra of the oxide layer at the points A, B and C as indicated in the figure. Spectra at the point A and B show the titanium presence, while spectrum C (acquired on the coating) shows only the main constituent elements of the coating. Gold signal is due to the 10 nm coating deposited on the non conductive sample before SEM analysis. Figure 6.11.c presents the top view area of coating PET-B after low-pressure static mode DPI test. In addition, titanium EDX map (d) shows the transfer of titanium on top of the coating during the test.

6.5 Conclusion

A protective coating for Ceradyne ThermoSil[®] 220 ceramic SPF dies, made of a low CTE aluminosilicate, has been investigated in this chapter. Two firing procedures have been developed and the resulting coatings have been tested under SPF conditions with the low-pressure static mode DPI test. The outcomes of the DPI test regarding coating performance are important for the selection of eligible protective coating solutions for SPF ceramic dies.

The coating deposition procedure is divided into three steps: preparation of the slurry; deposition of the slurry on the substrate; firing of the slurry. For the firing

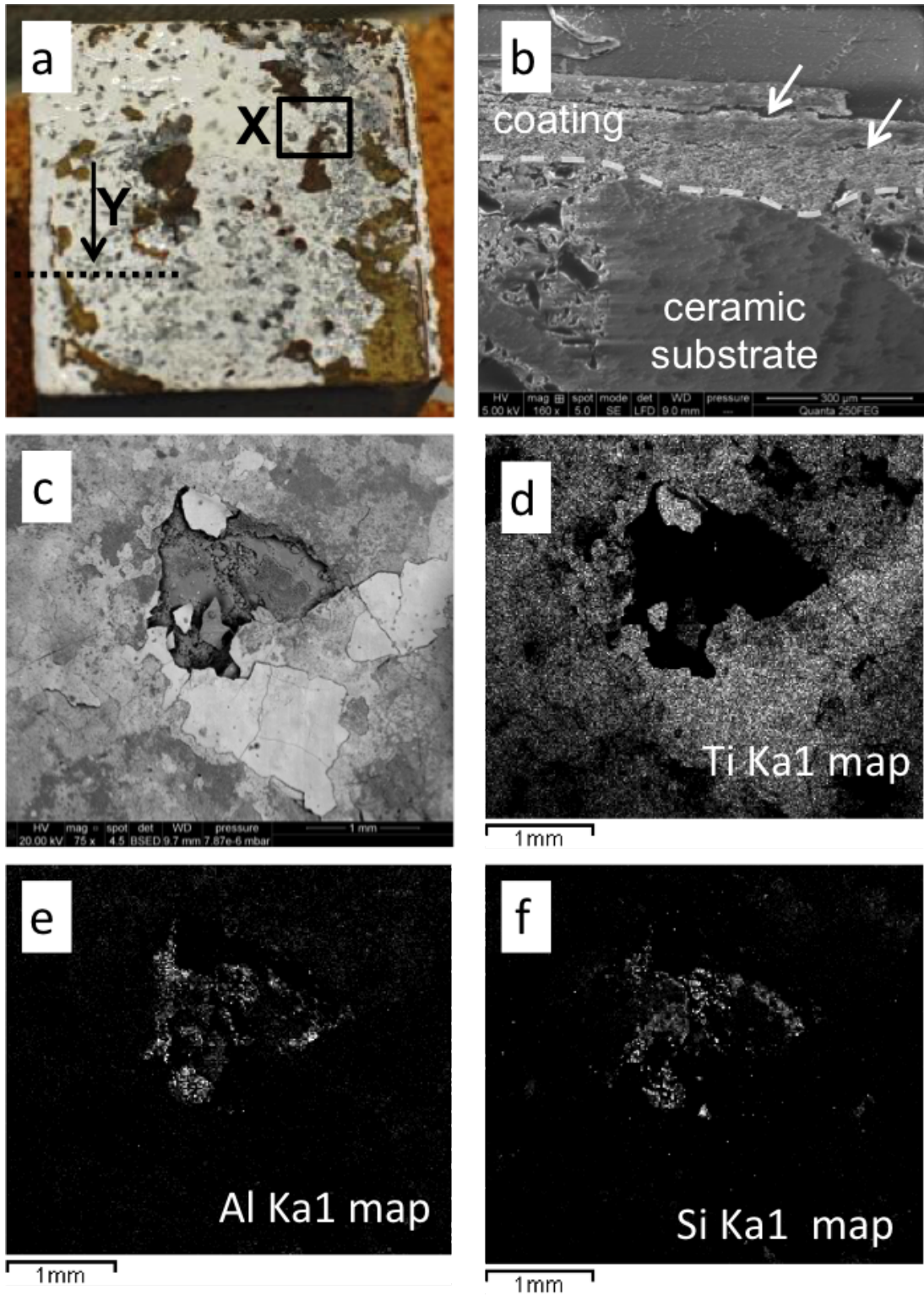


Figure (6.10) Coating PET-A after low-pressure static mode DPI test is presented in (a). (b) is the cross section of the coating (marked as Y), (c) is the top view highlighted as X and EDX maps of the top view have been acquired for titanium (d), aluminium (e) and silicon (f).

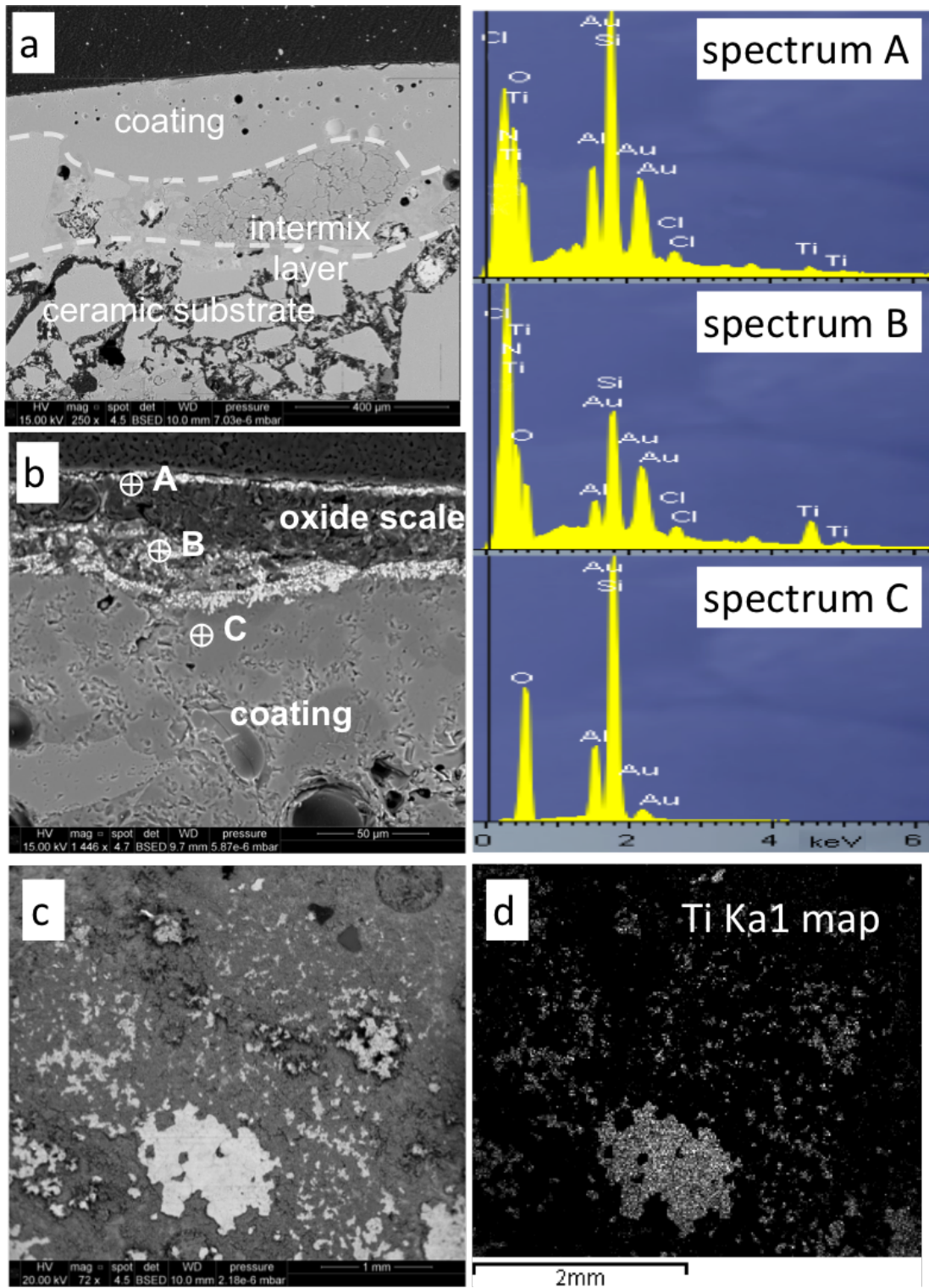


Figure (6.11) Coating PET-B before test cross section is showed in (a). The cross section of the coating after low-pressure static mode DPI test is showed in (b) and the acquired EDX spectra at the points A, B and C are presented. (c) is the coating PET-B top surface after low-pressure static mode DPI and the titanium EDX map is presented in (d).

step two procedures have been developed, labelled as firing A and firing B. The firing procedures differ in temperature and time, where firing A employ a thermal treatment at lower temperature but longer time than firing B. The resulting coating from firing A, coating PET-A, is white and opaque. The coating obtained with firing B, coating PET-B, has a dark translucent phase and the surface is characterised by waviness due to nucleation of the coating particles during the firing process.

Wear is identified on coating PET-A surface through thermal images. In addition the roughness study indicates that wear is characterised by removal of material from the coating. SEM images explain the loss of material, which is due to the presence of cracks in the coating parallel to the substrate surface, thus at each titanium removal a layer of coating is removed.

Coating PET-B shows good adhesion and resistance during the low pressure DPI test. The roughness study suggests that, during the test, peaks of coating material are smoothed and valleys are filled with material (boron nitride and oxides) released from the titanium sample. Cross section SEM images of the coating reveals an intermix layer between the coating and the ceramic substrate that enhances the adhesion of the coating. After the DPI test, a multilayer of oxides grows on the top of the coating.

The outcomes from this study show that the coating resulting from firing B has a better adhesion to the substrate, due to the intermix layer presence. Furthermore, no cracks parallel to the substrate are found on coating PET-B, thus the resulting coating does not suffer spallation. Coating PET-B has then been selected for further studies on protective coating performance under dynamic mode DPI test, and results will be shown in chapter 7.

6.6 Summary

Ceradyne ThermoSil[®] 220 has been selected in chapter 5 to be employed for the protective coating study. In this chapter petalite protective performance have been assessed with the DPI experiment. Petalite have been deposited through dip coating technique starting from a slurry (30% wt. and water as solvent). Two firing procedures, which differs in firing temperature and time, have been developed and the resulting coatings have been tested under SPF conditions. Coating PET-A has been obtained from a lower firing temperature and a longer firing time than coating PET-B. The two coatings have been tested under the DPI test and results have been compared with the uncoated ceramic material. The chapter outcomes can be summarised as follow:

- Coating PET-A is white and opaque after firing. During the test the coating is affected by drastic wear after four titanium samples. Roughness studies and SEM image analysis showed that wear is characterised by removal of material.

- Coating PET-B is dark and translucent after firing. During the test the coating peaks are smoothed and valleys are filled with material (boron nitride and oxides). SEM images show an intermix layer between the coating and the substrate, indicating good adherence. In addition, a multilayer of oxides is deposited on top of the coating, showing chemical interaction between the coating and the titanium sample.
- The surface degradation study shows that coating PET-B has a better performance under SPF condition than coating PET-A, but the uncoated ceramic CT wear is smaller than that of coating PET-B.

Chapter 7

Performance evaluation of protective coating solutions

In this chapter different coating solutions have been tested under SPF conditions employing the DPI experiment. The coated ceramic materials are tested in both static and dynamic mode and the results will show the effectiveness of the DPI test to make strategic decisions on the use of protective coatings materials for SPF ceramic dies.

7.1 Introduction

In the following study three coating materials have been tested as protective coatings for Ceradyne ThermoSil[®] 220 (CT in chapter 5) ceramic material with the DPI test. The coating performances are compared with uncoated ceramic from chapter 5 and coating PET-B from chapter 6. The three coating materials employed in this chapter have been selected by the author from a research of available commercial coatings. The coating material have been selected according to the following requirements in order of priority:

1. Availability in the market;
2. Working temperature; and
3. Coating CTE that would match with the substrate¹;

The three selected coating materials are presented in table 7.1. Two coatings are supplied by Ferro Corporation and one coating is supplied by James Kent Group. The coatings' technical sheets are available in appendix C and appendix D. The coatings ID (given in table 7.1) will be used to refer to the coating materials. The coatings have

¹Cardyne ThermoSil[®] 220 CTE is $1.7 \times 10^{-7} \text{ }^\circ\text{C}$ [95]

Table (7.1) Coatings technical properties.

Coating ID	Supplier	Product No.	Firing Range (°C)	CTE (10^{-7} / °C)	Softening point (°C)
F-50	Ferro Corp	50 1046	1150 - 1250	33	950
JK-N8	James Kent Group	N8228	1000 - 1100	nd	950
F-40	Ferro Corp	40 580 TF	1250 - 1300	60	1180
PET-B	MinChem Ltd	nd	1000 - 1350	<10	nd

been deposited via dip coating following their suppliers suggested procedure, which are summarised in appendix E.

This study focuses on the use of the DPI test to compare the different coating materials. Results are used to assess each coating performance under SPF condition.

7.2 Experimental conditions

The coating solutions under discussion have been subjected to both the static and dynamic modes of the DPI test. All the coatings have been deposited on Ceradyne ThermoSil[®] 220 cubes (50.0 x 50.0 x 50.0 mm), as in the experiments carried in chapters 5 and 6. The static mode DPI test evaluates resistance to thermal cycles and die surface degradation typical of the adhesion areas (cf. figure 2.6), while the dynamic mode DPI test simulates corner and sliding areas of the SPF die (cf. figure 2.6). In addition, the dynamic mode DPI test gives information regarding friction of the different ceramic surfaces.

The static mode DPI test, as discussed in section 5.1.2.1, consists of a series of thermo-mechanical cycle loads at standard SPF conditions. Time, temperature and applied load are kept the same as the low-pressure condition (cf. figure 5.1 and table 5.1) of the studies discussed in chapters 5 and 6 for comparison. The metal sheet samples are made of commercial SPF grade Ti-6Al-4V alloy with dimensions 40.0 x 60.0 x 1.2 mm, which are cleaned and sprayed with boron nitride (Kenametal, WJMB grade) suspension before the DPI test.

The dynamic mode DPI experiment is carried out as well in this study. The dynamic mode DPI test comprises three runs where different shear conditions are simulated.

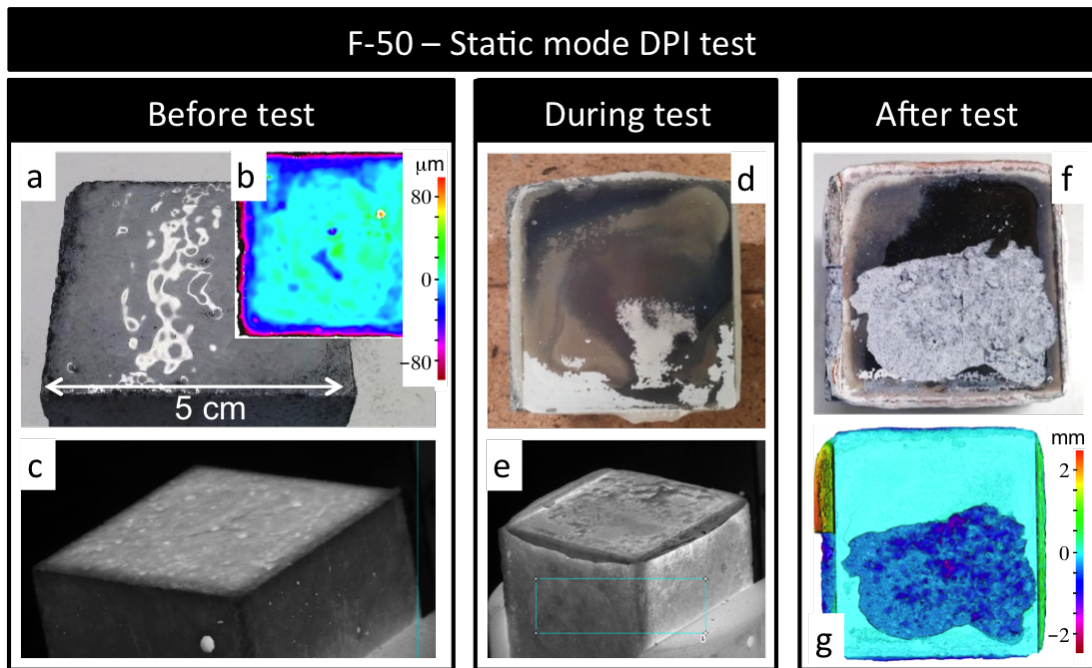


Figure (7.1) Coating F-50 before low-pressure static mode DPI test picture (a), pseudo-colour of the surface topography (b) revealed with confocal microscope technique and thermal image (c). Coating F-50 after one cycle (d) and corresponding thermal image (e). Coating F-50 at the end of the low-pressure DPI test picture (f) and pseudo-coloured surface topography (g).

The dynamic mode DPI test comprises three run. For each run one new untested ceramic sample is employed against one Ti-6Al-4V sample. All samples testing surfaces are polished before the dynamic mode DPI experiment in order to get a surface roughness below $10.0 \mu\text{m}$. As in chapter 5, three pressure levels have been tested, corresponding to three cycle duration (cf. figure 5.2 and table 5.2).

7.3 Results

7.3.1 Coating hot cracking and surface degradation

7.3.1.1 Static mode DPI test

Three coating materials have been investigated with the low-pressure static mode DPI test. **Coating F-50** before the test, which is showed in figure 7.1.a, is white and translucent, thus is difficult to see the surface roughness with bare eye. The pseudo-coloured image (cf. figure 7.1.b), acquired with the confocal microscope, shows the real surface morphology of the coating before the DPI test. During the test, thermal images are recorded at each unloading of the titanium sample and the starting surface condition

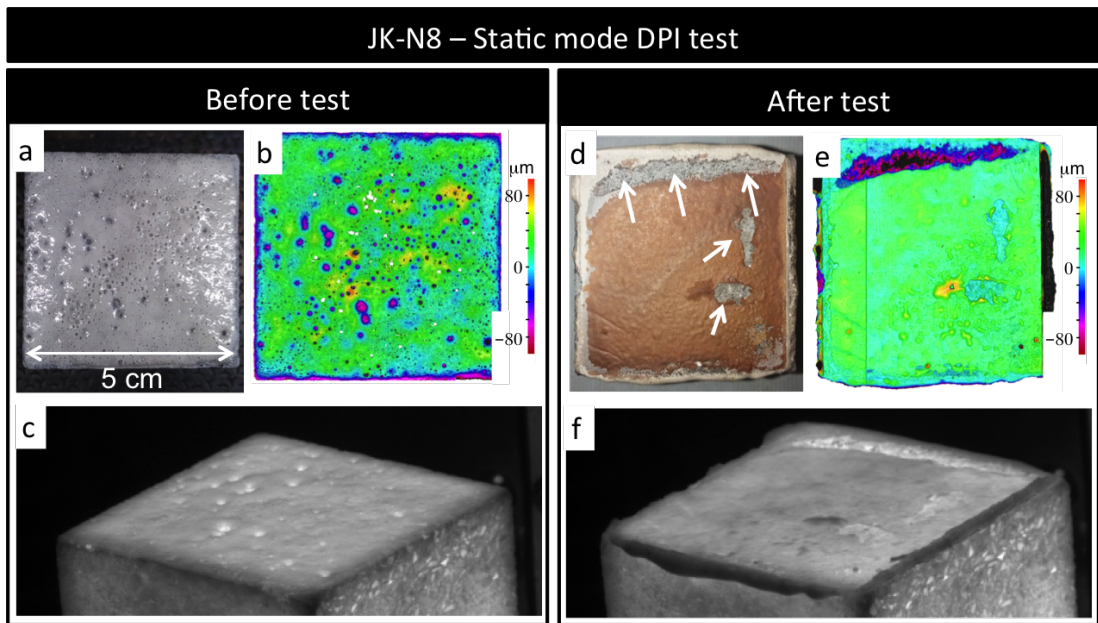


Figure (7.2) Coating JK-N8 before low-pressure static mode DPI test picture (a), pseudo-colour of the surface topography (b) and thermal image (c). Coating JK-N8 at the end of the low-pressure DPI test picture (d), pseudo-coloured surface topography (e) and thermal image (f).

is shown in figure 7.1.c. Figure 7.1.d shows the coating after removal of the first titanium sample, and the corresponding recorded thermal image is shown in figure 7.1.e. Both figures reveal that coating F-50 loses its mechanical properties and become soft under SPF conditions. The dark-brown/blue coating on the top suggests the presence of several oxides on the surface. The transfer of material from the titanium sample to the coating causes sticking between the two, making the removal of the titanium sample more difficult at each cycle. Consequently, coating F-50 failed after five cycles; the coating and part of the matrix of the ceramic substrate stuck to the titanium sample during the unloading, generating a hole on the working surface that extended for more than half of the contacting area (cf. figures 7.1.f and 7.1.g). The starting surface roughness of coating F-50 before test is $(15.4 \pm 0.6) \mu\text{m}$. The measured roughness of the overall coating F-50 after low-pressure static mode DPI test is $(77.1 \pm 0.8) \mu\text{m}$, while the roughness measured only in the area without considering the cracks is $(7.4 \pm 0.3) \mu\text{m}$. The surface roughness change denotes a damage on the coating surface, while the region of the coating not damaged shows a decreased surface roughness as a consequence of the coating softening.

Coating JK-N8 before test is showed in figure 7.2.a. The coating is white and it presents with porosities, which are more visible on the pseudo-coloured surface topography in figure 7.2.b. Porosities, which are also visible on the thermal image in figure 7.2.c,

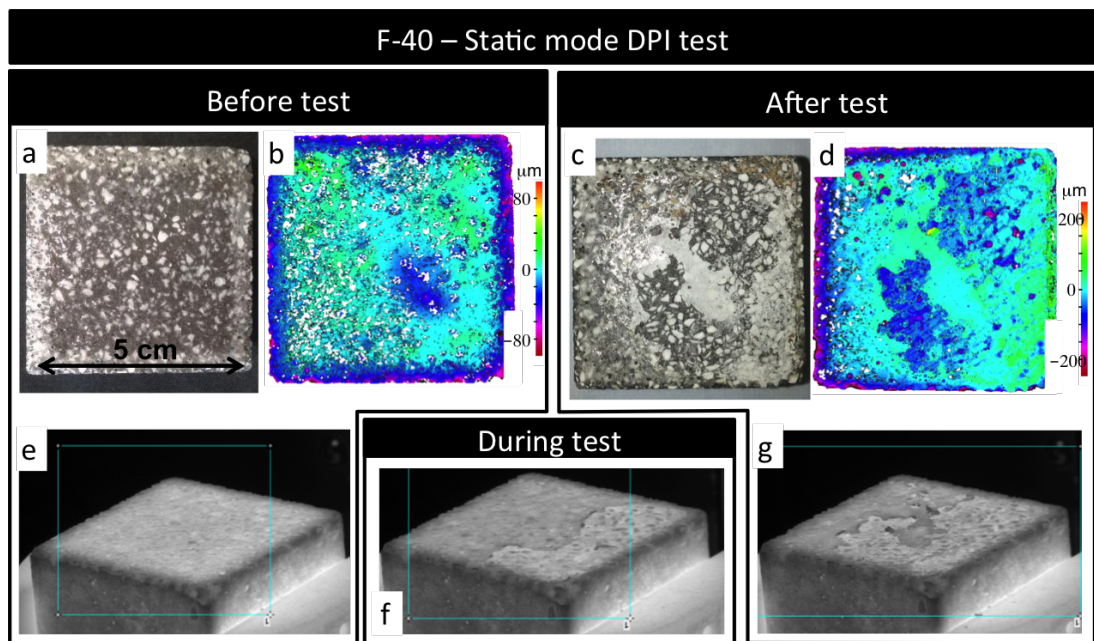


Figure (7.3) Coating F-40 after deposition picture (a) and pseudo-colour of the surface topography (b). Coating F-40 response after low-pressure static mode DPI test picture (c) and pseudo-coloured surface topography (d). Coating F-40 thermal image recorded before test (e), after one cycle (f) and at the end of the low-pressure static mode DPI test (g).

are caused by release of gasses as a product of the chemical reactions that take place during the firing process. The adhesion between coating and titanium sample is higher than the one experienced while removing titanium samples during the test with coating F-50. As a result, coating JK-N8 can stand only two cycles before breaking. The outcomes of the test are showed in figure 7.2.d, where the arrows highlight the coating spallation that exposed the ceramic substrate. Along the borders of the ceramic sample the coating is white, indicating a non-contact area with the titanium sample during the experiment. The area of the coating in contact to the titanium sample becomes red after the DPI test, denoting oxides formation. The pseudo-coloured image in figure 7.2.e reveals absence of the initial porosities of the coatings. The thermal image in figure 7.2.f shows the wear of the coating. In addition, coating material is moved out from the titanium part on the cube borders, as a result of the coating softening under SPF conditions. Before test the measured roughness of coating JK-N8 surface is $(64.1 \pm 0.7) \mu\text{m}$ and after low-pressure static mode DPI test it is $(38.9 \pm 1.2) \mu\text{m}$. Due to the coating softening, the overall surface roughness decreased and the porosities at the surface disappeared after the experiment.

The deposition of **coating F-40** results in a black translucent layer as shown in figure 7.3.a, where the pseudo-coloured surface topography in figure 7.3.b reveals the

presence of porosities at the coating surface. Therefore, the measured surface roughness before test is $(65.4 \pm 1.6) \mu\text{m}$. Under low-pressure static mode DPI test coating F-40 is able to stand three cycles before failure. In figure 7.3.c and 7.3.d the resulting coating surfaces after test are shown. The pseudo-coloured surface topography acquired with the confocal microscope (figure 7.3.d) helps to identify the remaining coating on the ceramic surface (light blue and green areas) and the exposed substrate surface (dark blue). Thermal images have been recorded before the experiment (figure 7.3.e), after the removal of the first titanium sample (figure 7.3.f) and at the end of the experiment (figure 7.3.g). Thermal images show no squeezing of the coating along the ceramic sample borders, hence, coating F-40 does not suffer of softening under SPF conditions. In addition, thermal images show the coating spallation during the DPI test. The measured roughness of coating F-40 surface after low-pressure static mode DPI test is $(80.0 \pm 1.8) \mu\text{m}$, which is higher than the starting roughness as indication of the coating surface wear.

7.3.1.2 Dynamic mode DPI test

The dynamic mode DPI test is employed to examine the coating resistance to hot cracking under shearing of a titanium sample on a coated die surface at SPF conditions. The three selected coating materials and coating PET-B from chapter 6 are tested with the dynamic mode DPI experiment. Figure 7.4 illustrates the resulting surface wear recorded with thermal camera after unloading of the sample for their respective run number.

Figures 7.4.a, 7.4.b and 7.4.c show the resulting **coating PET-B** surfaces for Run 1, Run 2 and Run 3 respectively. Due to the difference in emissivity of the coating material and the release agent, sprayed on each titanium sample, the brighter area denotes the coating surface and the dark area on the coating surface is mainly boron nitride transferred from the titanium sample to the coating surface. Run 1 and Run 2 are characterised by a great amount of boron nitride transferred on the coating surface if compared with Run 3.

Coating F-50 thermal images are showed in figures 7.4.d, 7.4.e and 7.4.f. Under dynamic mode the softening of the coating is more evident. Coating material is moved out of the circular track during rotation of the titanium sample (as indicated with the arrows), and this aspect is more visible when rotation speed and load are increased in Run 2 and Run 3.

The softening of the coating is visible in **coating JK-N8** thermal images as well (cf. figures 7.4.g, 7.4.h and 7.4.i). In addition, coating JK-N8 is damaged by the titanium sample removal during Run 3.

Coating F-40 thermal images are showed in figures 7.4.j, 7.4.k and 7.4.l for Run 1,

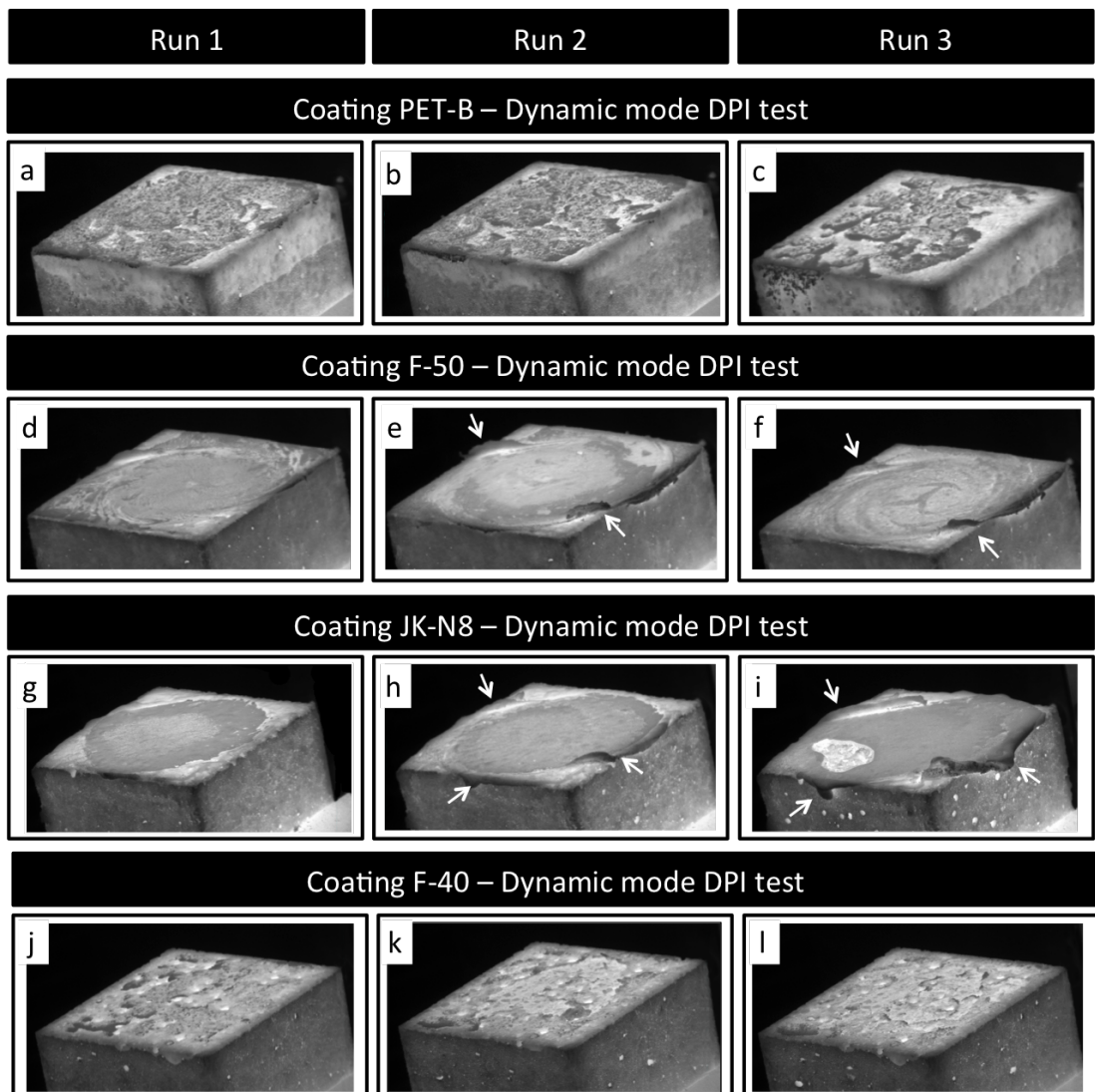


Figure (7.4) Thermal images recorded during the dynamic mode DPI test for coating PET-B at Run 1 (a), Run 2 (b) and Run 3 (c). Thermal images recorded during the dynamic mode DPI test for coating F-50 at Run 1 (d), Run 2 (e) and Run 3 (f). Thermal images recorded during the dynamic mode DPI test for coating JK-N8 at Run 1 (g), Run 2 (h) and Run 3 (i). Thermal images recorded during the dynamic mode DPI test for coating F-40 at Run 1 (j), Run 2 (k) and Run 3 (l).

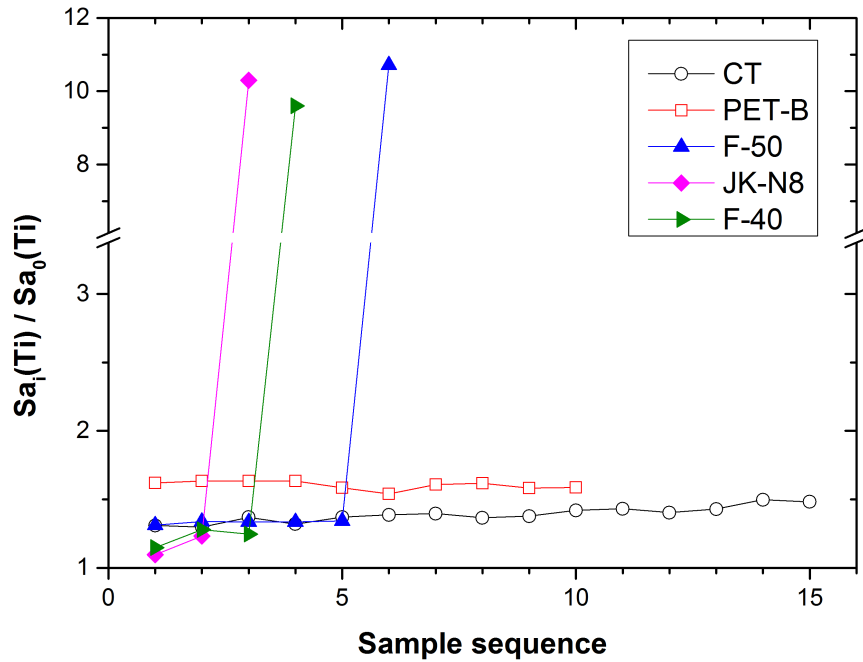


Figure (7.5) Titanium samples roughness normalised by their initial roughness. In empty black circles is represented the ceramic CT uncoated surface degradation for low-pressure condition (as reference). In empty red squares is represented the coating PET-B surface degradation (from chapter 6). In full blue triangles is represented the coating F-50 surface degradation. In full magenta diamonds is represented the coating JK-N8 surface degradation. In full green triangles is represented the coating F-40 surface degradation. All the samples have been tested at low-pressure static mode DPI test conditions.

Run 2 and Run 3 respectively. Coating F-40 does not reveal softening during the dynamic mode DPI test. On the other hand, the coating removal is visible in every test condition.

7.3.2 Titanium part surface degradation

The coating surface degradation cannot be analysed during the DPI test after each cycle, but the surface roughness change of each titanium sample is measured to observe the coating surface wear. During the DPI test, the titanium sample is in its super-plastic region, thus the applied pressure induces the titanium sample to mirror the die surface [86]. The titanium sample surface roughness, $Sa_i(Ti)$, is studied as a function of the sample sequence, and normalised with their starting roughness, $Sa_0(Ti)$. Figure 7.5 shows the resulting normalised values of the titanium surface roughness trends, $Sa_i(Ti)/Sa_0(Ti)$, from the low-pressure static mode DPI test for the coating F-50 in

full blue triangles, the coating JK-N8 in full magenta diamonds, the coating F-40 in full green triangles, the uncoated ceramic (as reference) in empty black circles and coating PET-B in empty red squares.

The starting value of the coating materials studied in this study is similar of below the uncoated ceramic, while coating PET-B from a previous study (see chapter 6, has a starting value of 1.6. Coating F-50 titanium normalised surface roughness starts from a value of 1.3, similar to uncoated ceramic, but the trend suddenly changes and the value increases almost one order of magnitude after five cycles, indicating wear of the coating. A similar trend is exhibited in coating JK-N8 after only two cycles and in coating F-40 after the third cycle.

As discussed at page 70 the Vmp values of the titanium sample are compared with the Vvv values of the coating, and the Vvv titanium sample values are compared with the Vmp values of the coating.

Figure 7.6 shows the Vmp and Vvv values measured on the titanium samples tested on coating F-50, JK-N8 and F-40 respectively. For each coating material a graph reports the valley void volume of titanium samples, $Vvv(Ti)$, plotted against the peak material volume of the coating surface measured before, $Vmp_i(Die)$, and after, $Vmp_f(Die)$, test. In addition, a second graph reports the peak material volume of titanium samples, $Vmp(Ti)$, plotted against the valley void volume of the coating surface measured before, $Vvv_i(Die)$, and after, $Vvv_f(Die)$, test. These graphs shows the relation between the volume surface parameters of the tested titanium samples against the coating surface condition. In figure 7.6 the Vmp and Vvv parameters of the titanium samples show a trend that starts from the initial Vvv and Vmp parameters of the coating and tends to the coating final value, indicating that the titanium samples are replicating the wear of the coating. This trend validates the use of titanium samples roughness value to control the coating surface degradation. In addition, it is possible to monitor the coating surface degradation at each cycle.

Coating F-50 Vvv and Vmp trends show that both the coatings' peak material volume, $Vmp(Die)$, and valley void volume, $Vvv(Die)$, increase during the DPI test. This trend, considering the outcomes showed in section 7.3.1, denotes a stable wear for the first four cycles and then a generation of valleys and peaks on the coating surface during the last two cycles (cracking of the coating). The absolute values of Vmp and Vvv are higher if compared with the other coatings or the values seen in the previous case studies, indicating that the generation of peaks and valleys is quite important. If we consider the coating surface without the crack, the final Vmp and Vvv values are 0.45 and 0.77 $\text{ml}^3/\mu\text{m}^2$, indicating that the coating surface have been smoothed by the softening of the coating, eroding asperities and filling the porosities. The wear mechanisms of coating F-50 are characterised by scale build up and removal of coating

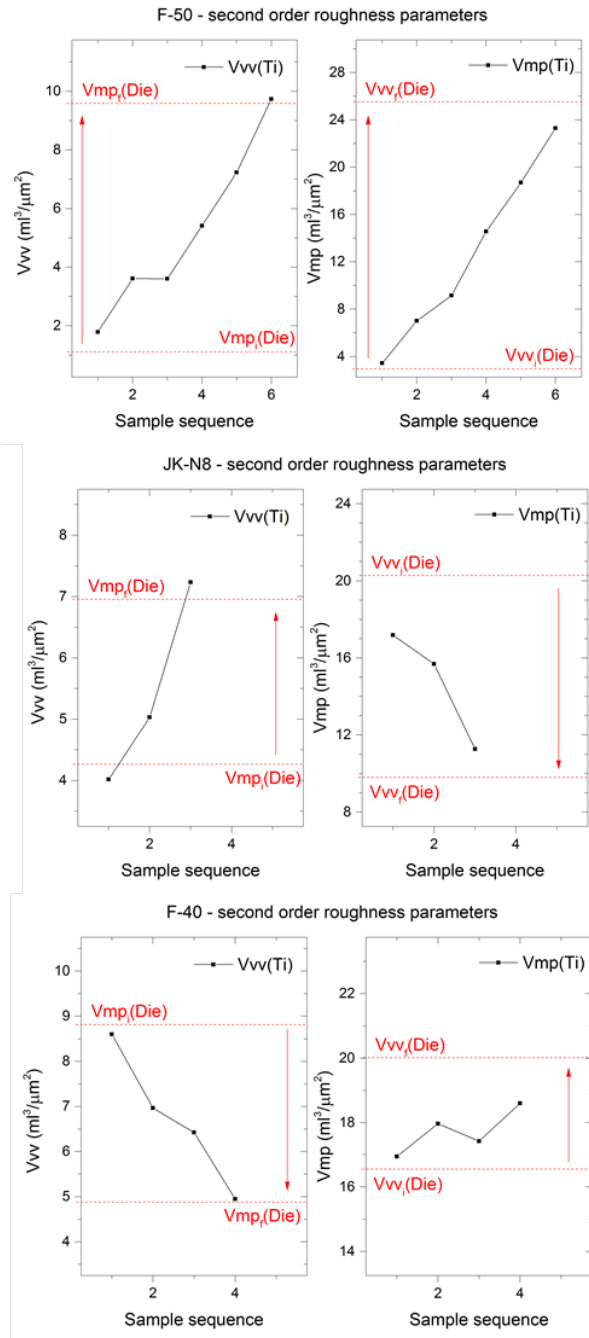


Figure (7.6) The measured material peak volume per unit area, Vmp , and the void valley volume per unit area, Vvv , are showed for coating F-40, JK-N8 and F-50. For each coating the void valley volume measured on the titanium samples, $Vvv(Ti)$, is evaluated with the material peak volume measured on the coating before ($Vmp_i(Die)$) and after ($Vmp_f(Die)$) the DPI test; the material peak volume measured on the titanium sample, $Vmp(Ti)$, is evaluated with the void valley volume measured on the coating before ($Vvv_i(Die)$) and after ($Vvv_f(Die)$) the DPI test.

material, generating deep valleys on the surface, as seen in figure 7.1.

Coating JK-N8 shows a similar trend to coating F-50 when considering the coating Vmp , and due to the similar hot cracking of the coating the Vvv is expected to have the same trend as coating F-50. Figure 7.6 shows that the coating JK-N8 Vvv decreases during the experiment, in contrast with coating F-50 trend. The reason why the volume of void valleys decreases in coating JK-N8 during the experiment instead of increasing (there are visible valleys generated during the experiment) is due to the high starting porosity of the coating before the experiment. The wear mechanisms of coating JK-N8 are characterised by deposition of material on the coating surface and removal of material as seen in figure 7.2, even if the Vvv value measured is affected by the high-porosity concentration on the starting coating.

Coating F-40 Vmp value is decreasing during the DPI test, while Vvv value is increasing. This trend indicates that asperities have been eroded and material has been removed from the coating leaving void valleys on the surface during the experiment. The wear mechanism of coating F-40 is characterised by spallation of the coating, which has been eroded and removed from the substrate, leaving voids on the surface as seen in figure 7.3.

7.3.3 Chemical interactions

Under SPF conditions the titanium sample and the coating interact and scale builds up on the die surface. Cross section and top view SEM images are useful to investigate the chemical interaction at the die-part interface. Ceramic samples are cut, lapped and polished following standard procedures. Samples are dried under vacuum for at least 48 hours before SEM inspection.

Figure 7.7.a shows **coating F-50** after the low-pressure static mode DPI test, where a top surface X and a cross section Y have been cut and prepared for SEM inspection. In figure 7.7.b a cross section of the coating after firing is shown. The interface coating/substrate is well defined and there is no presence of an intermix layer as in coating PET-B. The coating is 400 μm thick and considerable porosities are visible in the coating, with diameters up to 200 μm . Figure 7.7.c shows the cross section Y after test, which exhibits high porosity mainly concentrated at the coating-substrate interface. Porosities have been seen before the test dispersed in the coating (cf. figure 7.7.b), and after the DPI test the porosity concentration migrates to the coating-substrate interface. These results suggest that under SPF condition the diffusion of porosity already in the coating is promoted to move toward the substrate. Another possible cause of high porosities concentration at the coating-substrate interface after the DPI test is the release of trapped gasses from the intrinsic porosities of the substrate during the DPI test. The coating thickness (measured from an extended cross section) after test

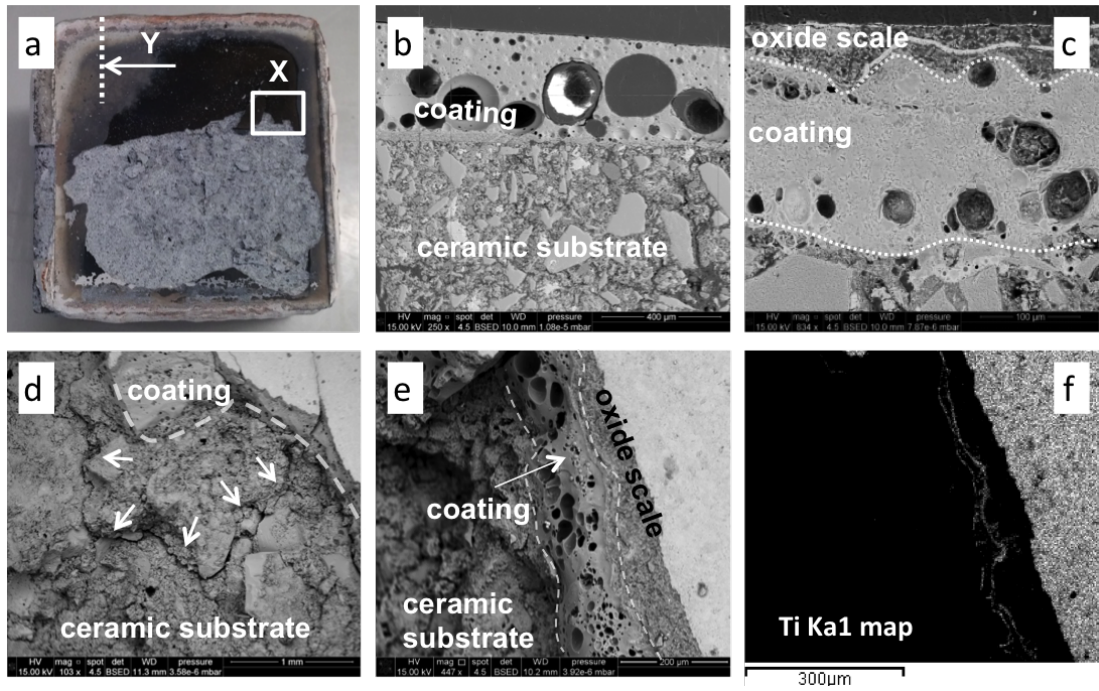


Figure (7.7) Coating F-50 after low-pressure static mode DPI test (a) where areas of interest are highlighted. SEM image of coating F-50 cross section after deposition (b). SEM images of the cross section Y (c) after DPI test. The area X top view SEM image have been acquired (d) and its magnification (e) and EDX map of titanium element (f) are presented. All SEM images are acquired with backscattered electron detector.

decreases to about $50 \mu\text{m}$. In addition, a scale layer is visible on top of the coating.

The top surface SEM image of the coating fracture (figure 7.7.d) shows the cracks generated on the substrate ceramic matrix during the unloading of the titanium sample. The porosities at the coating-substrate interface have been identified, where bubbles of trapped gasses are highly concentrated and they can drastically decrease the coating mechanical properties, being one of the causes of the coating failure. A magnification of the coating (figure 7.7.e) have been acquired together with EDX map of titanium element to identify the titanium layer. From the EDX map (figure 7.7.f) the different layers of titanium oxide are visible.

Coating JK-N8 cross section SEM image before testing is showed in figure 7.8.a, where the coating presents a thickness of approximately $800 \mu\text{m}$ and a net interface with the substrate. The coating presents some porosities of different sizes, mainly with a diameter of approximately $100 \mu\text{m}$. In addition, cracks due to thermal shrinkage are visible in the coating. After low-pressure static mode DPI test, the coating top view area (X) and cross section (Y) have been analysed with SEM and are highlighted in figure 7.8.b. The top view (cf. figure 7.8.c) shows the coating fracture surface, where a crack parallel to the substrate surface is visible. Such a crack can causes spallation of

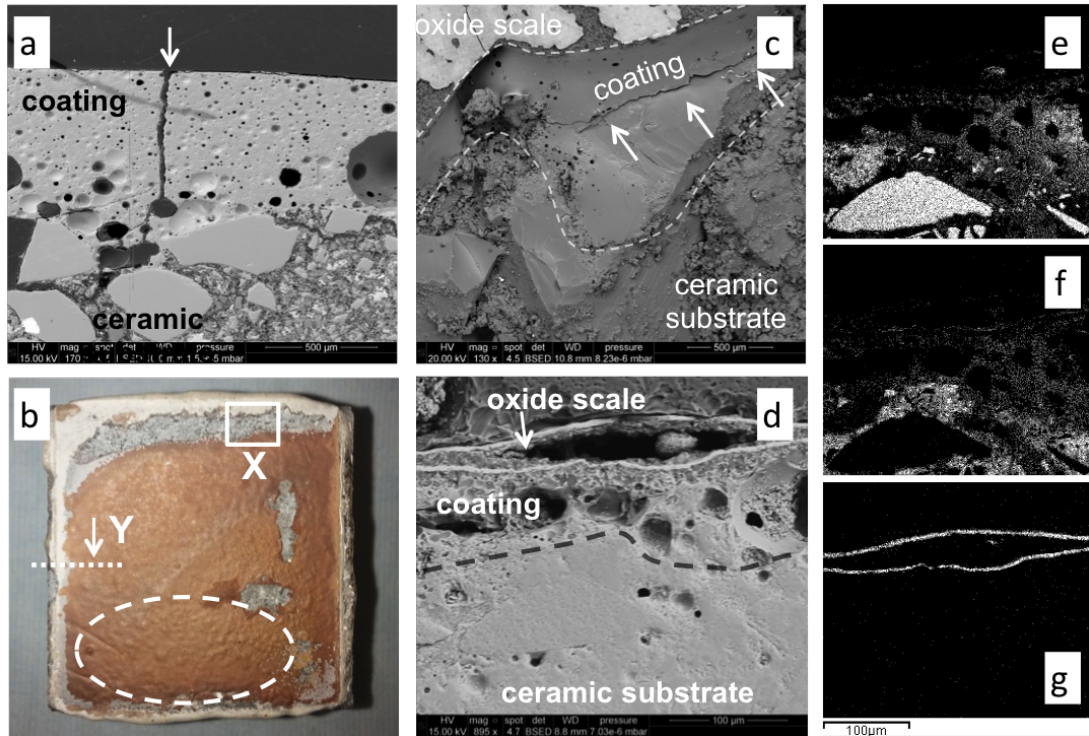


Figure (7.8) SEM image of coating JK-N8 cross section after deposition (a). Coating JK-N8 after low-pressure static mode DPI test (b) where areas of interest are highlighted. SEM image of area X top view (c) is presented. SEM image of the cross section Y (d), and its EDX acquired maps for silicon (e), aluminium (f) and titanium (g) elements are presented. All SEM images are acquired with backscattered electron detector.

the coating. On top of the coating, in white, there is accumulation of titanium oxide, identified with EDX spectra, transferred from the titanium sample to the coating, as a result of chemical interaction. The cross section of the coating after test is shown in figure 7.8.d. The coating-substrate interface is difficult to identify without the help of EDX maps for silicon and aluminium elements (cf. figure 7.8.e and 7.8.f). The coating shows porosities at the interface with the substrate and it is approximately $100 \mu\text{m}$ thick. On the top of the coating an oxide layer is visible, where the brighter layer is titanium rich as shown in the EDX map in figure 7.8.g. Inside the oxide layer is visible a void where material is trapped. These voids are spread all over the coating surface and are visible in figure 7.8.b as under-coating bubbles (highlighted in the white ellipse). The presence of bubbles can be explained by a chemical interaction between the coating top surface and the deposited oxide layer. This interaction may occur during the heat-up time, before a new titanium sample is tested and a new oxide layer is deposited. The interaction releases gasses, which are trapped under the oxide top layer.

Figure 7.9 shows the SEM images acquired from **coating F-40**. The coating, before

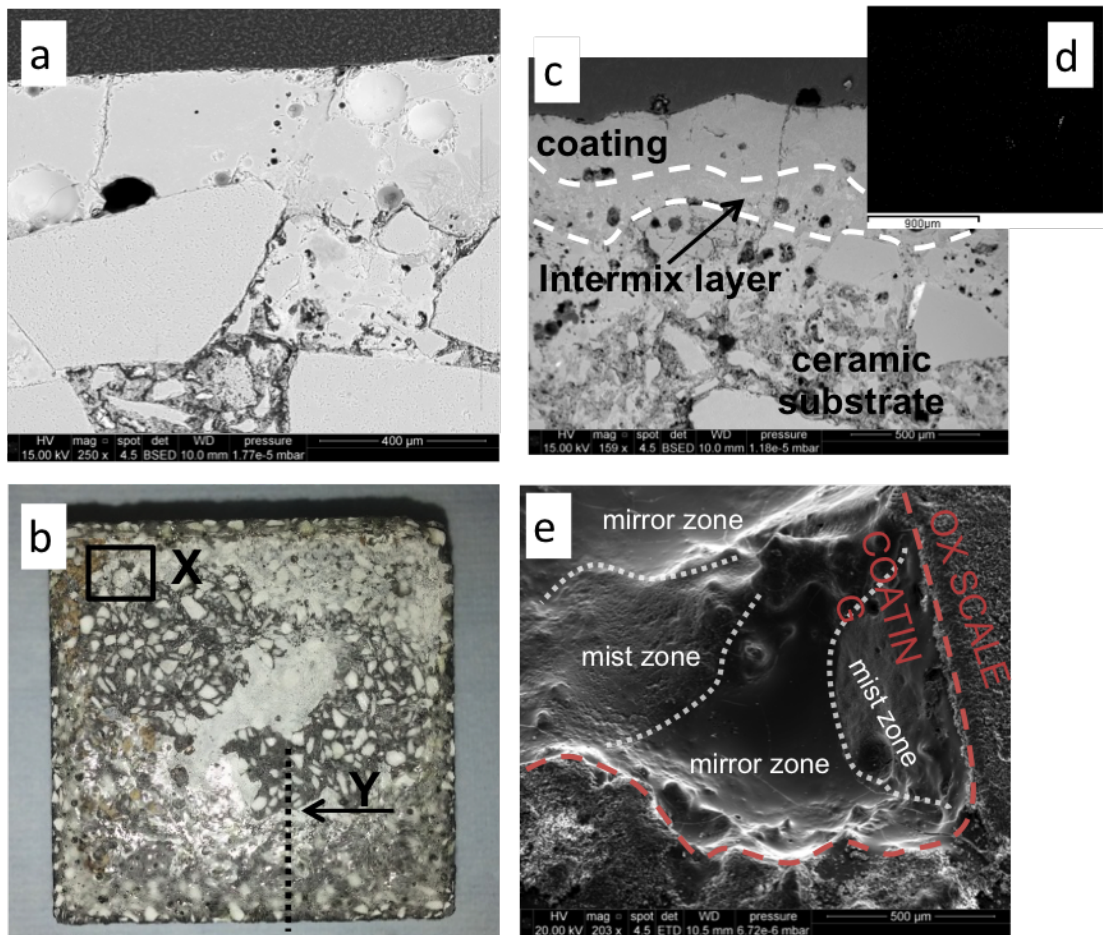


Figure (7.9) SEM image of coating F-40 cross section after deposition (a). Coating F-40 after low-pressure static mode DPI test (b) where areas of interest are highlighted. Top view SEM image of the area X (c) and cross section Y (d), with its EDX acquired maps for titanium element (e).

the experiment (cf. figure 7.9.a) is approximately $500 \mu\text{m}$ thick and there is no evidence of intermix between the coating and the substrate. A few porosities of about $50 \mu\text{m}$ diameter are present in the coating, and some cracks as well are visible transverse to the substrate deposition plane, which are generated by thermal shrinkage within the coating due to CTE mismatch with the substrate (cf. table 7.1). After low-pressure static mode DPI test, a top view area (X) and a cross section (Y) of the coating (cf. figure 7.9.b) are investigated with SEM. Examining the cross section Y, where a thicker coating survived to the experiment, SEM image (cf. figure 7.9.c) shows the presence of a small concentration of porosities in the coating. After the DPI experiment, the coating exhibits an intermix layer, which was absent before the test. In addition, there is no presence of oxide layer on the top; the titanium-rich layer seen in the other coating is not visible in the EDX map for the titanium element (cf. figure 7.9.d). This result

suggests that the coating did not chemically interact with the titanium samples as much as the other coatings assessed.

On the other hand, the top view SEM image (cf. figure 7.9.e) shows the coating fracture surface from the top view. In figure 7.9.e is visible the border between the oxide scale and the remaining coating (red line). Within the coating two zones are identified: the mirror zone, which is characterised by a smooth surface roughness, and a mist zone, where the surface roughness increase. These two zones, beside the hackle zone, which is missing, are similar to the brittle material fracture morphology [113, 114].

However, in this case, the mirror zone can identify the coating left after the experiment, while the mist zone shows the intermix layer, where most of the coating material has been locally removed, leaving the intermix layer exposed.

7.3.4 Friction

The dynamic mode DPI test gives information regarding the estimated coefficient of friction (COF) between the ceramic material and the titanium sample under SPF conditions. In the dynamic mode DPI experiment three operational set-up (runs) have been tested; Run 1 is a low-pressure/low-speed condition, Run 3 is a high-pressure/high-speed condition and Run 2 is a middle point. Figure 7.10 shows the measured COF of uncoated ceramic (white), coating PET-B (red), coating F-50 (blue), coating JK-N8 (magenta) and coating F-40 (green). The error bars are measured as the standard deviation of the average.

The resulting COF shows a trend from Run 1 to Run 3: at lower pressure and speed the resulting COF is lower than at higher pressure and speed for all the coatings. From the analysis of variance (ANOVA) of the means values of COF for each run, considering a significance level of 0.05 (thus a confidence level of 95%), results that the uncoated ceramic CT has the lowest COF value and coating JK-N8 has the highest for all the test conditions (runs). In addition, within all the tested coatings, PET-B and F-40 are the coatings that show a lower COF compared with the other coatings. The ANOVA reveals that in Run 1, at the 0.05 level of confidence, there is no significant difference between the means values of COF for PET-B and F-40; in Run 2 PET-B has a lower value of mean COF than F-40; in Run 3 F-40 has a lower value of mean COF than PET-B.

The COF gives an idea of the interaction at SPF temperature between the ceramic surface and the titanium sample. In addition, this data could be employed in finite element modelling for a more accurate simulation of the SPF process with ceramic materials.

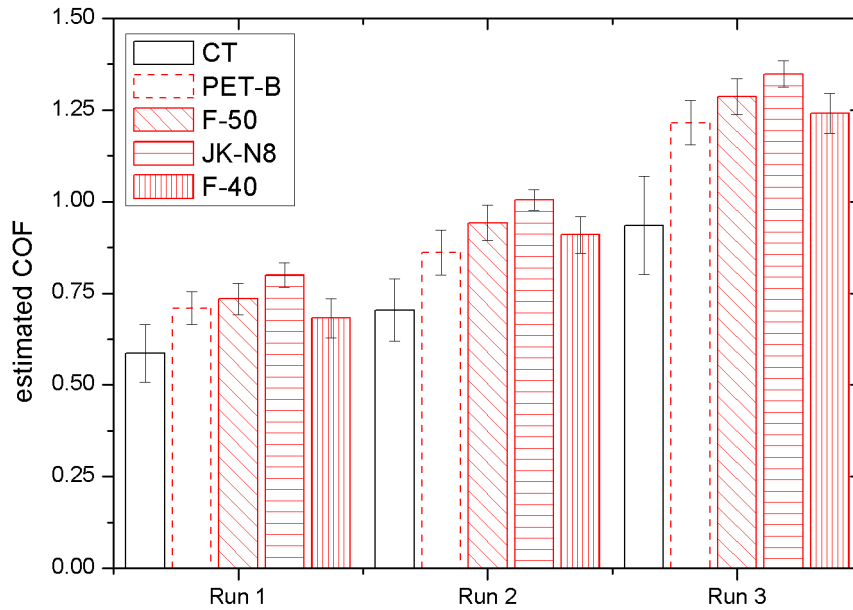


Figure (7.10) Coefficient of friction (COF) measured during the dynamic mode DPI test in each set of SPF conditions (run) for uncoated ceramic CT (as reference), coating PET-B, coating F-50, coating JK-N8 and coating F-40. Run 1 is characterised by a slower pressure and rotation speed than Run 3, while Run 2 is a midpoint level.

7.4 Conclusion

Three coating solutions have been investigated in this study and coating performances under SPF conditions have been compared with uncoated ceramic CT and coating PET-B. All the coatings have been deposited following suppliers suggested procedure. The outcomes of the DPI test regarding coatings performance gives important information for the selection of eligible protective coating solutions for SPF ceramic dies.

Coating F-50 under static DPI test shows softening and it can stand five cycles before breaking. Under dynamic DPI test, it shows softening as well and a high COF, indicating a high mechanical (and chemical) interaction between the coating and the titanium part. The chemical interaction is investigated with SEM images. Before DPI test, the coating is 400 μm thick and it does not show an intermix layer, as coating PET-B. and there are porosities within the coating. After DPI test, the porosities are concentrated at the substrate-coating interface and on the top coating surface an oxide layer transferred from the titanium part is visible.

Coating JK-N8 shows softening as well under both static and dynamic DPI test. The coating can stand two cycles before breaking under static DPI test, while the softening of the coating results in a high COF under dynamic DPI test. SEM image of the coating before test shows high porosity concentration within the coating. In addition, the coating is about 800 μm thick and thermal shrinkage cracks are visible. After the test, SEM images reveal cracks parallel to the substrate surface that are cause of the coating spallation. In addition, the porosities are concentrated at the coating-substrate interface. An titanium-rich oxide layer is visible on the top surface of the coating, which is the result of the chemical interaction between the coating and the titanium part. In addition, this layer is reactive at high temperature, generating gas that is trapped within the layer, causing voids within the top of the coating.

Coating F-40 does not show softening under SPF conditions. Under static DPI test, the coating fails after three cycles. In dynamic mode DPI test the coating suffers material removal. SEM images shows that the coating failure is due to poor adhesion to the substrate. In addition, SEM images show that the coating before test is 500 μm thick and it shows few porosities and cracks due to thermal stresses. SEM images acquired after test show the brittle fracture of the coating and the presence of an intermix layer between the coating and the substrate, which was absent before the test, indicating that there is margin of improvement of the coating adhesion. In addition, there is no oxide layer deposited on top of the coating, indicating limited chemical interaction between the coating and the titanium parts.

The recorded coatings' COFs during the dynamic mode DPI test show that the uncoated ceramic has the lowest COF, while coating JK-N8 has the highest COF. In addition, within the coated ceramics, coating PET-B and coating F-40 have a lower COF then the other tested coatings. In conclusion, the DPI test has been successfully employed to assess different coating materials and can be implemented for a systematic study of several coating solutions, in order to identify these that could be transferred in mass production.

7.5 Summary

In this chapter the DPI test has been employed to assess three coatings' performance under SPF condition. The test outcomes have been compared with the uncoated substrate (ceramic CT) from chapter 5 and coating PET-B from chapter 6. The chapter outcomes can be summarised as follow:

- Coating F-50 results in softening under SPF conditions that compromises the coating performance;

- Coating JK-N8 shows softening as well and poor performance under SPF conditions;
- Coating F-40 does not show softening or oxide layer on the top surface. The coating performance is compromised by the poor adhesion of the coating to the substrate, which could be improved.

Chapter 8

Discussion of collated results

The following chapter focuses on the discussion of the results obtained from all the three studies carried in chapter 5, 6 and 7. The results obtained in this research work have been crucial to develop a test protocol to be implemented to assess SPF ceramic die surface wear. The test protocol, which is discussed at the end of the chapter, comprises the static and dynamic modes of the DPI experiment.

8.1 Introduction

The DPI test has been employed with several ceramic die conditions: in this work two different uncoated ceramic material have been tested for comparison in chapter 5, two deposition procedures of the same coating material have been assessed in chapter 6, and several coating materials' performances have been investigated in chapter 7. Through the DPI experiment it has been possible to investigate different wear mechanisms, depending on the material properties. This chapter aims to compare the key metrics employed to evaluate the surface wear and coating performance in order to identify the major wear mechanisms that take places during the DPI experiment.

8.2 Die hot cracking and surface degradation

The DPI test enables the investigation of the interaction at the die-part interface under SPF conditions. Two uncoated ceramic materials and four coating materials, one of which it has been deposited with two different firing procedures, have been tested with the DPI test. Figure 8.1 presents an overview of the resulting behaviour of all the materials tested under the static mode DPI test. The material response have been quantified with an increasing grade from one to five, for the static mode DPI test, as follows:

- One denotes that the material breaks after less than five cycles;

Static mode DPI test										
	Low pressure					High pressure				
Rank	1	2	3	4	5	1	2	3	4	5
description	< 5 cycles	> 5 cycles	survived; degraded	survived; adhesion	survived; minor damage	< 5 cycles	> 5 cycles	survived; degraded	survived; adhesion	survived; minor damage
Uncoated ceramic CT										
Uncoated ceramic HC										
Coatings - substrate ceramic CT										
PET-A						NOT TESTED				
PET-B						NOT TESTED				
F-50						NOT TESTED				
JK-N8						NOT TESTED				
F-40						NOT TESTED				

Figure (8.1) Materials response to static mode DPI test. Coating performance has not been tested under high-pressure condition.

- Two denotes that the material breaks after more than five cycles;
- Three indicates that the material does not break but it degrades during the experiment;
- Four indicates that the main wear is adhesion of release agent from the titanium sample to the die;
- Five indicates minor degradation.

The DPI test outcomes show that under low pressure conditions the uncoated ceramic CT and HC have better performance than the tested coatings. Within the coatings, PET-B shows the best performance. Due to the poor performance of the coatings under low pressure conditions, the high-pressure static mode DPI tests have been conducted only on the uncoated ceramics for validation purpose of the developed test method.

With the data collected so far from the DPI experiments is possible to build a performance indicator that gives quantitative information regarding the surface wear diagnosis. In figure 8.2 the control charts of surface roughness parameter $Sa(Ti)$ of uncoated ceramic CT, coating PET-B and F-50 are presented. The control chart is usually employed for statistical control of any process stability [115]. The centre line is the average value ($\bar{S}a(Ti)$) calculated for the whole sample sequence, while the upper and lower control limits (UCL and LCL) are calculated as $\bar{S}a(Ti) \pm 3s$ where s is

the standard deviation of the sample in consideration. For example, for the uncoated ceramic CT there are fifteen $Sa(Ti)$ measurements and

$$\mu = \frac{\sum_{i=1}^{15} Sa(Ti)_i}{15} \quad (8.1)$$

and the standard deviation s is calculated as

$$s = \sqrt{\frac{\sum_{i=1}^{15} (Sa(Ti)_i - \bar{Sa}(Ti))^2}{14}} \quad (8.2)$$

The control chart identify if the process is in control within the interval six times the standard deviation. In addition, the centre, UCL and LCL lines have to be calculated from a sample greater than twenty samples [115]. Figure 8.2 shows that the uncoated ceramic CT roughness parameter is in control over the fifteen cycles that have been carried on the DPI rig¹. In figure 8.2 are presented the control chart made for PET-B and F-50 coatings as well. The center, UCL and LCL lines for coating F-50 have been calculated without considering the last measurement, which is clearly an out-of-control measure. The control charts here have been presented to shows the possibility of using a statistical process control tool to determine whether the surface degradation of the die surface is in-control or out-of-control. In the cases presented in figure 8.2 the uncoated ceramic CT and coating PET-B are within the UCL and LCL range, thus the surface degradation is in-control, while coating F-50 control chart shows the drastic surface degradation on the sixth sample. This tool can be employed to have a quantitative measure to determine the surface degradation during the DPI test (or SPF trials).

The dynamic mode DPI test have been carried out on the uncoated ceramic CT and HC and on ceramic CT coated with PET-B, F-50, JK-N8 and F-40 respectively. Figure 8.3 shows the overall results of the dynamic mode DPI test.

For the dynamic mode DPI test the material responses have been quantified in a range from *I* to *III*, where *I* indicates that the material cannot stand the shear stress and breaks, *III* indicates good resistance to shearing, and *II* is a middle point.

The uncoated ceramic materials, CT and HC, have been tested under static mode DPI test using both low- and high-pressure conditions, where the HC material showed better performance than CT. The dynamic mode DPI test revealed that HC is not suitable for SPF applications as it drastically suffers shear stresses.

Under dynamic mode DPI test, coating PET-B reveals better response than the other coatings, but still a lower performance compared to the uncoated ceramic CT.

The suitable protective coating should be able to maintain good protective performance at high temperature under load (static mode) and shear (dynamic mode). In

¹There are other rules to determine if the process is in control, but this is beyond the scope of this discussion. For further information about the topic refer to [115].

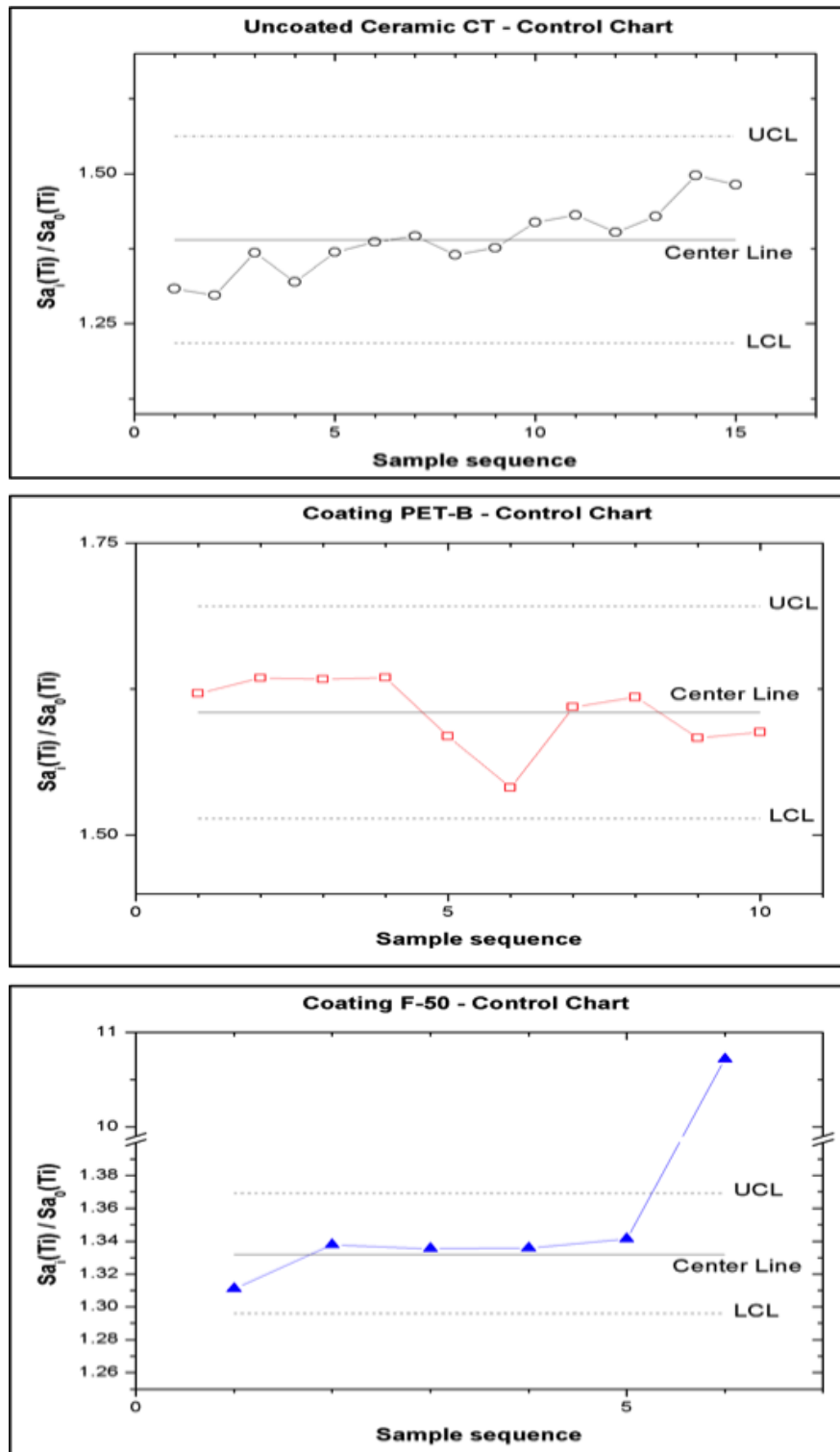


Figure (8.2) Control chart of uncoated ceramic CT, coating PET-B and coating F-50

Dynamic mode DPI test			
Rank	I	II	III
description	major damages	minor damages	unaffected by shear
Uncoated ceramic CT			
Uncoated ceramic HC			
Coatings - substrate ceramic CT			
PET-A	NOT TESTED		
PET-B			
F-50			
JK-N8			
F-40			

Figure (8.3) Materials response to dynamic mode DPI test. Coating PET-A has not been tested under dynamic mode DPI experiment.

addition, under static mode, it should be able to stand both low and high pressure conditions.

8.3 Wear mechanisms

The titanium samples' change of roughness during the static mode DPI test has been used to monitor the surface degradation of the die. The first order roughness parameter Sa plotted against the sample sequence gives an immediate feedback of the die surface conditions during SPF trials. In addition, the second order roughness parameters, or 3D areal functional parameters, such as the material peak volume (Vmp) and the void valley volume (Vvv), give an indication of the wear mechanism that is taking place at the die surface during the DPI test. When $\Delta Vmp(Die)$ increase, deposition of material on the top surface occurs, while a decrease of $\Delta Vmp(Die)$ indicates erosion of material from asperities. On the other hand, the increase of $\Delta Vvv(Die)$ value indicates removal of material which increase the volume of void valleys (such as porosities or cracks), while the decrease of $\Delta Vvv(Die)$ value indicates filling with material of the pre-existing porosities. The evolution of 3D areal functional parameters have been employed in literature to investigated surfaces wear in different application, such as scuffing during plastic deformation of sliding surfaces [116], or lubrication retention [117]. Table 8.1 summarises all the possible wear scenarios depending on the change of the roughness parameters $\Delta Vmp(Die)$ and $\Delta Vvv(Die)$. The findings from the second order roughness parameters study can be summarised as below:

- Wear of the uncoated ceramic CT under low-pressure conditions is characterised by gain of material on the top surface (increase of Vmp) and filling of porosities (decrease of Vvv). Under high-pressure conditions the wear is characterised by gain of material on the top surface (increase of Vmp) and increase of voids (increase of Vvv) due to removal of material where cracks arise.
- The uncoated ceramic HC is characterised by small changes in roughness, which indicate no great wear is occurring. Under high-pressure condition a small increase of Vmp indicates accumulation of material on the top surface, as visible in the pictures.
- The petalite coating PET-A is characterised by erosion of asperities (decrease of Vmp) and removal of material generating voids (increase of Vvv).
- Coating PET-B wear comprises erosion of asperities (decrease of Vmp) and filling of porosities (decrease of Vvv).
- Coating F-50 wears by gain of material on the top surface (increase of Vmp) and increase of voids (increase of Vvv) due to removal of material where the crack arise.
- Coating JK-N8 wears by gain of material on the top surface (increase of Vmp) and decrease of porosities (decrease of Vvv).
- Coating F-40 wear is made of erosion of asperities (decrease of Vmp) and removal of material generating voids (increase of Vvv).

Two of tested coatings undergo to softening during the DPI test. The combination of temperature and pressure parameters employed during the experiment shows that coatings F-50 and JK-N8 suffer softening. In order to have a better interpretation of the wear mechanisms involved during the DPI test, a more accurate second order surface roughness parameters (Vmp and Vvv) analysis has been carried for coating F-50 and JK-N8 due to their softening behaviour. In figure 8.4 the Vvv and Vmp trends have been measured considering the coating surface area where softening is arisen during testing, neglecting the cracks areas. In this case, both coatings F-50 and JK-N8 show a decrease of Vmp and Vvv on the die, indicating a decrease of material peaks and filling of voids due to softening instead of erosion or material transfer. When the coating softens, it becomes viscous, enabling self-levelling of the surface roughness under the pressure of the titanium part. In table 8.1 the softening phenomena have been highlighted for the two coatings under discussion. These data alone, do not explain the different wear mechanisms that take places with each tested surface, but they need to be combined with SEM analysis for a better interpretation.

Table (8.1) Summary of the wear mechanisms that can be identified with the study of the die's second order roughness parameters V_{mp} and V_{vv} .

$\Delta V_{mp}(\text{Die})$	$\Delta V_{vv}(\text{Die})$	Effect	Affected coatings
+	+	Deposition of material on the top surface AND Removal of material from porosities or generation of new porosities	Ceramic CT (HP) Coating F-50*
+	-	Deposition of material on the top surface AND Filling of voids (porosities) with material	Ceramic CT (LP) Coating JK-N8*
+	=	Deposition of material on the top surface	Ceramic HC (HP)
=	+	Removal of material from porosities or generation of new porosities	
=	-	Filling of voids (porosities) with material	
=	=	No considerable change	Ceramic HC (LP)
-	+	Erosion of material form asperities AND Removal of material from porosities or generation of new porosities	Coating PET-A Coating F-40
-	-	Erosion of material form asperities AND Filling of voids (porosities) with material	Coating PET-B Coating F-50** Coating JK-N8**
-	=	Erosion of material form asperities	

Coatings F-50 and JK-N(are affected by softening during the experiment.

* Surface roughness parameters measured considering the whole area

** Surface roughness parameters measured without considering cracks areas

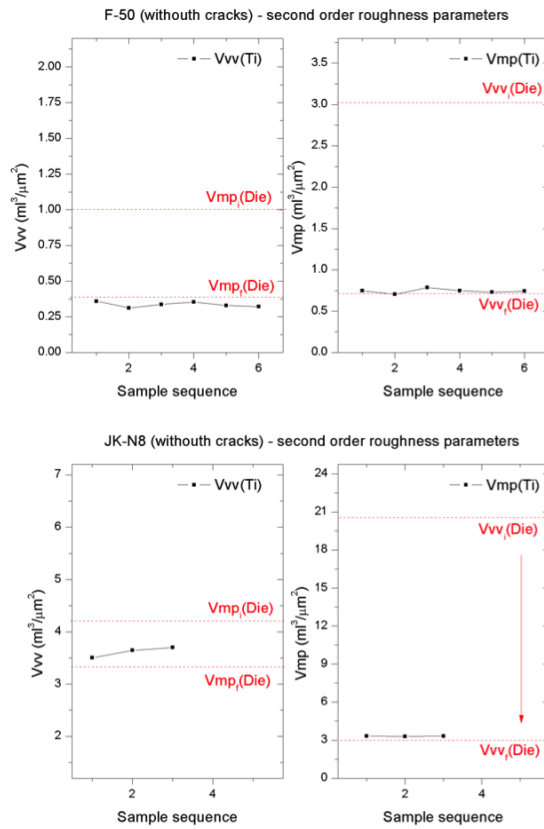


Figure (8.4) The measured material peak volume per unit area, Vmp , and the void valley volume per unit area, Vvv , are showed for coating F-40 without considering cracked area.

8.4 Chemical interaction

The uncoated ceramic CT surface wear is characterised by deposition of release agent from the titanium sample to the ceramic. At low pressure, the transferred boron nitride keeps its white colour, suggesting that no chemical reaction has occurred, but only physical transfer of a release agent layer on the ceramic surface. When tested at high pressure, the deposited layer is red-brown coloured, indicating that a chemical reaction has occurred. The surface of a ceramic CT sample after high-pressure static mode DPI test investigated with SEM and EDX (cf. figure ??) reveals the presence of titanium transferred to the die surface. The EDX technique identifies the atomic elements' presence, but it does not give information about the oxidation state of these elements. Further investigation with other techniques could validate the oxidation state of the titanium deposited on the ceramic surface. The high chemical interaction at high pressure results in the damage of the ceramic surface after the third test cycle.

After testing with the DPI experiment, the uncoated ceramic HC surface exhibits release agent transfer from the titanium sample to the ceramic in both high- and low-pressure conditions, but differently from ceramic CT, ceramic HC is not damaged during the high-pressure test. The main physical difference between the two ceramic materials is the amount of porosities at the surface: ceramic CT is more porous than ceramic HC due to the manufacturing procedure employed (the chrome infiltration process drastically decreases porosity [28]). Porosities affect both the physical and chemical interaction, and they can negatively affect mechanical properties as well. In addition, the presence of porosity acts as an oxygen source, where oxidation is promoted. An oxidising atmosphere in presence of titanium increase the chemical interaction between the titanium part and the die, resulting in adhesion of titanium oxide to the die working surface. Furthermore, porosity at the die-part interface increases the exposed surface, hence the interaction become stronger at higher pressure, as shown with ceramic CT.

Despite ceramic HC performing better than ceramic CT under static mode high-pressure conditions, ceramic HC breaks under shear stresses during the dynamic mode experiments, thus ceramic CT has been selected as substrate material.

To increase the wear resistance of ceramic CT SPF dies the surface porosity should be decreased, thus coating solutions have been selected for testing, which should reduce surface porosity. In addition, for the coating to be beneficial, it should not interact with titanium samples, hence the DPI test has been carried out to investigate the coating performance under SPF conditions.

Table 8.2 summarises the outcomes from the analysis of SEM images acquired from the coatings after deposition and after static mode DPI test. Petalite has been identified to fulfil the requirements imposed by the SPF process and the ceramic die material.

Table (8.2) Observations from SEM analysis.

Coating	Observations		Comments
	After deposition	After static mode DPI test	
PET-A	<ul style="list-style-type: none"> • White and opaque • Intermix layer absent 	<ul style="list-style-type: none"> • White and opaque with some glassified areas • Coating removed during test • Multiple cracks parallel to substrate surface • Accumulation of oxides on top surface • Coating fails after 4 cycles 	Poor sintering of the coating
PET-B	<ul style="list-style-type: none"> • Dark and translucent • 200µm external layer + 200µm intermix layer (good for adhesion) • Some porosities within the coating 	<ul style="list-style-type: none"> • Intermix layer still present • Some porosities within the coating • Erosion of coating material • Accumulation of oxides on top surface 	Further work needed to investigate different release agents
F-50	<ul style="list-style-type: none"> • White and opaque • 400µm thick • Intermix layer absent • Porosities within the coating 	<ul style="list-style-type: none"> • Dark-blue layer • Softening during test • Porosity concentrated at the interface substrate-coating • Accumulation of oxides on top surface • Coating fails after 5 cycles 	Not suitable for SPF applications
JK-N8	<ul style="list-style-type: none"> • White and opaque • 800µm thick • Intermix layer absent • Porosities within the coating • Cracks perpendicular to substrate surface (thermal stresses) 	<ul style="list-style-type: none"> • Brown layer • Softening during test • Accumulation of oxides on top surface • Porosity concentrated at the interface substrate-coating and within the deposited oxide layer • Coating fails after 2 cycles 	Not suitable for SPF applications
F-40	<ul style="list-style-type: none"> • Dark and translucent • 500µm thick • Intermix layer absent • Some porosities within the coating • Cracks perpendicular to substrate surface (thermal stresses) 	<ul style="list-style-type: none"> • Intermix layer arise during test • Some porosities within the coating • Coating removal during test • Coating fails after 3 cycles • No accumulation of oxide on top surface 	Further work needed to improve coating adhesion to substrate

Petalite is a lithium-rich aluminosilicate with very low CTE and it has been selected as potential protective coating. A deposition procedure has been developed, and two firing procedures have been investigated. The resulting coatings' performances have been tested with the DPI experiment. The coating obtained with firing procedure A, PET-A, is white and opaque. SEM images of coating cross section after DPI test show cracks parallel to the substrate surface, indicating that the sintering process is poor. During the DPI test part of the coating is removed and some areas show a shiny surface, indicating that the coating glassified in those regions as a result of an incomplete firing process. Further investigation could be conducted increasing the time of the firing procedure A.

Firing procedure B results in a more performing coating, where the material is fully sintered as cross section SEM images show. In addition, the coating exhibits an intermix layer that enhances the coating adhesion to the substrate. No coating spallation or

cracks in the coating have been found after the DPI test. In addition, the coating does not suffer softening during the DPI test, but it is affected by erosion of material and oxidation of the deposited release agent and titanium oxide on the working surface. On the coating, differently from PET-A, there is no adhesion of thick titanium layers and spallation of the coating does not occur; the results suggest that coating PET-B could be a good candidate for further work, for example investigating the chemical interaction using different release agents.

Few coatings are available in the market that can fulfil the SPF process and ceramic die requirements, and most of them have low commercial availability. Three coating materials, of those commercially available, have been tested in this work. Coating F-50 and coating JK-N8 shows inadequate performance under SPF conditions. Both the coating suffer softening, which increase the chemical interaction between coating and titanium sample. Coating F-50 exhibits a dark-blue layer on the working surface after the DPI test, while coating JK-N8 has a brown layer. The colour is due to the titanium oxidation number, thus the type of titanium oxide generated. Further investigation on the titanium oxidation number should clarify this aspect. The cross section of coating F-50 and coating JK-N8 analysed at the SEM shows high porosity in the coating. The porosity may be due to the oxygen released from the (porous) ceramic substrate, where gasses are trapped in the coating during the firing. Future works may focus on the optimization of the firing process with porous substrates. In conclusion, the results obtained with coating F-50 and coating JK-N8, with the current firing procedure, suggest that these materials are not suitable for SPF applications.

Coating F-40 is another of the coatings selected from the market. The firing procedure employed has been suggested from the supplier and the obtained coating has not produced any intermix layer with the substrate, but the cross section of the coating after test analysed with SEM shows that an intermix layer between the coating and the substrate has arisen after keeping the coating for prolonged time at the testing temperature. This result indicates that, if the deposition process is optimised, it is possible to obtain a dense protective coating well adhered to the ceramic substrate. In addition, coating F-40 does not present scale built-up on the working surface, as seen in all the other situations. The coating failed during the DPI test because of low adhesion with the substrate. These results suggest that further investigation should be conducted on the optimisation of the coating firing procedure in order to obtain a better adhesion with the substrate. This has not been undertaken in this study as the focus of this thesis is on validating a test methodology.

From the outcomes of the DPI test the uncoated ceramic CT results to be the best option in terms of surface degradation resistance and chemical interaction with the titanium parts. Two coatings undergo to softening during the test conditions,

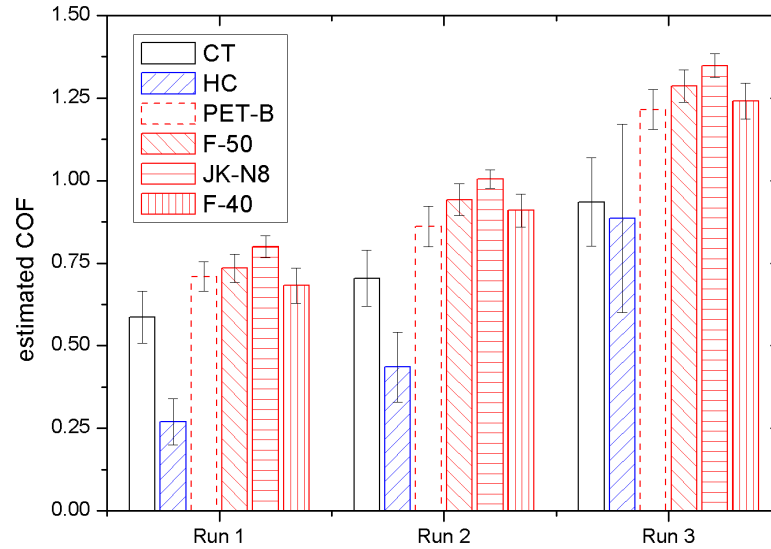


Figure (8.5) COF from dynamic mode DPI test for all the tested materials. Due to rupture of the ceramic HC sample during Run 3, the COF is affected by high variability of the reading value, thus high standard deviation.

which results in strong adhesion between the die and titanium part that makes difficult the unloading of titanium part at the end of each cycle and generates cracks at the die surface. Coatings F-50 and JK-N8 are thus not employable for SPF applications. Results from coatings F-40 and PET-A show that further work should be conducted to optimise adhesion between coating and substrate. Coating PET-B shows interesting results in terms of surface degradation under SPF conditions, but the coating suffers of strong chemical interaction with titanium oxide under SPF conditions compared with the uncoated substrate (ceramic CT).

8.5 Friction

The dynamic mode DPI test gives information regarding the COF between the ceramic material and the titanium sample under SPF conditions. The measurement of COF is explained in section 4.2.4, where a circular geometry has been considered for an easier calculation of the COF. The resulting COF, calculated implying this simplification, is underestimated. In order to achieve a more accurate measure of the COF, a circular geometry of the titanium sample should be used during the dynamic mode DPI test. However, the estimated COF resulting from this testing method is used for comparison studies. In the dynamic mode DPI test Run 1 is a low-pressure/low-speed

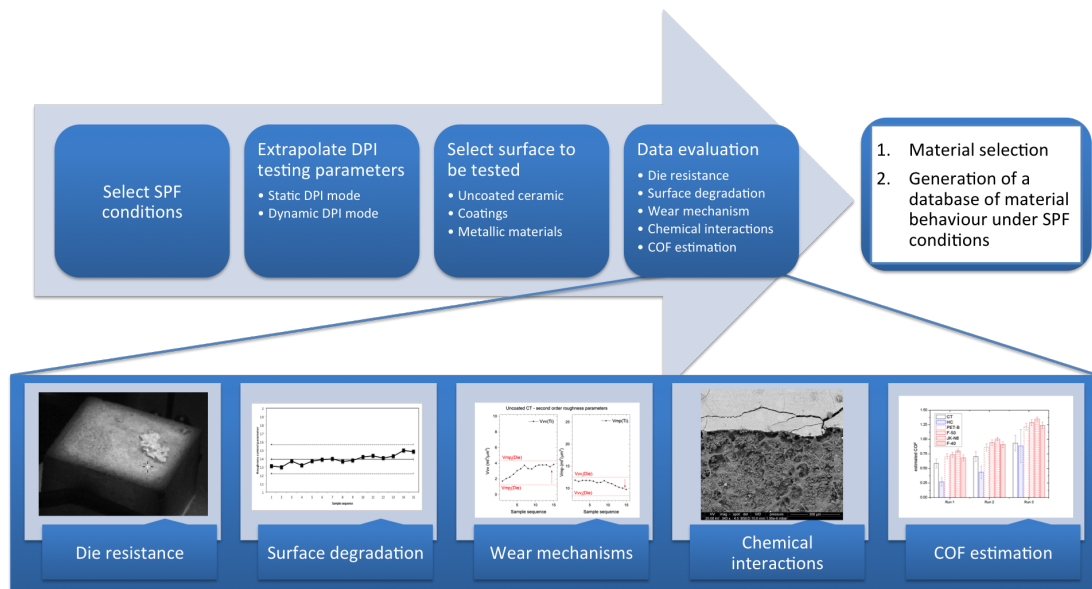


Figure (8.6) The Die-Part Interface test protocol

condition, while Run 3 is a high-pressure/high-speed condition and Run 2 is a middle point; figure 8.5 presents the resulting coefficient of friction measured for all the surface conditions tested. The analysis of variance (ANOVA) for all the average COF values for each run, weight for their standard deviation, and considering a significance level of 0.05 (thus a confidence level of 95%), indicates that the uncoated ceramics (CT and HC) have the lowest COF value and coating JK-N8 has the highest for all the test conditions (runs). Coatings F-50 and JK-N8 have the highest COF in all runs, due to softening of the coatings under SPF conditions, which makes the coatings viscous, increasing the adhesion with the titanium part, thus resulting in a higher COF. Between the uncoated ceramics, HC has a lower COF than ceramic CT in Run 1 and Run 2, while is comparable in Run 3, but higher standard deviation due to cracking of the ceramic HC block during testing.

The COF gives an idea of the interaction at SPF temperature between the ceramic surface and the titanium sample. Data in figure 8.5 give a quick overview of the mechanical and chemical interaction at the die-part interface, showing that all the tested coatings interactions are greater than the uncoated ceramics. In addition, this estimated data could be employed in finite element modelling for a more accurate simulation of the SPF process with ceramic materials.

8.6 The die-part interface test protocol

The results obtained in the previous chapters have been used to formulate a test protocol to be employed for future surface wear assessment of different die materials and/or protective coatings under SPF conditions at a laboratory scale.

The test protocol is summarised in figure 8.6 and it gives a precise guideline to proceed with SPF die-surface wear assessment. The aim of the test protocol is to establish a database of material's behaviour under SPF conditions, which will help materials engineer to select the proper die material and protective coating depending on the die geometry, formed part alloy and SPF cycle. As shown in figure 8.6, the first step of the test protocol is to select the SPF conditions. In this step the die geometry, material of formed part, forming temperature and SPF cycle are established. The next step is to extrapolate the DPI testing parameters from the SPF conditions defined in the previous step, as explained in section 4.1.4 and section 5.1.2. The materials to be tested are then selected: they can be metallic materials, ceramic materials, protective coatings or surface treatments. Once the DPI tests are carried, the data analysis evaluates the key metrics parameters. Die resistance is evaluated through visual inspection of the surface, using thermal images and 3D topography with confocal microscope technique. The acceptable surface degradations during the test is monitored through control charts of first order surface roughness parameter. If the selected surface roughness parameter, normalised with the initial surface roughness, increase for more than 3σ (where σ is the standard deviation of the measured roughness parameter value for each test run), then the surface degradation is considered as unacceptable. The wear mechanisms are assessed employing second order surface roughness parameters, such as Vmp and Vvv , and chemical interaction analysis with SEM and EDX techniques. Friction studies are carried as COF comparisons with benchmarks.

The results obtained in the previous chapters have been useful for the formulation of the guidelines illustrated in the test protocol in figure 8.6. Furthermore, the results obtained have been crucial for the determination of the Ceradyne ThermoSil[®] 220 surface wear properties under SPF condition. These data are employed to generate a comparative baseline for all the tested material so far and in the future.

8.7 Summary

Several wear mechanisms occur on the die surface during the SPF process, which are competitive, such as gain or loss of material. The DPI test have been employed to identify these wear mechanisms under SPF conditions and the outcomes can be summarised as follows:

- Uncoated ceramic CT degrades under high-pressure, while uncoated ceramic HC is not able to stand shearing on the surface, thus ceramic CT has been selected as the SPF die candidate for the study on protective coatings. Such protective coatings should enhance the ceramic CT properties under high-pressure conditions.
- Petalite coating, in the form of PET-B, shows interesting results such as the intermix layer with the ceramic substrate and moderate wear, thus further investigation on different release agents is recommended.
- Coatings F-40 and JK-N8 suffer softening under SPF conditions, interacting with the titanium parts and damaging the ceramic die. These materials are not suitable as protective coatings.
- Coating F-50 does not show good protective performance, but SEM images suggest that further work aimed to increase adhesion of the coating to the substrate could lead to a successful coating.

In addition, a test protocol has been presented in this chapter, to address future studies on SPF die wear assessment.

Chapter 9

Conclusion

This chapter concludes this work, focusing on the potential of the DPI test to answer the research questions. In addition, recommendations for further work are given.

Superplastic forming (SPF) is a metal sheet manufacturing process that employs the exceptional ductility of superplastic materials. This research work focused on ceramic die materials for high-temperature SPF, and in particular on the surface wear of ceramic die and coatings. The literature review revealed a shortage of knowledge on the ceramic materials wear mechanisms involved during the SPF process of titanium alloys. This knowledge gap is due to the cost related to test ceramic materials into SPF manufacturing presses and to the shortage of laboratory tests that are able to simulate SPF surfaces interactions.

This aspect is crucial for the development and improvement of SPF technology, thus the main research question of this work focuses on a laboratory test assessment of ceramic die surface wear.

The research contribution lies on the development of a test protocol that enables the assessment of surface wear of ceramic materials under SPF conditions. Researcher at the Advanced Forming Research Centre have previously developed a Die-Part Interface (DPI) test rig capable of simulating SPF conditions at a laboratory scale. The author contribution focuses on the methodology employed in the DPI rig to select testing parameters depending on the SPF forming process to be simulated (geometry of the die, SPF pressure cycle, strain rate, etc.). In addition, the author proposed a guideline for the interpretation of the roughness parameters data, combined with SEM analysis and friction data, to explain the wear mechanisms involved at the working surface during the experiment. The coating selection have been discussed as well; the author proposed four coating materials in order to gather data on different materials behaviour under SPF conditions employing the DPI test.

The DPI test discussed in this work is an experimental method for assessing wear of

ceramic surface under SPF conditions, and it comprises two experimental configurations (static and dynamic) to simulate the different die-part interactions occurring during the SPF process. The test recreates wear conditions on the die surface and analysis of both ceramic die and titanium parts gives information on surface wear mechanisms involved. The key metrics that the DPI test protocol evaluates are: the die resistance to thermal cycles and surface degradation, the titanium scale accumulation, the chemical interaction and friction between die and part.

In this thesis three separate studies have been reported where the DPI test has been employed in order to validate its effectiveness. In chapter 5 two uncoated ceramic materials, Ceradyne ThermoSil[®] 220 (ceramic CT) and Horizon Chrome infiltrated (ceramic HC), have undergone the DPI test. The DPI test revealed that Ceradyne material degrades under high-pressure conditions, but it shows better resistance during shear of titanium parts on the ceramic surface. The DPI test helped the author to select the ceramic material substrate for protective coating studies, which are discussed in chapter 6 and 7.

The protective coatings studies show that the DPI test can evaluate wear of several different coating materials, assessing their performance under SPF conditions. Chapter 6 shows the employment of the DPI test to optimise coating deposition parameters when the optimal deposition variables are unknown. The DPI test compared two different depositions of the same coating material in order to obtain a performant protective coating under SPF conditions.

In addition, the DPI test has been employed to assess the performance under SPF conditions of four different coating materials (PET-B, F-50, JK-N8 and F-40) in chapter 7. The DPI test reveals that the uncoated Ceradyne has better response under SPF conditions than the coated Ceradyne samples. The surface roughness evaluation of each formed titanium part is one of the key metrics evaluated to assess wear of surfaces. This data is helpful to characterise the wear mechanisms that take place during wear under SPF conditions, which are summarised in table 8.1 of Chapter 8 for each tested material and condition. Furthermore, SEM analysis reveals chemical interactions at the interfaces substrate-coating and coating-titanium part. These data are crucial for the understanding of wear-resistant protective coatings, and they are taken into consideration for the recommendations of future research work.

9.1 Recommendations for future work

The DPI test is a powerful tool for the assessment of SPF ceramic die surface wear, but due to the complexity of the manufacturing process it is trying to simulate, there are some intrinsic limitations. The SPF process is characterised by the superplastic

stretching of a metal sheet, which slides on the die surface. Due to technological limitations, the DPI test simulates this effect with sliding imposed by torque of the titanium sample on the ceramic surface neglecting the plastic deformation of the metal sheet. The superplastic stretching of the titanium sample generates new (non-oxidised) surfaces which are then exposed to the die surface. Neglecting the superplastic stretching result in an underestimation of the chemical interaction and COF underestimation between die and part during the DPI test. In addition, chemical interaction inspection could be improved with other characterisation techniques, such as Raman and infra-red spectroscopy, that could give additional information regarding the state of oxidation of the elements identified with EDX maps.

Although these limitation factors, the developed DPI test enables a great number of research activities for the future, such as systematic studies on wear assessment under SPF conditions of:

- A detailed study on the effect of oxygen released by the ceramic die porosities on SPF formed parts;
- The effect of oxygen barrier coatings on SPF formed parts;
- Further protective coatings for ceramic die materials;
- The use of release agent different from boron nitride for ceramic and metallic dies;
- Other metallic die materials; and
- Enamels and coatings for metallic die materials.

The author would suggest evaluating coating PET-B performance through the DPI test employing different release agents to boron nitride, or even to test the coating without the use of any release agent on the titanium samples.

Furthermore, effort should be spent to improve the adhesion properties of coating F-40 on Ceradyne ThermoSil[®] 220 substrate, evaluating other firing procedures or the use of a slip layer between the substrate and coating to decrease the thermal expansion coefficient mismatch between coating and substrate materials.

Appendices

Appendix A

Coating materials

In this appendix are described the coating materials that have been employed in different applications to SPF and could be of interest for SPF ceramic dies. A desirable protective coating should be able to protect the ceramic surface from wear during the SPF process, enhancing the die life. A review of potential coatings has been conducted in order to identify interesting coating materials and to assess their performance under SPF conditions with the DPI test.

A suitable surface treatment can introduce important benefits to the working surface of ceramic dies, protecting the die-part interface from wear, and preventing the formation of cracks [38, 7, 32]. The appendix is divided into three sections, following the rationale of the coating investigation. A first category of identified coating materials regards these employed for ceramic dies in applications similar to SPF. A second category of identified coating materials focuses on these with low or adjustable thermal expansion, thus they can fit the low CTE of ceramic dies. A third category focuses on anti-oxidation barrier coatings employed on titanium alloys. This last category of coating materials should give an indication of materials with low chemical interaction with titanium alloys.

A.1 Coating materials for ceramic dies employed in similar applications

The Boeing Company, in 2005, patented a durable die liner employed for protection purposes of ceramic forming dies [118]. The proposed liner is a thick coating (2.0 to 3.2 mm) composed of a more durable material than the ceramic die body, thus increasing the die lifetime. The patent proposes an invention for the fabrication of composite materials in hot press, without limiting the scope of the invention to further applications. The patent suggest to deposit the liner during the casting of the die body. In addition, some liner solutions have been proposed such as:

- A slip casted Silicon-Nickel system; and
- An aluminosilicate matrix reinforced by silicon carbide fibres.

The patent does not mention the application of this invention for SPF ceramic dies, but if the ceramic composite can sustain the SPF process temperature, this solution can be integrated as a protective coating.

A.1.1 Rare earth alumino-silicates glasses

Rare earth oxides, or yttria, can be added to common ceramic glass systems in order to obtain high-temperature resistant materials. Those glasses are interesting as they show glass transformation temperature above 850°C [119]. Furthermore, rare-earth aluminosilicate glasses show high hardness and elastic moduli, chemical durability at high temperature and moderate thermal expansion, and for these reasons they have been employed [120] and patented [121]) as thermal barrier coatings in high temperature environments. The limited interest to use these coatings in SPF applications can be explained by the high cost of rare earth oxides.

A.2 Coatings and materials that fulfil thermal expansion requirements

A systematic review has been conducted on protective coating materials employed in similar applications to SPF. Data were collected if one or more of the following criteria were fulfilled:

- The use of coatings for titanium and titanium alloys at high temperatures;
- The use of ceramic and ceramic-glass coatings at high temperatures; and
- The use of ceramic and ceramic-glass coatings on ceramic substrates.

A.2.1 Adjustable thermal expansion materials

The relationship between the CTE and the volume fraction of titania (TiO_2) into zirconia (ZrO_2) matrix has been investigated by Jiang and Zhang [122, 2], in order to obtain a compound with linear CTE close to that of Ti-6Al-4V ($8.92 \times 10^{-6} \text{ }^\circ\text{C}^{-1}$) at 930°C). In Table A.1 the single components CTE are summarised. The study focuses on the manufacture of a ceramic die for SPF application where the CTE mismatch between the die and the Ti-6Al-4V was minimized.

According to Velay, et al. [123], the unloading step is critical for the prevention of crack generation on the working surface, since most of the die stress is concentrated

Table (A.1) CTE of zirconia, titania and Titanium alloy (Ti-6Al-4V)

	Density ($g\ cm^{-3}$)	CTE ($\times 10^{-6}\ ^\circ C^{-1}$)
ZrO_2	5.75	9.6
TiO_2	4.20	8.2
$Ti - 6Al - 4V$	4.43	8.92

on the die surface during the part unloading. The amount of TiO_2 mass fraction and relative density has influence on the final CTE. Furthermore, the addition of TiO_2 into ZrO_2 prevents any chemical interaction between the die and the titanium alloy, which results in an easier unload of the formed part at the end of the process.

The investigation is related to bulk materials for ceramic dies in SPF, but the results could be interesting as for transferring it on the design of a protective coating using a similar composition.

A.2.2 Low thermal expansion ceramic-glasses

Low thermal expansion ceramics are scientifically and industrially useful materials, and they are employed in thermal shock resistance applications, electronic devices, heat-engine components and high-performing optical mirrors for space. Ceramic materials can be successfully employed if they demonstrate dimensional integrity and microcracking resistance during thermal cycles. Microcracking occurs when the lattice, when it expands due to high temperature, undergoes large anisotropic movement. Therefore, a suitable ceramic should show either low bulk coefficient of thermal expansion and low or no anisotropy in the lattice expansion. Ceramic materials can be divided into three classes depending on the CTE value (α):

- High expansion ceramics ($\alpha > 8 \times 10^{-6}\ ^\circ C^{-1}$)
- Intermediate expansion ceramics ($2 \times 10^{-6}\ ^\circ C^{-1} < \alpha < 8 \times 10^{-6}\ ^\circ C^{-1}$)
- Low expansion ceramics ($0 < \alpha < 2 \times 10^{-6}\ ^\circ C^{-1}$)

Materials with negative expansion can be included in the last category depending on the absolute CTE value.

Low thermal expansion ceramic can be divide in four families:

1. Magnesium aluminosilicates (MAS) family;
2. Lithium aluminosilicates (LAS) family;

3. $NaZr_2P_3O_{12}$ (NZP) family;
4. Silica family.

A.2.2.1 MAS family

The MAS family is composed of the ternary system based on magnesia, alumina and silica. As discussed in Section 2.4.1, cordierite is part of this family, and the crystal structure of $2MgO - 2Al_2O_3 - 5SiO_2$ consists of an open framework structure. As discussed previously, cordierite exists in one metastable form and two polymorphic forms depending on the temperature. Cordierite composition modification (adding iron, manganese, gallium and germanium) has been studied [124, 125] to determine the CTE dependency.

A.2.2.2 LAS family

The ternary system composed of lithia, alumina and silica $LiO_2 - Al_2O_3 - SiO_2$ was investigated for the first time, in terms of low thermal expansion properties, in 1951 [126]. Hummel discovered ultralow thermal expansion polymorphs of the LAS system such as β -spodumene ($LiAlSi_2O_6$), β -eucryptite ($LiAlSiO_4$), and their solid solutions. The LAS system shows two negative thermal expansion areas, and useful compositions that has nearly zero thermal expansion [127]. Some of the commercialised glasses that are from the LAS family are *Zerodur*, *Pyroceram* and *Cer-Vit*.

A.2.2.3 NZP family

In 1980s the $NaZr_2P_3O_{12}$ thermal properties were discovered and a new family of low thermal expansion materials discovered and named NZP [128]. The NZP family is characterised by low CTE and superionic conductivity, which makes this material a good candidate for storing radioactive waste. NZP properties are attributed to the unique crystal structure, where there are holes completely or partially occupied by sodium or another substituent ion. The structure shows high flexibility in the substitutions of ions in the lattice, leading to numerous possible compositions with tailored α [129]. NPZ materials are being used or tested on applications such as port-liners for diesel engines, optical benches, braze fixtures for aircraft engine repair, high temperature nozzles and in the heating industry.

A.2.2.4 Silica family

Silica and silicate glasses are widely used as shock-resistant materials, due to their low CTE. The order of silica molecules in the solid state determines mechanical, chemical and thermal properties of the bulk material. Silica glass has the same material

composition of quartz, but a different crystal order, where quartz is the ordered structure of silica tetrahedron, while in the glass structure the order is missing. The low CTE of silica glass, in conjunction with other properties of glass such as chemical inertness and non-porous nature, etc., made it an attractive material for ceramists. Silica glass with addition of B_2O_3 is known as *Pyrex*. $SiO_2 - TiO_2$ glass system, commercially known as *ULE Titanium Silicate* (Code 7971), exhibits almost zero CTE over a wide range of temperature.

A.3 Anti-oxidation barrier coatings

Titanium alloys, such as Ti-6Al-4V, are employed for medical applications, in particular for dental prostheses where titanium is cast into a mould to obtain the desired shape of the part [33]. Investment casting of Ti-6Al-4V cannot use traditional moulds, because of its high reactivity, even in an inert gas atmosphere. The high reactivity of titanium alloy, particularly with oxygen, causes the generation of the so called α -case at the surface of the final manufactured part. The α -case is an oxygen-rich layer that shows several drawbacks, such as enhanced hardness and brittleness, reduced ductility and fatigue resistance [5].

Several methods have been evaluated to minimise the interaction between the mould and the melted metal, in order to avoid the formation of the α -case. One proposed solution is to employ barrier coating on the wax pattern. Different coating solutions have been investigated as a barrier layer that is thermodynamically stable when in contact with the melted Ti-6Al-4V. Yttrium oxide (Y_2O_3) showed good stability, compared with uncoated wax pattern [130]. Further investigations show that other refractory oxides have good stability with the melted metal, such as ZrO_2 [131], $ZrO_2 - Al_2O_3$ systems [132], and spinel-type oxides ($MgO - Al_2O_3$) [133].

Investment casting is a completely different process to SPF. However, the protective coatings employed in the wax pattern could be interesting for the application into SPF ceramic dies.

A.4 Summary

This appendix discusses coating materials that have been employed in different application to SPF that can be of interest for future protective coating studies. The identified coating materials are divided into three categories, as follows:

- Coating materials for ceramic dies employed in application different from SPF;
- Coating materials that fulfil thermal expansion requirements; and

- Anti-oxidation barrier coatings

Appendix B

Surface roughness data acquisition and processing

The following appendix regards the confocal microscope data acquisition and data processing carried out with the Alicona InfiniteFocus microscope and IF-MeasureSuite v4.1 software.

B.1 Data acquisition

Surface topography has been acquired using a 5x magnification, 400 nm vertical resolution and 55.99 μm lateral resolution. Brightness and contrast have been optimised for each acquisition in order to avoid too dark or too bright areas.

B.2 Data processing

Once the data of the surface topography has been acquired, the following procedure have been employed for data processing:

1. Selection of the coordinate system;
2. Form removal;
3. Roughness filter;
4. Roughness parameters extrapolation.

B.2.1 Selection of the coordinate system

The coordinate system xyz is imposed on the dataset with the following parameters:

- Method: a reference plane is used for adaptation of the coordinate system.

- Selection: the whole dataset is used for adjustment of the coordinate system.
- Computation: robust. The robust method is not influenced by peaks/valleys and will lead to a reference plane that is well fitted onto the even part of the dataset.

B.2.2 Form removal

A second order polynomial form is removed from the acquired dataset.

B.2.3 Roughness filter

A Roughness Gaussian filter (according to EN ISO 16610 [134]) is select in order to eliminate low frequency components from the profile. As the analysed surfaces are random surfaces, a synchronised x- and y-direction filter is selected.

B.2.4 Roughness parameters extrapolation

Roughness parameters are extrapolated, such as Sa that gives the average height of selected area. See table 2.4 for further details. In addition, the bearing area curve is measured on the selected area in order to calculate 3D roughness parameters as Vmp and Vvv .

Appendix C

Ferro coatings: technical information

Appendix D

James Kent coating N8-JK: technical information

Appendix E

Coating deposition procedures

In this appendix are available the coating deposition procedures employed for the DPI experiments in chapter 6 and chapter 7, which are:

- Petalite firing A, or PET-A
- Petalite firing B, or PET-B
- Ferro Corp. coating F-50
- James Kent Group coating JK-N8
- Ferro Corp. coating F-40

E.1 Deposition procedure of coating PET-A

The coating is deposited via dip-coating technique. A slurry made of 30% wt. petalite in water have been prepared and then the following procedure have been employed:

1. Dip the ceramic sample into the slurry and keep it for 30 seconds;
2. Remove the ceramic sample from the slurry without turning it. Allow the excess of slurry to drip from the ceramic surface for 30 seconds, and then turn the sample;
3. Leave the sample to dry in air for at least 24 hours.
4. Introduce the sample into a furnace at 1100°C and leave the sample for 60 minutes;
5. Move the sample into another furnace at 500°C and leave the sample for 120 minutes;
6. Turn off the furnace and let the sample inside to cool down.

E.2 Deposition procedure of coating PET-B

The coating is deposited via dip-coating technique. A slurry made of 30% wt. petal-ite in water have been prepared and then the following procedure have been employed:

1. Dip the ceramic sample into the slurry and keep it for 30 seconds;
2. Remove the ceramic sample from the slurry without turning it. Allow the excess of slurry to drip from the ceramic surface for 30 seconds, and then turn the sample;
3. Leave the sample to dry in air for at least 24 hours.
4. Introduce the sample into a furnace at 1350°C and leave the sample for 10 minutes;
5. Move the sample into another furnace at 500°C and leave the sample for 120 minutes;
6. Turn off the furnace and let the sample inside to cool down.

E.3 Deposition procedure of coating F-50

The coating is deposited via dip-coating technique. A slurry made of 20-30% wt. F-50 in water have been prepared and then the following procedure have been employed:

1. Dip the ceramic sample into the slurry and keep it for 30 seconds;
2. Remove the ceramic sample from the slurry without turning it. Allow the excess of slurry to drip from the ceramic surface for 30 seconds, and then turn the sample;
3. Leave the sample to dry in air for at least 24 hours.
4. Introduce the sample into a furnace at 1200°C and leave the sample for 10 minutes;
5. Move the sample into another furnace at 500°C and leave the sample for 120 minutes;
6. Turn off the furnace and let the sample inside to cool down.

E.4 Deposition procedure of coating JK-N8

The coating is deposited via dip-coating technique. A slurry made of 30% wt. JK-N8 in water have been prepared and then the following procedure have been employed:

1. Dip the ceramic sample into the slurry and keep it for 30 seconds;

2. Remove the ceramic sample from the slurry without turning it. Allow the excess of slurry to drip from the ceramic surface for 30 seconds, and then turn the sample;
3. Leave the sample to dry in air for at least 24 hours.
4. Introduce the sample into a furnace at 1050°C and leave the sample for 10 minutes;
5. Move the sample into another furnace at 500°C and leave the sample for 120 minutes;
6. Turn off the furnace and let the sample inside to cool down.

E.5 Deposition procedure of coating F-40

The coating is deposited via dip-coating technique. A slurry made of 30% wt. F-40 in water have been prepared and then the following procedure have been employed:

1. Dip the ceramic sample into the slurry and keep it for 30 seconds;
2. Remove the ceramic sample from the slurry without turning it. Allow the excess of slurry to drip from the ceramic surface for 30 seconds, and then turn the sample;
3. Leave the sample to dry in air for at least 24 hours.
4. Introduce the sample into a furnace at 1280°C and leave the sample for 10 minutes;
5. Move the sample into another furnace at 500°C and leave the sample for 120 minutes;
6. Turn off the furnace and let the sample inside to cool down.

Bibliography

- [1] Daniel G. Sanders. Superplastic forming manufacturing technology moves towards the twenty-first century. *Materials Science Forum*, 304-306:805–812, 1999.
- [2] Shao Song Jiang and Kai Feng Zhang. Superplastic forming of Ti6Al4V alloy using ZrO₂-TiO₂ ceramic die with adjustable linear thermal expansion coefficient. *Transactions of Nonferrous Metals Society of China*, 19(June):418–422, 2009.
- [3] Christoph Leyens and Manfred Peters. *Titanium and Titanium Alloys: Fundamentals and Applications*. Wiley-VCH Verlag GmbH & Co. KGaA, Weinheim, FRG, 2003.
- [4] G. Bernhart, F. Nazaret, and T. Cutard. Fiber reinforced refractory castables for SPF toolings. *Materialwissenschaft und Werkstofftechnik*, 39(4-5):317–321, 2008.
- [5] Gerd Lütjering and James C. Williams. *Titanium*. Springer Berlin Heidelberg, Berlin, 2007.
- [6] G. Bernhart, F. Nazaret, and T. Cutard. Fibre Reinforced Refractory Castables : an Alternative Solution for SPF Die Manufacturing. *Mater. Sci. Forum*, 551-552:37, 2007.
- [7] Daniel G. Sanders. A Production System Using Ceramic Die Technology for Superplastic Forming. *Materials Science Forum*, 447-448:153–158, 2004.
- [8] A. Mazzoni, G. Bernhart, and T. Cutard. Ceramic Fibre Reinforced Refractory Castables for Very High Temperature Superplastic Forming. *Materialwissenschaft und Werkstofftechnik*, 43(9):758–762, sep 2012.
- [9] Arianna T. Morales. Evaluation of die coatings for superplastic forming processes. In *Advances in superplasticity and superplastic forming : proceedings of a symposium held during the 2004 TMS Annual Meeting*, pages 51–64, Charlotte, Pennsylvania, US, 2004.
- [10] L E A Sanchez, J F G Oliveira, and R T Coelho. Detection of cracks in scratching tests in ceramic materials through acoustic emission. *Proceedings of the Institution*

- of Mechanical Engineers, Part B: Journal of Engineering Manufacture*, 219:685–693, 2005.
- [11] S I Jaffery and P T Mativenga. Study of the use of wear maps for assessing machining performance. *Proceedings of the Institution of Mechanical Engineers, Part B: Journal of Engineering Manufacture*, 223:1097–1105, 2009.
- [12] Q H Zhang, C L Wu, J L Sun, and Z X Jia. The mechanism of material removal in ultrasonic drilling of engineering ceramics. *Proceedings of the Institution of Mechanical Engineers, Part B: Journal of Engineering Manufacture*, 214:805–810, 2000.
- [13] G N Peggs, P G Maropoulos, E B Hughes, A B Forbes, S Robson, M Ziebart, and B Muralikrishnan. Recent developments in large-scale dimensional metrology. *Proceedings of the Institution of Mechanical Engineers, Part B: Journal of Engineering Manufacture*, 223(6):571–595, jun 2009.
- [14] Tiandan Chen and Martha L. Mecartney. Superplastic Compression, Microstructural Analysis and Mechanical Properties of a Fine Grain Three-Phase Alumina-Zirconia-Mullite Ceramic Composite. *Materials Science and Engineering A*, 410-411:134–139, 2005.
- [15] Ke Ke Zhang, Yun Yue, Z.L. Zhang, Ning Ma, S. Liu, Hong Xin Shi, Hua Yu, and Yao Li Wang. Compression Superplasticity of Ultrahigh Carbon Steel in Electric Field. *Materials Science Forum*, 682:177–183, mar 2011.
- [16] J D Beal, R Boyer, and D Sanders. Forming of Titanium and Titanium Alloys. In *ASM Handbook vol.14B - Metalworking: Sheet Forming*, page 656. ASM International, 2006.
- [17] C H Hamilton. Superplasticity in Titanium Alloys. In S P Agrawal, editor, *Superplastic Forming*, pages 13–22. American Society for Metals, 1985.
- [18] (MIT). Lab Report 3.12. Technical report, 1964.
- [19] Larry D Hefti. Taming titanium via superplastic forming, 2010.
- [20] Daniel Sanders, Paul Edwards, Glenn Grant, Mamidala Ramulu, and Anthony Reynolds. Superplastically formed friction stir welded tailored aluminum and titanium blanks for aerospace applications. *Journal of Materials Engineering and Performance*, 19(4):515–520, 2010.
- [21] D Lee and W Backofen. No Title. *Transactions of the Metallurgical Society of AIME*, 239:1034, 1967.

- [22] A. K. Ghosh and C. H. Hamilton. Mechanical behavior and hardening characteristics of a superplastic Ti-6Al-4V alloy. *Metallurgical Transactions A*, 10(6):699–706, 1979.
- [23] A.J. Barnes. Superplastic Forming 40 Years and Still Growing. *Journal of Materials Engineering and Performance*, 16(4):440–454, 2007.
- [24] G. Giuliano. Mathematical modelling of superplastic metal sheet forming processes. In Gillo Giuliano, editor, *Superplastic forming of advanced metallic materials*, chapter Chapter 6. Woodhead Publishing Limited, Oxford, 2011.
- [25] J Bonet and A Gil. Finite element modelling of thin metal sheet forming. In G Giuliano, editor, *Superplastic forming of advanced metallic materials*, chapter Chapter 7. Woodhead Publishing Limited, Oxford, 2011.
- [26] A. K. Ghosh and C. H. Hamilton. Superplastic Sheet Forming. In *ASM Handbook vol.14B - Metalworking: Sheet Forming*, page 345. ASM International, 2004.
- [27] Kuppuswamy Anantha Padmanabhan and Graeme John Davies. *Superplasticity*. Springer Berlin Heidelberg, Berlin, Heidelberg, 1980.
- [28] Lynne O’Hare and Hector Basoalto. SPF Tooling Cost Reduction : Ceramic Dies - Ceramic Material Testing. Technical report, Advanced Forming Research Centre, 2012.
- [29] T Y M Al-naib and J L Duncan. Super plastic metal forming. *Inst.J.Mech.Sci*, 12:463–477, 1970.
- [30] J F Hubert. Superplastic Forming Process: Advances in Tooling Materials. *Tooling & Production*, 42:74, 1977.
- [31] P Barnet and J P Moraux. 25 Years of Experiment in The Tools for Superplastic Forming of Ti Alloys Evolution of Metallic Materials and Design in Foundry. In *EuroSPF 2008*, Carcassonne, France, 2008.
- [32] G. Bernhart, P. Lours, T. Cutard, V. Velay, and F. Nazaret. *Processes and Equipment for Superplastic Forming of Metals*. Woodhead Publishing Limited, 2011.
- [33] R. Curtis. The suitability of dental investment materials as dies for superplastic forming of medical and dental prostheses. *Materialwissenschaft und Werkstofftechnik*, 39(4-5):322–326, apr 2008.
- [34] R. Curtis. Overview – Superplasticity Community. *Materialwissenschaft und Werkstofftechnik*, 39(4-5):265–274, apr 2008.

- [35] Shao Song Jiang and Kai Feng Zhang. Superplastic Forming and Thickness Distribution of Ti6Al4V Alloy Denture Base. *Materials Science Forum*, 551-552:427–432, 2007.
- [36] Daniel G. Sanders. Integral forming die system for superplastic metal forming, nov 1995.
- [37] G. Bernhart, F. Nazaret, A. Martinier, C. Gao, D. Garriga-Majo, T. Cutard, and P. Lours. Design of SPF Dies Based on Advanced Material Behaviour Models. *Materials Science Forum*, 447-448:123–130, 2004.
- [38] D G Sanders, M A Peterson, D C Van Aken, T D Weaver, S F Miller, and J D Smith. US 6,692,844 - Glaze for ceramic superplastic forming (SPF) dies, 2004.
- [39] J. Rösler, M. Bäker, and H. Harders. Mechanical behaviour of ceramics. In *Mechanical Behaviour of Engineering Materials*, chapter 7, pages 227–255. Springer Berlin Heidelberg, 2007.
- [40] K C Ludema. Sliding and Adhesive Wear. In *ASM Handbook vol. 18 - Friction, Lubrication, and Wear Technology*, page 236. ASM International, 2010.
- [41] Paul E. Krajewski and Arianna T. Morales. Tribological Issues During Quick Plastic Forming. *Journal of Materials Engineering and Performance*, 13(6):700–709, dec 2004.
- [42] J. F. Archard and W. Hirst. The Wear of Metals under Unlubricated Conditions. In *Proceedings of the Royal Society A: Mathematical, Physical and Engineering Sciences*, volume 236, pages 397–410, 1956.
- [43] T S All, S Jacobson, and O Vingsbo. Surface Damage. In *ASM Handbook vol. 18 - Friction, Lubrication, and Wear Technology*, page 176. ASM International, 2011.
- [44] W A Glaeser. Friction and Wear of Ceramics. In *ASM Handbook vol. 18 - Friction, Lubrication, and Wear Technology*, page 812. ASM International, 2011.
- [45] O O Ajayi and K C Ludema. The Effect of Microstructure on Wear Modes of Ceramic materials. In *Proceeding of the International Conference on Wear of Materials*, pages 307–318. American Society of Mechanical Engineers, 1991.
- [46] R A Vaughn and A Ball. The Effect of Hardness and Toughness on the Erosion of Ceramic and Ultrahard Materials. In *Proceeding of the International Conference on Wear of Materials*, pages 71–75. American Society of Mechanical Engineers, 1991.

- [47] Zhiping Chen and P.F. Thomson. Friction against superplastic aluminium alloys. *Wear*, 201(1-2):227–232, dec 1996.
- [48] S.S. Han. The influence of tool geometry on friction behavior in sheet metal forming. *Journal of Materials Processing Technology*, 63(1-3):129–133, jan 1997.
- [49] S Hao, B.E Klamecki, and S Ramalingam. Friction measurement apparatus for sheet metal forming. *Wear*, 224(1):1–7, jan 1999.
- [50] L. Anand and W. Tong. A Constitutive Model for Friction in Forming. *CIRP Annals - Manufacturing Technology*, 42(1):361–366, jan 1993.
- [51] M. Woydt and K.-H. Habig. High temperature tribology of ceramics. *Tribology International*, 22(2):75–88, 1989.
- [52] J.L. Andreasen, N. Bay, and L. De Chiffre. Quantification of galling in sheet metal forming by surface topography characterisation. *International Journal of Machine Tools and Manufacture*, 38(5-6):503–510, may 1998.
- [53] L. Figueiredo, A. Ramalho, M.C. Oliveira, and L.F. Menezes. Experimental study of friction in sheet metal forming. *Wear*, 271(9-10):1651–1657, jul 2011.
- [54] H. Kim, S. Han, Q. Yan, and T. Altan. Evaluation of tool materials, coatings and lubricants in forming galvanized advanced high strength steels (AHSS). *CIRP Annals - Manufacturing Technology*, 57:299–304, 2008.
- [55] L. Kirkhorn, K. Frogner, M. Andersson, and J.E. Ståhl. Improved Tribotesting for Sheet Metal Forming. *Procedia CIRP*, 3:507–512, 2012.
- [56] G. J. Wenzloff, T. A. Hylton, and D. K. Mattock. Technical note: A new test procedure for the bending under tension friction test. *Journal of Materials Engineering and Performance*, 1(5):609–613, oct 1992.
- [57] R.W. Davies, M.A Khaleel, S.G. Pitman, and M.T. Smith. Experimental determination of the coefficient of friction during superplastic forming of AA5083 aluminium alloy. In ASM International, editor, *Proceeding from International Symposium on Superplasticity and Spuerplastic Forming Technology*, pages 39–43, 2002.
- [58] F.H. Stott. High-temperature sliding wear of metals. *Tribology International*, 35(8):489–495, aug 2002.
- [59] H. Kashani, A. Amadeh, and H.M. Ghasemi. Room and high temperature wear behaviors of nickel and cobalt base weld overlay coatings on hot forging dies. *Wear*, 262(7-8):800–806, 2007.

- [60] Xiong Dangsheng. Lubrication behavior of Ni–Cr-based alloys containing MoS₂ at high temperature. *Wear*, 251(1-12):1094–1099, oct 2001.
- [61] H Kim, J Sung, F E Goodwin, and T Altan. Investigation of galling in forming galvanized advanced high strength steels (AHSSs) using the twist compression test (TCT). *Journal of Materials Processing Technology*, 205(1-3):459–468, 2008.
- [62] Hasan Sofuoglu, Hasan Gedikli, and Jahan Rasty. Determination of Friction Coefficient by Employing the Ring Compression Test. *Journal of Engineering Materials and Technology*, 123(3):338, 2001.
- [63] S.B. Petersen, P.A.F. Martins, and N. Bay. An alternative ring-test geometry for the evaluation of friction under low normal pressure. *Journal of Materials Processing Technology*, 79(1-3):14–24, jul 1998.
- [64] P A Friedman, S G Luckey, W B Copple, R Allor, C E Miller, and C Young. Overview of Superplastic Forming Research at Ford Motor Company. *Journal of Materials Engineering and Performance*, 13:670, 2004.
- [65] J F Song and T V Vorburger. Surface Texture. In *ASM Handbook vol. 18 - Friction, Lubrication, and Wear Technology*, pages 334–345. ASM International, 2010.
- [66] (ISO). BSI Standards Publication Geometrical product specifications (GPS) — Surface texture : Areal Part 601 : Nominal characteristics of contact, 2010.
- [67] BS EN ISO. BS EN ISO 4287:1998+A1:2009 - Geometrical Product Specifications (GPS) – Surface texture: Profile method – Terms, definitions and surface texture parameters, 2009.
- [68] E.J. Abbott and F.A. Firestone. Specifying surface quality: a method based on accurate measurement and comparison. *Mechanical Engineering*, 55:569–572, 1933.
- [69] BS EN ISO. ISO 13565-2:1998 - Geometric Product Specifications (GPS) - Surface texture : Profile method - Surfaces having stratified functional properties, 1998.
- [70] MichiganMetrology. Methrology parameters, 2010.
- [71] M A Schmidt and R D Compton. Confocal Microscopy. In *ASM Handbook vol. 18 - Friction, Lubrication, and Wear Technology*, pages 357–361. ASM International, 2010.

- [72] M Richardson. Confocal Microscopy and 3-D Visualization. *American Laboratory*, 11:19–24, 1990.
- [73] G Kino and T Corle. Confocal Scanning Optical Microscopy. *Physics Today*, 9:55–62, 1989.
- [74] D. K. Bowen and C. R. Hall. *Microscopy of Materials*. Macmillan Education UK, London, 1975.
- [75] J I Goldstein, D E Newbury, P Echlin, D C Joy, C E Fiori, and E Lifshin. *Scanning Electron Microscopy and X-Ray Microanalysis*. Plenum Publishers, New York, 3rd editio edition, 2004.
- [76] L K Ives. Electron Microscopy. In *ASM Handbook vol. 18 - Friction, Lubrication, and Wear Technology*, page 376. ASM International, 2011.
- [77] D C Joy, A D Roming, and J I Goldstein. *Principles of Analytical Electron Microscopy*. Plenum Publishers, New York, 1st editio edition, 1986.
- [78] D T Weaver, F S Miller, D C Van Aken, and J D Smith. Development of Cordierite Coatings for Low Thermal Expansion Refractory Concretes. In *Proceedings of the 1st International Thermal Spray Conference*, pages 829–835, 2000.
- [79] R B Graf, F M Wahl, and R E Grim. Phase transformations in silica-alumina-magnesia mixtures as examined by continuous X-ray diffraction. *The American Mineralogist*, 48:150–158, 1963.
- [80] K Y Blohowiak and C W Newquist. US 5,947,187 - Method for protecting a die, 1999.
- [81] Andrea Staiano, William Ion, and Lynne O’Hare. Thermal sprayed protective coatings for superplastic forming ceramic dies: a monitoring system of die condition. *Proceeding of the International Thermal Spray Conference*, 302(1):301–305, 2014.
- [82] Claes Wohlin, Per Runeson, Martin Höst, Magnus C. Ohlsson, Björn Regnell, and Anders Wesslén. Empirical Strategies. In *Experimentation in Software Engineering*, pages 9–36. Springer Berlin Heidelberg, Berlin, Heidelberg, 2012.
- [83] Ravi Jain, Harry Charalambos Triandis, Cynthia Wagner. Weick, and Wiley InterScience (Online service). *Managing research, development and innovation : managing the unmanageable*. Wiley, 2010.
- [84] Richard M. Felder and Linda K. Silverman. Learning and Teaching Styles in Engineering Education. *Engineering Education Journal*, 78(7):674–681, 1988.

- [85] Thuy Mai. Technology Readiness Level, 2015.
- [86] R. Zante and C. Knowles. Advances in Monitoring Die Condition during Superplastic Forming. *Key Engineering Materials*, 549:557–564, jun 2013.
- [87] Andrea Staiano. *A working surface monitoring system for ceramic superplastic forming dies*. Master dissertation, University of Strathclyde, 2014.
- [88] H Czichos, T Saito, and L Smith. *Springer Handbook of Metrology and Testing*. Springer-Verlag, Berlin, Heidelberg, 2nd editio edition, 2011.
- [89] S Christiansen and L De Chiffre. Topographic characterization of progressive wear on deep drawing dies. *Tribology Transactions*, 40(2):346–352, 1997.
- [90] Buehler. Buehler Product Catalog, 2014.
- [91] P a Friedman and S G Luckey. *High-temperature lubricants for superplastic forming materials*. Woodhead Publishing Limited, 2011.
- [92] A. Gomez-Gallegos, Andrea Staiano, M Farrell, and N Zuelli. A comparative study assessing the wear behaviour of different ceramic die materials during superplastic forming. In *EuroSPF 2016*, Toulouse, 2016.
- [93] A. A. Gomez-Gallegos, M. Farrell, N. Zuelli, and A. Staiano. A comparative study assessing the wear behaviour of different ceramic die materials during superplastic forming. *Materialwissenschaft und Werkstofftechnik*, 48(10):983–992, oct 2017.
- [94] A. Gomez-Gallegos. D.2 - Literature Review on Ceramic Tool Materials. Publication No. 451. Technical report, Advanced Forming Research Centre, Inchinnan, 2016.
- [95] Ceradyne-Thermo. Ceradyne Thermo-Sil Product information.
- [96] Wojciech Wieleba. The statistical correlation of the coefficient of friction and wear rate of PTFE composites with steel counterface roughness and hardness. *Wear*, 252(9-10):719–729, may 2002.
- [97] Leigh Brown. *The use of 3D surface analysis techniques to investigate the wear of matt surface finish femoral stems in total hip replacement*. PhD thesis, University of Huddersfield, 2006.
- [98] Marko Sedlaček, Bojan Podgornik, and Jože Vižintin. Correlation between standard roughness parameters skewness and kurtosis and tribological behaviour of contact surfaces. *Tribology International*, 48:102–112, apr 2012.

- [99] A.Z. Eguren. *The use of 3D surface topography analysis techniques to analyse and predict the alteration of endosseous titanium dental implants generated during the surgical insertion*. PhD thesis, Mondragon Unibertsitatea, 2015.
- [100] Don Cohen. 3D Functional Parameters - Michigan Metrology.
- [101] Lynne O'Hare and Hector Basoalto. D8.1.1 SPF tooling cost reduction plan - AFRC0005. Technical report, AFRC, University of Strathclyde, 2010.
- [102] Lynne O'Hare and Hector Basoalto. D8.1.2/3 Progress report & die design methodology - AFRC00046. Technical report, AFRC, University of Strathclyde, 2011.
- [103] R. Bhattacharya. D8.1.A4 Ceramic Literature Review - AFRC00105. Technical report, 2012.
- [104] C. Knowles and P Anderson. REPORT ON LOW-COST TOOLING: D75 CERAMIC DIE. Technical report, AFRC, University of Strathclyde, 2015.
- [105] Andrea Staiano, Lynne O'Hare, William Ion, and N Zuelli. Protective coatings for superplastic forming ceramic dies: An initial study on protective coatings performance. In *EuroSPF 2016*, Toulouse, 2016.
- [106] A. Staiano, W. Ion, L. O'Hare, and N. Zuelli. Protective coatings for ceramic superplastic forming dies: An initial study on protective coating performance. *Materialwissenschaft und Werkstofftechnik*, 48(10):1009–1016, oct 2017.
- [107] Andrea Staiano. D1.1_A - Summary report on protective coatings for ceramic dies. Publication No. Technical report, Advanced Forming Research Centre, Inchinnan, 2014.
- [108] Andrea Staiano. AFRC_CORE_HSF 14/15 D1.3 – Annex to the Report on Ceramic Die Coating. Publication No. 341. Technical report, Advanced Forming Research Centre, Inchinnan, 2015.
- [109] Andrea Staiano. AFRC_CORE_HSF 14/15 D1.3 – Report on Ceramic Die Coating. Publication No. 322. Technical report, Advanced Forming Research Centre, Inchinnan, 2015.
- [110] Andrea Staiano and A. Gomez-Gallegos. D4.1 – Report on Ceramic Die Protective Coating. Publication No. 537. Technical report, Advanced Forming Research Centre, Inchinnan, 2016.

- [111] D T Weaver, D C Van Aken, and J D Smith. The role of bulk nucleation in the formation of crystalline cordierite coatings produced by air plasma spraying. *Materials Science and Engineering A*, 339:96–102, 2003.
- [112] F G Razavy, D C Van Aken, and J D Smith. Effect of laser surface melting upon the devitrification of plasma sprayed cordierite. *Materials Science and Engineering: A*, 362:213–222, 2003.
- [113] A. Rabinovitch, G. Belizovsky, and D. Bahat. Origin of mist and hackle patterns in brittle fracture. *Physical Review B*, 61(22):14968–14974, jun 2000.
- [114] J. Rösler, M. Bäker, and H. Harders. Fracture Mechanics. In *Mechanical Behaviour of Engineering Materials*, chapter 5, pages 129–164. Springer Berlin Heidelberg, jan 2007.
- [115] D Montgomery. *Statistical Quality Control*. 7th editio edition, 2012.
- [116] A Suh, A Polycarpou, and T Conry. Detailed surface roughness characterization of engineering surfaces undergoing tribological testing leading to scuffing. *Wear*, 255:556, 2003.
- [117] Jack R Clark and Marion B Grant. The effect of surface finish on component performance. *International Journal of Machine Tools and Manufacture*, 32:57, 1992.
- [118] M. R. Matsen, R. W. Brown, J. R. Fischer, and B. L. Kirkwood. US 6,855,917 - Induction processable ceramic die with durable die liner, 2005.
- [119] J E Shelby and J Kohli. Rare-Earth Aluminosilicate Glasses. *Journal of the American Ceramic Society*, 73(1):39–42, 1990.
- [120] K N Lee. Comprised of rare earth silicate material; strength and durability in high temperature and chemically hostile environment, 2004.
- [121] C Louchet-Pouillier, H Tawil, and E Bouilon. Composite material part with a silicon-containing ceramic matrix protected against corrosion, 2012.
- [122] Shao Song Jiang and Kai Feng Zhang. Study on controlling thermal expansion coefficient of ZrO₂-TiO₂ ceramic die for superplastic blow-forming high accuracy Ti-6Al-4V component. *Materials & Design*, 30(9):3904–3907, oct 2009.
- [123] V. Velay, T. Cutard, and N. Guegan. Thermal behaviour modelling of superplastic forming tools. *Materialwissenschaft und Werkstofftechnik*, 43(9):799–804, sep 2012.

- [124] D K Agrawal, V S Stubican, and Y Mehrotra. Germanium-modified cordierite ceramics with low thermal expansion. *Journal of the American Ceramic Society*, 69:847–51, 1986.
- [125] H Ikawa, T Otagiri, O Imai, M Suzuki, and K Urabe. Crystal structures and mechanism of thermal expansion of high cordierite and its solid solutions. *Journal of the American Ceramic Society*, 69:492–8, 1986.
- [126] F. A. Hummel. Thermal expansion properties of some synthetic lithia minerals. *Journal of the American Ceramic Society*, 34:235–239, 1951.
- [127] E J Smoke. Ceramic compositions having negative linear thermal expansion. *Journal of the American Ceramic Society*, 34:97–90, 1951.
- [128] R Roy, D K Agrawal, J Alamo, and R A Roy. [CTP]: a new structural family of near-zero expansion ceramics. *Materials Research Bulletin*, 19(471-7), 1984.
- [129] J Alamo and R Roy. Crystal chemistry of the $\text{NaZr}_2(\text{PO}_4)_3$ NZP or CTP structure family. *Journal of Materials Science*, 21:444–50, 1986.
- [130] T Okabe, H Shimizu, M Woldu, M Brezner, L Carrasco, and K Watanabe. Mechanical properties of titanium cast using yttria face-coating. In *THERMEC 2000*, 2000.
- [131] T Shafer, Z Cai, L Carrasco, and T Okabe. Porcelain binding to cast titanium made from oxide face-coated patterns. *Journal of Dental Research*, 81:A–261, 2002.
- [132] M Nakamura, K Jyohzaki, T Kimura, T Togaya, and K Ida. Ceramic dental molds for the precision casting of titanium and titanium alloys. *Journal of the American Ceramic Society*, 73:35–38, 1990.
- [133] O Miyakawa, K Watanabe, S Okawa, S Nakano, and M Kobayashi. Reaction layers of titanium cast in molds containing spine. *Dental Materials*, 14:560–568, 1995.
- [134] BS EN ISO. BS EN ISO 16610-21:2012 - Geometrical product specifications (GPS). Filtration. Linear profile filters: Gaussian filters, 2012.